REACTOR MATERIALS

OCT 15 1968
MICHIGAN STATE UNIVERSITY

A Quarterly Technical Progress Review

Prepared for DIVISION OF TECHNICAL INFORMATION, U. S. ATOMIC ENERGY COMMISSION,
by BATTELLE MEMORIAL INSTITUTE, COLUMBUS LABORATORIES

Fall 1968

● VOLUME 11

● NUMBER 3

TECHNICAL PROGRESS REVIEWS

The United States Atomic Energy Commission publishes the Technical Progress Reviews to meet the needs of industry and government for concise summaries of current nuclear developments. Each journal digests and evaluates the latest findings in a specific area of nuclear technology and science. *Nuclear Safety* is a bimonthly journal; the other three are quarterly journals.

Isotopes and Radiation Technology
P. S. Baker, A. F. Rupp, and Associates
Isotopes Information Center, Oak Ridge National Laboratory

Nuclear Safety
Wm. B. Cottrell, W. H. Jordan, J. P. Blakely, and Associates
Nuclear Safety Information Center, Oak Ridge National Laboratory

Reactor and Fuel-Processing Technology
Argonne National Laboratory

Reactor Materials
E. M. Simons and Associates
Battelle Memorial Institute, Columbus Laboratories

All are available from the U. S. Government Printing Office. See the back cover for ordering instructions.

The views expressed in this publication do not necessarily represent those of the United States Atomic Energy Commission, its divisions or offices, or of any Commission advisory committee or contractor.

Availability of Reports Cited in This Review

United States Atomic Energy Commission (USAEC) reports are available at USAEC depository libraries and are sold by the Clearinghouse for Federal Scientific and Technical Information (CFSTI), National Bureau of Standards, U. S. Department of Commerce, 5285 Port Royal Road, Springfield, Va. 22151. All reports sold by CFSTI are $3.00 for printed copy and $0.65 for microfiche. Each separately bound part of a report is priced as a separate report. Some reports may not be available because of their preliminary nature; however, the information contained in them will generally be found in later progress or topical reports on the subject.

Other U. S. Government agency reports identified in this journal generally are available from CFSTI.

Private-organization reports should be requested from the originator.

United Kingdom Atomic Energy Authority (UKAEA) and Atomic Energy of Canada Limited (AECL) reports are available at USAEC depository libraries. UKAEA reports are sold by Her Majesty's Stationery Office, London; AECL reports are sold by the Scientific Document Distribution Office, Atomic Energy of Canada Limited, Chalk River, Ontario, Canada. UKAEA and AECL reports issued after March 1, 1967, are sold by CFSTI to purchasers in the United States and its territories.

Contents

Reactor Materials
Vol. 11, No. 3, Fall 1968

Fuel and Fertile Materials (Section I)
Uranium Metal and Alloys 145
Plutonium 148
Thorium 150
Metal–Ceramic Fuels 150
Coated-Particle Fuels 150
Uranium and Thorium Oxides 151
Carbide and Nitride Fuels 151
Basic Studies of Irradiation Effects in Fuel Materials 153
References 154

Moderator and Control Materials (Section II)
Graphite 157
Beryllium and Beryllium Alloys 158
Beryllium Oxide 160
Solid Hydrides 160
References 162

Cladding and Structural Materials (Section III)
Corrosion by Aqueous and Gaseous Media . . 164
Corrosion by Nonaqueous Liquids 166
Radiation Effects in Structural Materials . . 172
Metallurgy of Refractory Metals 177
Metallurgy of Common Cladding and Structural Materials 179
Nonfueled Refractories 182
Ceramic Technology 185
References 187

Special Fabrication Techniques (Section IV)
Cast and Wrought Materials 191
Powder-Metallurgy Materials 194
Pressure Bonding 195
Plating 196
High-Energy-Rate Processes 197
Welding and Brazing 197
Nondestructive Testing 200
References 201

Superintendent of Documents, U. S. Government Printing Office, Washington, D. C. 20402, $2.50 per year

Reactor Materials

is one of a series of technical progress reviews broadly covering the field of nuclear science and technology. Under the auspices of the USAEC Division of Technical Information, *Reactor Materials* is prepared by Battelle personnel from worldwide literature. It covers properties, behavior, and fabrication processes of materials applicable to nuclear reactor components and associated equipment.

The reader will recognize that the scope of this Review is too broad to permit detailed coverage of every topic. Rather, the authors and editors attempt to combine the highlights of significant new developments into an information summary of current research for both management and the technical specialist. As a rule, enough of the results are presented to define the research and summarize the findings. For readers desiring more information on any particular topic, a complete set of references is provided at the end of each section.

Each quarter a number of bibliographies, monographs, and books appear on subjects within the scope of *Reactor Materials*. Although the main purpose of this Review is to call attention to findings that are new and significant, such publications are noted in the text because they often represent excellent compilations of available information on important materials topics.

E. M. SIMONS
S. W. POREMBKA, JR.
D. L. KELLER

Battelle Memorial Institute
Columbus Laboratories

Issued quarterly by the U. S. Atomic Energy Commission. Use of funds for printing this publication approved by the Director of the Bureau of the Budget on July 8, 1966.

Section I

Reactor Materials

Fuel and Fertile Materials

Uranium Metal and Alloys

Unalloyed Uranium

French investigators[1] have studied the diffusion of uranium (at concentrations of 10^{-7} to 10^{-8}) in beta titanium and gamma iron. The diffusion coefficients obey the equation

$$D = D_0 \exp(-H/RT)$$

with

$D_0 = 2 \times 10^{-3}$ cm^2/sec and $H = 1.43$ ev/atom for Ti

and

$D_0 = 7 \times 10^{-5}$ cm^2/sec and $H = 1.38$ ev/atom for Fe

The mechanical and physical properties of cast, highly enriched (97.5% ^{235}U) uranium were determined at Oak Ridge.[2] Where possible, these measurements were made in the temperature range −65 to 165° F (−54 to 74° C). A statistical analysis of the test results indicated that a high degree of uniformity of properties exists among castings and within castings. These properties are given in Table I-1.

Taplin and Cocks[3] have studied the creep-rupture mechanisms of adjusted* uranium, with the following results:

1. In the range 250 to 400° C, the mechanism of failure was similar to normal ductile rupture. The brittle U(OCN) dendritic and cuboid inclusions fractured transversely to the stress direction at an early stage in the life of a specimen. The voids so formed grew by plastic flow (and perhaps vacancy condensation), merged, and linked to cause failure. At higher temperatures (and lower stresses), fracture of inclusions became less pronounced; and little effect of temperature upon ductility was observed. In general, ductility was relatively low in this adjusted uranium, owing to the large volume fraction of inclusions present.

2. In the range 400 to 520° C, intergranular creep–cavitation predominated as the mechanism of failure, and ductility remained relatively low. Some inclusions and dendritic cracking were observed, but the main path of failure was intergranular: grain-boundary sliding initiated cavitation at grain corners and grain edges, and these grew and linked by such processes as sliding, tearing, vacancy condensation, and gas collection to cause failure.

3. Around 600° C, failure was still initiated by cavities formed at grain boundaries, but because of easy stress relaxation at the cavity apices, these cavities did not readily propagate transversely to the stress direction. Thus large voids elongated in the stress direction were produced owing to growth largely by plastic flow. These voids merged at a late stage by internal necking and gave rise to a high ductility.

The French[4] have discussed the use of activation-energy measurements to study the creep mechanism in uranium. Other papers of interest include "Preparation of Uranium by Means of Reduction of UO_3 by Calcium Vapor,"[5] "Work-Hardening Characteristics of Polycrystalline Alpha Uranium in the Temperature Range 20 to 640° C,"[6] and "Study of the Plastic Consolidation of Polycrystalline Uranium During Tensile Tests Carried Out in the Alpha Phase at Different Rates."[7]

Alpha-Phase Uranium Alloys

Phase diagrams of the U–Ru, U–Rh, and U–Ir systems have been detailed by the National Bureau of Standards.[8] These diagrams are given in Figs. I-1, I-2, and I-3, respectively.

Other papers dealing with alpha-phase uranium alloys include "Nucleation and Growth of Martensite in Some Uranium–Chromium Alloys,"[9] and "Transformation Mechanisms on Rapid Cooling of Uranium–1.5 wt.% Molybdenum from the Gamma Phase."[10]

Gamma-Phase Uranium Alloys

Westinghouse Astronuclear[11] investigated a U–8 wt.% Mo alloy as gamma-ray shielding for SNAP-23A. Table I-2 presents the tensile properties of the cast alloy in the γ and $\gamma + \alpha$ conditions. Thermal-conductivity values for U–8 wt.% Mo in the stable $\gamma + \alpha$ form and thermal-expansion characteristics of the γ-phase alloy were also obtained at temperatures up to about 1400° F (760° C). As noted by other investigators, thermal-conductivity values increased essentially linearly with temperature, ranging from 10 Btu/(hr)(ft)(° F) at 400° F (204° C) to 22 Btu/(hr)(ft)(° F) at slightly over 1400° F. Thermal-expansion data showed a 1.8% length change at 1400° F with an inflection point in the curve at about 1100° F (593° C).

*Uranium containing approximately 500 ppm iron, 250 ppm aluminum, 600 ppm carbon, and 20 ppm nitrogen.

Table I-1 MECHANICAL AND PHYSICAL PROPERTIES[2] OF CAST, HIGH-PURITY URANIUM(97.5% ^{235}U)

Tensile Properties

Specimen direction	Temperature, °F	Number of measurements	Average	Limit of error of average	Limits within which approximately 95% of the measurements would be included
			Tensile strength		
			psi	psi	psi
Transverse	RT	9	63,778	±3,167	54,279–73,277
Longitudinal	RT	18	61,269	±2,728	49,701–72,837
Longitudinal	–65	4	51,012	±4,637	41,738–60,286
	0	3	52,283	±5,361	43,009–61,557
	115	4	70,938	±4,637	61,664–80,212
	165	4	75,575	±4,637	66,301–84,849
			Yield strength		
			psi	psi	psi
Transverse	RT	9	24,822	±5,080	9,583–40,061
Longitudinal	RT	19	28,095	±2,610	16,714–39,476
Longitudinal	–65	4	31,225	±5,484	20,256–42,194
	0	3	24,917	±6,340	13,948–35,886
	115	4	26,512	±5,484	15,543–37,481
	165	4	24,112	±5,484	13,143–35,081
			Elongation		
			%	%	%
Transverse	RT	9	6.7	± 1.4	2.4–11.0
Longitudinal	RT	19	5.7	± 0.4	3.7–7.7
Longitudinal	–65	4	2.5	± 1.7	0.0–5.9
	0	3	5.0	± 2.0	1.6–8.4
	115	4	7.5	± 1.7	4.1–10.9
	165	4	16.8	± 1.7	13.4–20.2
			Reduction in area		
			%	%	%
Transverse	RT	8	9.8	± 3.0	1.4–18.2
Longitudinal	RT	18	7.7	± 1.4	1.9–13.5
Longitudinal	–65	4	3.8	± 3.1	0.0–9.9
	0	3	2.4	± 1.9	0.0–5.6
	115	4	8.6	± 3.3	1.9–15.3
	165	4	15.6	±10.6	0.0–36.8

Compressive Properties

Specimen direction	Number of measurements	Average yield strength, psi	Limit of error of average, psi	Limits within which approximately 95% of the measurements would be included, psi
Transverse	11	33,795	±3,232	23,065–44,525
Longitudinal	11	36,473	±2,747	27,353–45,593

Charpy Impact Properties

Test direction	Temperature, °F	Number of of measurements	Average Charpy value, ft-lb	Limit of error of average, ft-lb	Limits within which approximately 95% of the measurements would be included, ft-lb
Transverse	RT	11	17.6	±2.9	7.6–27.6
Longitudinal					
Casting 2	RT	2	21.8	±2.0	19.0–24.6
Castings 1, 3, and 4	RT	7	17.6	±1.1	14.6–20.6
Longitudinal	–65	3	10.6	±3.1	5.3–15.9
	0	2	11.9	±3.8	6.6–17.2
	115	1	21.2	±5.3	15.9–26.5
	165	3	24.2	±3.1	18.9–29.5

Poisson's Ratio

Casting number	Number of measurements	Average Poisson's ratio, %	Limit of error of average, %	Limits within which approximately 95% of the measurements would be included, %
1 and 4	10	0.18	±0.02	0.11–0.25
2 and 3	8	0.27	±0.03	0.20–0.34

Table I-1 (Continued)

Specimen direction	Number of measurements	Average expansion, 10^{-6}/°F	Limit of error of average, 10^{-6}/°F	Limits within which approximately 95% of measurements would be included, 10^{-6}/°F
Coefficient of Thermal Expansion				
		−65 to 75°F		
Transverse	10	8.1	±0.3	7.0–9.2
Longitudinal	8	8.4	±0.3	7.6–9.2
		75 to 165°F		
Transverse	10	8.0	±0.5	6.5–9.3
Longitudinal	8	8.5	±0.3	7.7–9.3

Number of measurements	Average density, g/cm³	Limit of error of average, %	Limits within which 95% of measurements would be included, g/cm³
Density			
22	18,762	±0.008	18.72–18.80

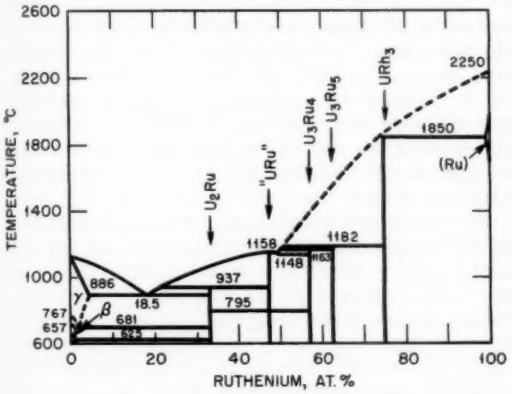

Fig. I-1 The U–Ru system.[8a]

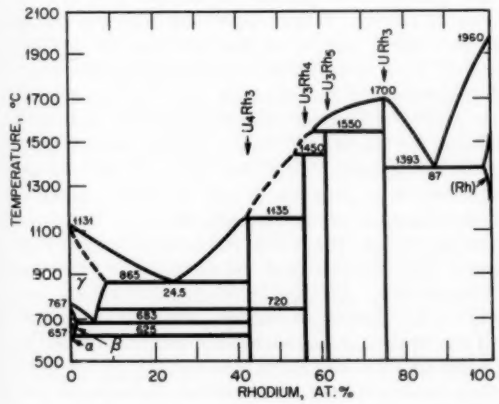

Fig. I-2 The U–Rh System.[8b]

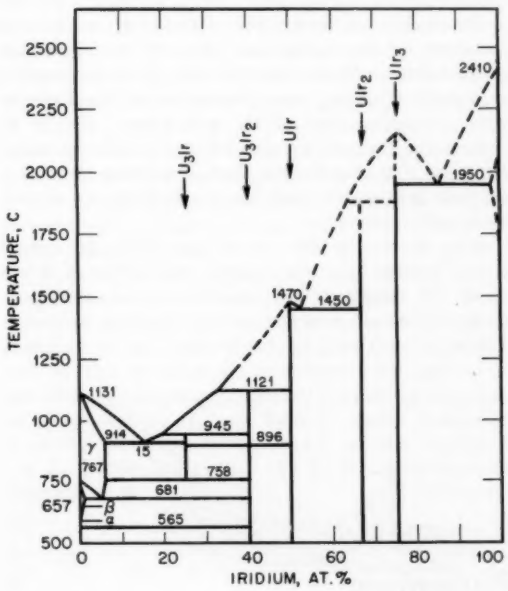

Fig. I-3 The U–Ir system.[8c]

Table I-2 TENSILE PROPERTIES* OF AS-CAST U–8 WT.% Mo (REF. 11)

Test temp., °F	Tensile strength, 1000 psi	Elongation, %	Comments
RT	133.8	3.3	Material tests in the as-cast condition, metastable γ structure
200	104.1	2.7	
400	78.1	2.7	
600	70.9	12.0	
800	65.8	5.3	
1000	56.3	10.7	
1200	24.8	36.7	
1400	16.9	25.3	
RT	109.4	Nil	Material tested in the as-cast-and-aged condition, γ + α specimens aged at 900°F for 114 hr
200	137.5	0.6	
400	135.0	0.6	
600	121.5	0.6	
800	117.7	Nil	
1000	63.9	Nil	

*Strain rate for all tests was 0.05 min^{-1}. Elevated-temperature tests were conducted in flowing argon.

Low-Uranium Alloys

Phase relations in aluminum-rich alloys of the Al–Sm–U and Al–Dy–U systems[12,13] have been determined. No ternary intermetallic compounds were found in the Al–Sm–U system. The pseudobinary system $SmAl_2$–UAl_2 was found to exist, and an orthorhombic $(U,Sm)Al_4$ intermetallic compound was found to be in equilibrium with the aluminum-rich solid solution. In the Al–Dy–U system, the ternary compound $U_2Dy_3Al_{15}$ was identified and the pseudobinary system $DyAl_2$–UAl_2 was found. The U–Al compounds UAl_4, UAl_3, and UAl_2 all exhibited solubility for dysprosium. The fabrication characteristics of these ternary alloys in the region of Al–24 wt.% U were also examined.

Other work has been performed by the Germans[14] on the system Al–UAl_2–$ZrAl_2$. The system is dominated by extended heterogeneous phase equilibria involving the intermetallic phase UAl_3 in most cases. Although UAl_3 is able to dissolve up to 16.9 at.% zirconium, the solubility of zirconium in UAl_4 is very low. The process of the reaction implies an extended two-phase range marked by UAl_3 inclusions in an aluminum matrix, a fact that could make the use of aluminum-rich Al–U–Zr alloys interesting as reactor fuel. (M. S. Farkas)

Plutonium

The solubility of plutonium in iron was studied by the French[15] using diffusion couples of iron against Fe–4 wt.% Pu; these were evaluated by X-ray microanalysis techniques. The results showed that between 850 and 880°C the solubility of plutonium in iron is less than 0.1 wt.%, and above the eutectic at 1165°C the diffusion produced in the presence of a liquid phase is very rapid. Below the eutectic, only intergranular diffusion occurs, which results in the formation of three zones:

1. A zone of pure iron where plutonium diffuses only in the grain boundaries.
2. A single-phase zone wherein the plutonium concentration corresponds to the saturation concentration of plutonium in iron.
3. A biphase zone.

Of particular interest because of their simplicity were the techniques used in India to produce a high-efficiency Pu–Be alloy neutron source.[16] The source was prepared by mixing 18.75 g of –200-mesh PuO_2 and 18.28 g of –200-mesh beryllium until there was no measurable increase in neutron output. The mixture was then compacted into two pellets and sintered in argon at 1265°C. During sintering, the mixture alloyed to yield a source with over 90% efficiency.

Alloys of Al–Pu are being utilized at Battelle–Northwest in two programs: the Phoenix program[17] and High Exposure Plutonium Studies.[18] The former concerned the utilization of plutonium-fueled systems for extra long reactivity lifetime. Computer studies have been made which show that ^{240}Pu has the potential to be employed as a convertible poison. Initially, the plutonium would act as a poison but would be converted to the fissionable ^{241}Pu isotope. This type of poisoning is contemplated for use in fuel of the Materials Testing Reactor (MTR) type.

The high-exposure plutonium studies concern the neutron and gamma dose rates that will be present when handling chemically separated plutonium that has been irradiated to the exposures now recommended for power reactors. Fuel plates of Al–20 wt.% Pu were fabricated from high-exposure plutonium. Each plate (0.040 × 2.5 × 23 in., with 0.020-in. aluminum cladding) emitted about 1200 neutron counts/min at a distance 1.7 ft from the source. Stacking the plates increased the dose rate linearly with the number of plates. Dose-rate attenuations by lead-loaded gloves were on the order of 32 to 37% for 50-mil thickness. Other data confirmed the thesis that the major portion of the dose rate from high-exposure PuO_2 is due to the low-energy gamma rays.

A summary of fuel-element development for the Zero Power Plutonium Reactor (ZPPR) has been published by Argonne.[19] This comprehensive report covers all phases of the development through the production of a pilot lot of fuel elements. Included are descriptions of the equipment used, the techniques employed, and a cost analysis of the process. Since it was required that the elements be practical to manufacture, all the techniques developed are amenable to quantity production. The development of a casting technique, mold designs that permit multiple castings, the simplified can design, and the can-loading technique are all intended to increase the output of a given facility. It is estimated that the cost for the 15,547 elements for the ZPPR fabricated

by a commercial vendor will be in excess of $10 million.

Argonne is continuing their studies of U–Pu–Zr alloys.[20,21a,22] Density measurements of annular sections of fuels after irradiation in the Experimental Breeder Reactor No. 2 (EBR-II) to burnups of 4.6 at.% show that the least-dense fuel is consistently in the middle zone and the most-dense fuel is in the center zone. Chemical analyses for technetium in this fuel and a similar fuel irradiated to 3.9 at.% burnup show that the less-dense middle zone contains appreciably less technetium than either the center or the outer zone. Apparently the technetium has migrated to either or both of the other two zones.

Delta-stabilized plutonium alloys continue to be of interest in both the United Kingdom and the United States. In the United Kingdom the effect of cold treatment at 80°C upon the alpha-phase precipitation in a Pu–3 at.% Ga alloy has been investigated.[23] The alloy was cast to produce a cored delta-phase structure, and the subsequent cold treatment transformed the gallium-deficient regions to the alpha phase. The precipitation of the alpha phase produced a strengthening of the delta phase to a degree dependent upon the dispersion of the solute phase.

Ductile behavior of a Pu–1 wt.% Ga alloy has been observed at Dow Chemical.[24] The yield and tensile strengths decreased 30% as the temperature was increased from −60 to 77°C and uniform elongation was decreased 20%. No significant effect on yield or tensile strength was noted with an increase in strain rate. (N. E. Daniel)

Plutonium Compounds

The thermal diffusivity of UC, $(U_{0.8}Pu_{0.2})C$, and PuC from 500 to 1500°C has been determined by Argonne investigators using the flash technique with a lead sulfide detector.[21b] The specimen characteristics are reported in Table I-3 and the test results plotted in Fig. I-4. Differences in the thermal diffusivity of the three compounds evaluated decrease as the temperature is increased. At 1300°C the diffusivity value for PuC is approximately equal to that for the mixed carbide, $(U_{0.8}Pu_{0.2})C$. Since reliable heat-capacity values are not available for carbides containing appreciable oxygen and nitrogen, calculations of the thermal conductivity were not attempted.

Table I-3 CARBIDE FUEL SPECIMEN CHARACTERISTICS[21]

Material	UC, arc-cast	UC sintered (1800°C)	$(U_{0.8}Pu_{0.2})C$, sintered (1800°C)	PuC, sintered (1400°C)
Density, % of theoretical	99.0	78.8	74.8	83.8
Carbon, wt.%	4.93	4.69	4.66	4.12
Oxygen, wt.%	0.0117	0.106	0.202	0.567
Nigrogen, wt.%	0.0021	0.0228	0.0206	0.0440
Equivalent carbon, wt.%	4.94	4.79	4.83	4.58
Equivalent carbon, at.%*	50.8	49.9	50.2	48.9

*Equivalent carbon: wt.% = wt.% carbon + 12 to 16 wt.% oxygen + 12 to 14 wt.% nitrogen.

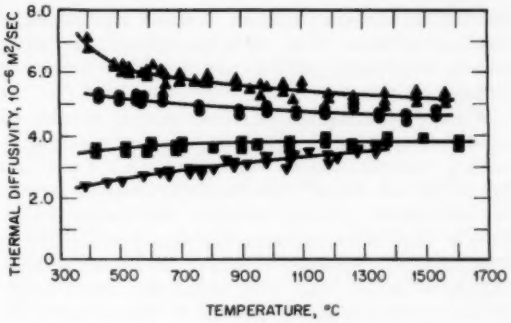

Fig. I-4 Thermal diffusivity of uranium and plutonium monocarbides.[21b] ▲, arc-cast UC; ●, 79% dense UC; ■, 75% dense $(U_{0.8}Pu_{0.2})C$; ▼, 84% dense PuC.

The phase behavior and thermodynamic properties of the Pu–N binary system were reviewed in an Oak Ridge literature report[25] which tabulates and analyzes data from 27 sources.

An effort to prepare standards for the alpha autoradiographic evaluation of mixed $(U,Pu)O_2$ fuel homogeneity is under way at Nuclear Materials and Equipment Corporation.[26] Plutonia microspheres from 5 to 350 μ in diameter are blended in amounts varying from 0 to 30 wt.% with coprecipitated $(U,Pu)O_2$. Plutonia microspheres 10 μ in diameter can be clearly defined by alpha autoradiography. Work is in progress to improve resolution so that 5-μ-diameter PuO_2 microspheres can be defined by autoradiography.

General Electric investigators[27] have measured the thermal conductivity of mixed $(U,Pu)O_2$ of varying stoichiometry using a modified radial-heat-flow technique. The conductivity of $UO_{1.97}$ to $UO_{2.01}$ and $(U_{0.8}Pu_{0.2})O_{1.98}$ to $(U_{0.8}Pu_{0.2})O_{2.25}$ was studied in the temperature range 800 to 1900°C. Figure I-5 shows the data obtained for the three mixed-oxide stoichiometries. Between 1000 and 1900°C, UO_2 of 95%

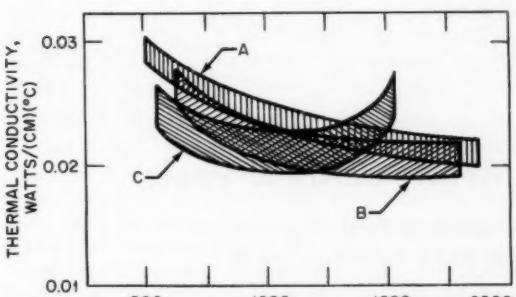

Fig. I-5 Thermal conductivity[27] of $(Pu–U)O_2$. A, $(Pu–U)O_{2.00}$; B, $(Pu–U)O_{1.98}$; C, $(Pu–U)O_{2.05}$ (possible microcracks in pellet).

theoretical density exhibits thermal conductivities similar to those of the stoichiometric mixed oxide (curve A). Below 1000°C the thermal conductivity of UO_2 is higher.

Alpha autoradiography of mixed-oxide microspheres prepared by Babcock & Wilcox investigators by contacting UO_2-gel spheres with hexavalent and trivalent plutonium has shown[28] that the Pu(VI) resides largely on the sphere surface, whereas the Pu(III) is uniformly distributed through the sphere after firing. The rate of plutonium pickup with Pu(III) is substantially lower than that observed with Pu(VI). However, the oxidation damage to the gel is more severe with Pu(VI). (D. F. Askey)

Thorium

A collection of scientific papers presented at the Second International Thorium Fuel Cycle Symposium in May 1966 has been released in book form by the AEC.[29] The papers reflect the widespread interest in this cycle, and its ability to produce economically competitive power is viewed optimistically. Of particular interest to reactor-materials specialists are the sections on fuel preparation and irradiation testing (seven papers) and fuel fabrication (seven papers), with emphasis on coated particles containing thorium oxide or carbide.

Workers at Los Alamos have found the Th–ThP eutectic to be at 1608 ± 20°C and at a P/Th ratio of 0.11 ± 0.02.[30] The phase transition between saturated face-centered cubic and body-centered cubic thorium occurs at 1360°C. The ThP phase is stable over a range of compositions with a minimum P/Th ratio of 0.98. The ThP phase melts congruently with the P/Th ratio of 0.99 ± 0.02 at 2990°C.

The Pu–Th phase diagram has been investigated by French workers with metallographic, dilatometric, thermal analytical, and X-ray techniques.[31] A peritectic transformation was found at 596 ± 6°C, liquid (Th, Pu) + β (Th, Pu) $\rightleftharpoons \zeta$. The compound ζ is defined as Pu_7Th_3 with a density of 15.5 g/cm^3. A eutectoid transformation was found at 582 ± 5°C, β (Th–Pu) $\rightleftharpoons$ α (Th–Pu) + ζ, at a plutonium content of 49 ± 3 at.%. (R. L. Martin)

Metal–Ceramic Fuels

Dispersion Fuels (Less Than 50 Vol.% Ceramic Phase)

An investigation by Idaho Nuclear[32] has shown that dispersion-type aluminum-clad fuel plates containing UAl_3 powders as the fuel phase are advantageous for high-flux, high-power-density nuclear reactors. The use of powder-metallurgy techniques in the fabrication of fuel elements containing UAl_3 for the Engineering Test Reactor (ETR) has increased the fuel-element life 50%. Previously it was difficult to fabricate fuels with uniformly dispersed aluminides and a burnable poison by the conventional procedures when the uranium content exceeded 25%. The uranium aluminide powders were prepared by arc melting and crushing, and the fuel cores were fabricated by standard powder-metallurgy techniques, adding boron or B_4C as a burnable poison to the dispersion blend. The plates were then roll clad with 1100 or 6061 aluminum alloy at 600 and 500°C, respectively.

Studies are in progress at Idaho Nuclear[33] to minimize the fuel-core thickness variation in dispersion-type, powder-metallurgy fuel plates. One process that shows promise is prerolling the compacted powder core to an intermediate thickness and trimming to size before assembling into the picture frame for final roll bonding. This prerolling and trimming approach would enable the Advanced Test Reactor (ATR) elements to be made from one die rather than the 19 die sizes presently required. Although thickening at the core ends is still prevalent, the economic advantage of reducing the die requirements has encouraged continued development of the process. (D. E. Lozier)

Cermet Fuels (Over 50 Vol.% Ceramic Phase)

Factors and mechanisms controlling the growth of cermets during thermal cycling have been investigated by Battelle–Columbus.[34] The first mechanism is described as "growth during cooling" in which the higher contracting dispersed fuel particles crack or separate from the matrix upon cooling. The second mechanism is described as "fuel-particle ratcheting" in which cracked and/or separated particles continually realign during cycling. Cracks and separations that do not close during heating result in an increase in the "at temperature volume" of each particle site. Failure modes identified were fuel-particle cracking, fuel-matrix separation, and matrix failure. Data are presented which show that the effect of selected geometric variables (fuel-particle size, shape, and loading) on the magnitude of thermal-cycling growth will be reversed with continual thermal cycling. This reversal is related to a change in the growth mechanism or failure mode. Factors shown to be most effective in reducing growth are: (1) small fuel-particle size, (2) low fuel-matrix thermal-expansion differential, (3) high matrix ductility, and (4) increased holding time at the upper thermal-cycling temperature. (R. A. Smith)

Coated-Particle Fuels

Oak Ridge[35] has successfully operated a 5-in.-diameter fluidized-bed coater for the application of

pyrolytic carbon (PyC) coatings on nuclear fuel particles. The unit is remotely controlled and capable of coating 10 kg of nuclear fuel particles per day. The development of the coating unit is considered to be an important step toward installation of a fueled-graphite fabrication line in the Thorium Uranium Recycle Facility (TURF). The purposes of TURF is to recycle ^{233}U-bearing fuels for the High Temperature Gas Cooled Reactor (HTGR). Although the major emphasis is shifting from coating development toward identification of simple procedures for bonding particles into fuel sticks,[35,36] some coating studies are still active. These include the deposition of PyC on PuO_2 particles and the deposition of SiC barriers within PyC coatings. Procedures and facilities have been established for the preparation of PuO_2 microspheres, and PyC coatings have been applied on PuO_2 in coating equipment housed in glove boxes. The economic feasibility of incorporating an SiC barrier within PyC coatings to retain the solid fission products barium and strontium is being investigated for use in the TURF fabrication line. Since the deposition of SiC has been studied elsewhere,[37,38] the work is limited to investigations of interest for possible TURF production application. Information obtained thus far indicates that the process is attractive for large-scale production. (Neil D. Veigel)

Uranium and Thorium Oxides

Behavior and Properties of Uranium and Thorium Oxides

Furuya and Yajima[39] have measured both lattice and grain-boundary diffusion of ^{233}Pa in sintered ThO_2 and a ThO_2–50 at.% UO_2 solid solution in the temperature range 1800 to 2000°C. The lattice diffusion coefficients are:

$$D_{ThO_2} = 2.91 \times 10^{-5} \exp(-75{,}400/RT) \text{ cm}^2/\text{sec}$$

and

$$D_{ThO_2-UO_2} = 1.88 \times 10^{-3} \exp(-91{,}800/RT) \text{ cm}^2/\text{sec}$$

The grain-boundary diffusion coefficients are:

$$2a\,D'_{ThO_2} = 6.66 \times 10^{-11} \exp(-30{,}600/RT) \text{ cm}^3/\text{sec}$$

and

$$2a\,D'_{ThO_2-UO_2} = 5.64 \times 10^{-3} \exp(-59{,}700/RT) \text{ cm}^3/\text{sec}$$

where D' and $2a$ are the grain-boundary diffusion coefficient and the grain-boundary width, respectively. Reynolds[40] studied the decay of surface scratches on UO_2 in the temperature range 1450 to 1700°C. This process was found to be controlled by a surface diffusion process, with the surface diffusion coefficient given by the reaction $D = 5.6 \times 10^6 \exp(-119{,}000/RT)$ cm^3/sec. (R. H. Barnes)

Preparation of Fuel Bodies

A patent has been issued on the fabrication of thoria fuel rods.[41] Powdered ThO_2 is admixed with a weak solution of HNO_3 to form a weak flocculated dispersion, which is concentrated to provide a sol that has a plastic claylike consistency. The sol can then be extruded into the desired configuration, dried, and sintered. Presintered and/or calcined powders can be added to the sol before extrusion to reduce shrinkage, eliminate cracking, improve dimensional control, and control the density of the final product.

W. R. Grace investigators have been issued a British patent[42] on the preparation of ThO_2–UO_2 aquasols. Preparation of the sols involves removal of the chloride ion from a $ThCl_4$–UCl_4 solution with an anion-exchange resin, filtering, and autoclaving the deionized filtrate.

Protsenko[43] described a method for obtaining U_3O_8 films by an internal electrolysis technique. A solution of uranium nitrate with glycerin as the complex-forming medium was employed as the electrolyte. The cathode was a platinum disk, and the anode was a zinc rod. Electrolysis occurred at a solution temperature of 70 to 80°C. The final product was obtained by roasting at 800°C. Among the advantages claimed for this process over the usual electrolytic precipitation process was greater uniformity and density of the film layer. (T. R. Wright)

Carbide and Nitride Fuels

A phase field of U(C, N, O) plus graphite is found at C:N atom ratios of 1:1 and 1:3 at 1700°C in the U–C–N–O system; but extended heat-treatments at a C:N atom ratio of 3:1 produced U(C, N, O) plus UC_2 plus graphite at low oxygen contents.[44] These results are qualitatively in agreement with other studies which have defined the equilibrium pressures of nitrogen over mixtures of U(C, N), UC_2, and graphite as a function of temperature.[45] The equilibrium nitrogen pressures (atmospheres) over such mixtures at temperatures near 2100°K are given by the expression: $\log p = -25{,}860/T + 12.26$. The general form of the U–C–N phase diagram suggested by these studies is shown in Fig. I-6.

At 1000°C the three-phase field known to exist between uranium, thorium, and (Th, U)C was reexamined.[46] The (Th, U)C in this field was found to contain 52.8 at.% thorium, 41.6 at.% carbon, and 5.5 at.% uranium. The thorium was found to contain 96.6 at.% thorium, 2.7 at.% uranium, and 0.7 at.% carbon. The uranium phase was believed to be at least 99% pure.

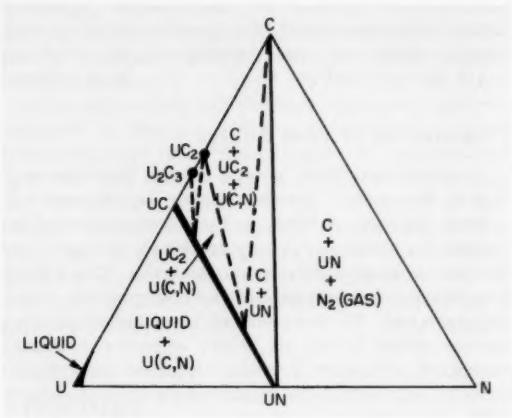

Fig. I-6 General phase diagram of U—C—N system[44] at 1500 to 1800°C and 1 atm.

The UN—ThN system was found to consist of a complete series of solid solutions with lattice parameters as listed in Fig. I-7. It was estimated that the three-phase field of uranium, thorium, and (Th, U)N contains (Th, U)N of the composition 50.5 at.% thorium, 46.5 at.% nitrogen, and 3.0 at.% uranium. The free energy of formation of ThN at 1000°C was estimated to be −51,900 cal/gram mole.

Some properties of refractory fuels have been determined[47] as follows: the solidus and liquidus of $(U_{0.81}Pu_{0.19})C_{0.99}$ are 2300°C and 2485°C, respectively. The lattice parameter of Pu_2C_3 shows an expansion with time by self-irradiation damage; at zero expansion the parameter is estimated to be 8.13 A for a bcc structure and 40 atoms/unit cell. The free energy of formation of PuN near 1000°K is given by the expression $\Delta G_f^\circ = -72.1 + 0.0219T$ kcal/gram mole. Thus PuN, like UN, is slightly less stable than ThN.

The thermal conductivity of UC is decreased[48] by the addition of oxygen to form U(C, O). At 1500°C the thermal conductivity of UC is 0.23 watt/(cm)(°C), whereas the conductivity of $U_{0.495}(C_{0.33}O_{0.17})$ is 0.16 watt/(cm)(°C).

A study of the rate of diffusion of iodine in UC (4.6 wt.% carbon) produced diffusion coefficients between 4×10^{-14} and 2×10^{-12} cm²/sec at temperatures[49] from 1500 to 1800°C. Since these coefficients are less than 1% of the coefficients for self-diffusion of uranium in UC, iodine is evidently being retained in UC in much the same way as the inert fission gases are retained at these temperatures.

Density changes of 1.6 to 2.0% were observed[50] after an irradiation of UC to approximately 8000 Mwd/metric ton of uranium at a peak cladding temperature of 450°C and a peak fuel temperature of 1100°C. These results are in good agreement with those obtained previously on cast, stoichiometric, and hyperstoichiometric UC. Gas release was negligible, and no defects were observed in the sintered aluminum powder (SAP) cladding. Interaction between the fuel and cladding was confined to a discontinuous layer about 0.001 in. thick.

After 1000 hr at 800°C, a 21-μ-thick, nickel-rich zone was observed in UP in contact with 304 stainless steel; and a 55-μ-thick, nickel-rich zone was observed in UP in contact with Hastelloy X.[22b] (W. Chubb)

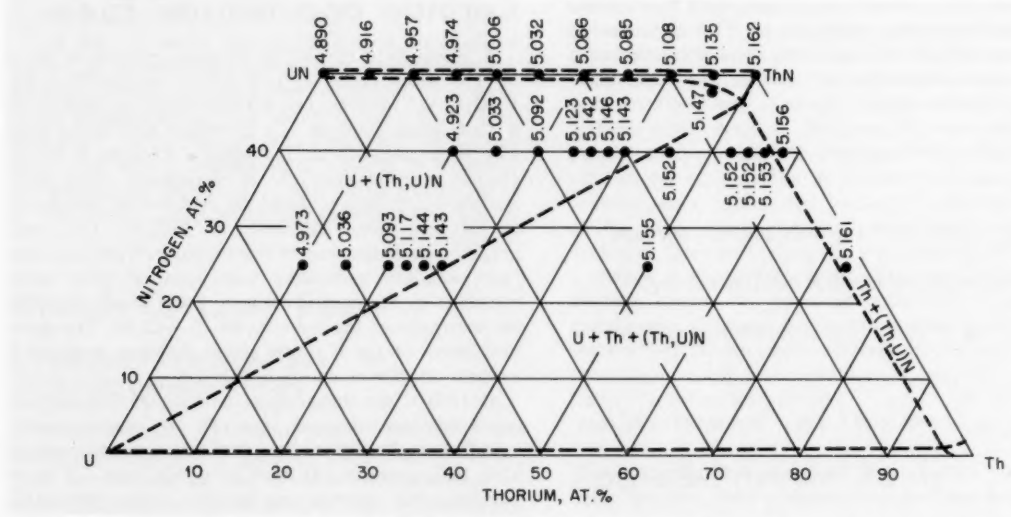

Fig. I-7 The equilibrium 1000°C partial isotherm of the Th—U—N system, which shows alloys examined and the lattice parameter of their (Th, U)N phase.[46]

Basic Studies of Irradiation Effects in Fuel Materials

Metals

The homogeneous nucleation of gas bubbles in metals occurs when the concentration of gas dissolved in the metal considerably exceeds the equilibrium concentration. A theoretical analysis of this phenomenon has been presented by Semenov[51] in which the nucleation process was considered as a phase transition and gaseous pores served as nuclei of the new phase. These pores constituted a "two-constituent alloy" of chaotically distributed gas atoms and vacancies. It was assumed that the evolution of the gas pores in time was described by the Becker–Döring mechanism.[52] Approximate mathematical solutions were obtained for the nucleation problem.

The influence of irradiation on the nucleation of gas bubbles in reactor fuels has been investigated at Harwell.[53] The atomic collision events resulting from the inherent fission-fragment irradiation of nuclear fuels can create a kinetic solubility of inert-gas atoms, thus affecting the stability of bubble nuclei. Calculations suggest that the formation and growth of gas bubbles will depend critically upon the operating temperature, the rating, and the gas-atom concentration. However, it was shown that, for technologically important gas concentrations, bubbles can nucleate homogeneously throughout the grains.

It has been suggested that the swelling of nuclear fuels might be reduced if the fission-gas bubbles are kept small and finely dispersed. One potential means for achieving this condition is to provide a dispersion of second-phase particles that act as traps for migrating bubbles. Ruedl[54] has conducted an experimental study of the trapping of bubbles by alumina particles in alpha-bombarded Al–Al_2O_3 alloys. The specimens, in the form of prethinned foils, were bombarded at room temperature and were subsequently examined by transmission electron microscopy. The foils were then annealed in vacuum at various temperatures. Effects of dislocations on bubbles were observed, and it was also noted that in areas of narrow interparticle spacing the bubbles were efficiently trapped by Al_2O_3 particles.

Studies are being conducted at Battelle–Northwest[55] to determine the effect of hydrostatic pressure on (1) fission-gas swelling in irradiated uranium, (2) the healing of irradiation-produced microtears in uranium, and (3) diffusion of fission gases in uranium and Zircaloy-2 cladding. The reversibility of volume changes due to microtearing and swelling has been demonstrated.

The results of some experiments on the emission time of nuclear reaction products driven into heated plates have been reported by Tarantin et al.[56] Diffusion coefficients for various substances in the plate material were determined, and the values appear to be consistent with those expected under the given experimental conditions.

Ceramics

A theoretical analysis of the formation and behavior of fission-gas bubbles in a nonuniform temperature environment has been developed at Harwell.[57] A homogeneous-nucleation model was used to describe the formation of gas-atom clusters during irradiation. The scale of nucleation was shown to be a function of temperature, so that the distribution of nuclei in a temperature gradient is nonuniform. The stresses that develop as nuclei grow to form gas bubbles were considered in addition to the forces acting on bubbles due to temperature and stress gradients. It was concluded that during irradiation, when supersaturation of vacancies is large, the energy gained by the matrix from the vacancies absorbed into bubbles provides the dominant driving force for bubble growth. The theory developed in this work was applied to a uranium carbide pellet operating under a specific set of conditions typical of those existing in a fast reactor environment.

The FIGRO computer program, developed at Westinghouse, permits calculations of internal temperatures and fuel volume swelling in bulk-oxide cylindrical fuel elements. The addition of a model of interfacial heat transfer, which includes conduction through a physical gap, has been described.[58] The size of the gap is determined by differential thermal expansion of the fuel and cladding and by fuel swelling. In addition, the thermal conductivity of the cladding is computed as a function of temperature, and that of the fuel–cladding gap is computed as a function of temperature and gas composition.

The release of krypton contained in a thin UC layer has been studied by Euratom.[59] Samples of UC, in powder form and of different grain sizes, were irradiated in an atmosphere consisting of a Kr–^{85}Kr mixture in a thermal-neutron flux at about 300°C. For integrated neutron fluxes of 4×10^{17} to 7×10^{18} neutrons/cm^2, about 10^{13} atoms of krypton were found in the UC per square centimeter of specimen surface and atmosphere of pressure (at ambient temperature). During heat-treatment, most of the gas was released below 430°C, the release curve indicating an activation energy of 10 to 20 kcal/mole. For temperatures between 430 and 1000°C, the release rate appeared to be independent of temperature. Above 1000°C the temperature dependence was characterized by an activation energy of 62 to 85 kcal/mole.

The effects of radiation damage and gas concentration on rare-gas diffusion in solids can also be investigated using nonfissionable solids. For example, at the North Carolina State University,[60] single crystals of CsI were doped with ^{133}Xe and the gas release was observed during heating. Deviations from

classical diffusion were observed which could be attributed to trapping processes occurring within the crystal. Clear single crystals of CsI containing a homogeneous dispersion of ^{133}Xe exhibited classical diffusion, whereas cloudy crystals gave a decreasing diffusion coefficient with time, which is consistent with trapping of gas atoms at naturally occurring defects. Diffusion was also classical for xenon which was recoiled into specimens from an external fissionable source, indicating that no enhanced diffusion along the fission-recoil track occurred. Radiation-damage effects were observed in crystals exposed to higher fission-recoil concentrations. Radiation exposure lowered the diffusion coefficient at low temperatures, and annealing of the damage at higher temperatures was reflected in a diffusion coefficient which increased with time. Radiation thus produced trapping of gas atoms in the lattice rather than enhanced diffusion. Release of xenon from uranium-doped crystals gave a rapid release (burst) of gas during initial heating, which was much more rapid than classical diffusion. This was followed by classical diffusion at longer heating times. The experimental results were more consistent with an interstitial model for xenon diffusion than with a vacancy model.

The possibility of locating fuel failures by fission-product deposition has been investigated at Chalk River.[61] Of particular interest was the observation that the release of ^{99}Mo and ^{132}Te occurred in bursts during fuel and power changes, either when the reactor was starting up or shutting down. During the long period of steady operation at high power, release rates were negligible.

Ferrari and Segre[62] determined the emission of uranium from uranium oxide under irradiation. The emitted material was examined by alpha-counting thin aluminum foils, which acted as catchers during irradiation, and by electron microscopy. A tentative phenomenological interpretation was given.

X-ray studies of the radiation damage in BeO-base dispersion fuels have been conducted by Walker and Hickman.[63] It was found that the matrix damage differed in two ways from that occurring in a fast-neutron flux. First, in regions traversed by recoiling fission fragments, the anisotropic lattice growth was much less than that predicted from the fast-neutron fluence, although the X-ray line broadening was increased. Second, beyond this recoil range the passage of beta particles arising from fission-product decay caused the anisotropic lattice growth to be greater than that produced by the neutron fluence alone. These observations were supported by the results of simulated experiments in which the effects of fission-fragment and beta-particle bombardment, in addition to neutron irradiation, were compared more directly with those of neutron irradiation alone. It was also observed that the fission-fragment bombardment produced a large macroscopic growth in BeO.

The effect of porosity on the thermal conductivity of UO_2 has been studied by MacEwan et al.[64] It was found, for example, that irradiation-induced reductions in thermal conductivity appear to be independent of pore volume fraction. The discrepancy between experimental results and theoretical expressions was attributed to probable deficiencies in the theory rather than to the effect of some other imperfection which varied in the same manner as fuel porosity.

A parameter of great importance in studies of migration of fission-gas bubbles in nuclear fuels is the surface diffusion coefficient of the fuel. The surface diffusion coefficient for UO_2 has been measured by Reynolds[65] through interferometric studies of the decay of surface scratches within the temperature range 1450 to 1700°C. The measured coefficient is given by

$$D_s = D_0 \exp\left(-\frac{Q}{RT}\right)$$

with

$$D_0 = (5.6 \pm 2.4) \times 10^6 \text{ cm}^2/\text{sec}$$

$$Q = 119{,}000 \pm 15{,}000 \text{ kcal/mole}$$

Three sessions on the topic "Gas Bubbles in Solids" were held at the 97th AIME Annual Meeting in New York City during February 1968. The abstracts of the papers presented at these sessions have been published in the *Journal of Metals*.[66]

(A. J. Markworth)

References

1. F. de Keroulas, Diffusion of Extremely Dilute Concentrations of Uranium in β-Titanium and γ-Iron, French Report CEA-R-3253, July 1967.
2. D. J. Legacy and W. J. Yaggi, Determination of Selected Mechanical and Physical Properties of Cast Very-High-Assay Uranium, USAEC Report Y-1593, Union Carbide Corp., Y-12 Plant, Jan. 29, 1968.
3. D. Taplin and G. Cocks, A Note on Creep-Rupture Mechanisms in Reactor Grade Uranium, *J. Nucl. Mater.*, 23: 245-248 (1967).
4. P. Grenier, Study of Elementary Mechanisms of Creep Deformation in Uranium as a Function of Temperature (150 to 760°C) by Activation Energy Measurements, French Report CEA-R-3187, November 1967.
5. T. Oki and J. Tanikawa, Preparation of Uranium by Means of Reduction of UO_2 by Calcium Vapor (in Japanese), *Nippon Kinzoku Gakkaishi*, 31: 1048-1052 (1967).
6. F. Jean-Louis, J. S. Daniel, and P. Lacombe, Work-Hardening Characteristics of Polycrystalline α-Uranium in the Temperature Range 20 to 640°C, *J. Inst. Metals*, 95: 314-315 (October 1967).
7. F. Jean-Louis, J. S. Daniel, and P. Lacombe, Study of the Plastic Consolidation of Polycrystalline Uranium During Tensile Tests Carried Out in α Phase at Different Rates (in French), *Mem. Sci. Rev. Met.*, 64: 593-603 (June 1967).
8. Reactions of Uranium with the Platinide Elements,

J. Res. Nat. Bur. Stand., A, 72A(1) (January–February 1968).
a. J. J. Park, I. The Uranium–Ruthenium System, pp. 1-10.
b. J. J. Park, II. The Uranium–Rhodium System, pp. 11-19.
c. J. J. Park and L. R. Mullen, III. The Uranium–Iridium System, pp. 19-25.
9. A. Bar-Or and G. Kimmel, Nucleation and Growth of Martensite in Some Uranium–Chromium Alloys, *Trans. Met. Soc. AIME,* 239: 1615-1619 (October 1967).
10. F. Giraud-Herand, J. Guillaumin, and R. Sifferlen, Mechanisms de Transformation des Alliages U–Mo 1.5% par Refroidissement Rapide a Parter de la Phase γ, *J. Nucl. Mater.,* 25: 16-23 (1968).
11. S. Cerni, SNAP-23A, Phase 1. Quarterly Progress Report, September 1–November 30, 1967, USAEC Report WANL-3800-9, Westinghouse Electric Corp., Astronuclear Laboratories, Dec. 15, 1967.
12. F. Casteels, P. Diels, and A. Cools, An Investigation of the Aluminum-Rich Alloys in the Aluminum–Samarium–Uranium and Aluminum–Dysprosium–Uranium Ternary Systems: I. The Aluminum–Uranium–Samarium System, *J. Nucl. Mater.,* 24: 87-94 (1967).
13. F. Casteels, P. Diels, and A. Cools, An Investigation of the Aluminum-Rich Alloys in the Aluminum–Samarium–Uranium and Aluminum–Dysprosium–Uranium Ternary Systems: II. The Aluminum-Rich Alloys in the Aluminum–Dysprosium–Uranium Ternary System, *J. Nucl. Mater.,* 24: 95-100 (1967).
14. G. Petzow, H. E. Exner, and A. K. Chakroborty, Die Phasengleichgewichte in Aluminum–Uran–Zirkinium–Legierungen des Teilbereiches Aluminum–UAl_2–$ZrAl_2$ (in German), *J. Nucl. Mater.,* 25: 1-15 (1968).
15. G. Moreau and D. Calais, Solubility of Plutonium in Iron, *J. Nucl. Mater.,* 24: 121-124 (1967).
16. P. R. Roy, R. G. Deshpande, and T. S. Laxminarayanan, Preparation of a Plutonium–Beryllium Alloy Neutron Source, Indian Report BARC-294, 1967.
17. D. D. Lanning and G. J. Busselman (Eds.), Phoenix Fuel Program Progress Report, USAEC Report BNWL-635, Battelle–Northwest, November 1967.
18. Battelle–Northwest, unpublished, February 1968.
19. A. B. Shuck, H. F. Jelinek, A. G. Hins, N. J. Carson, Jr., A. A. Denst, and T. A. Steele, The Development of a Design and Fabrication Method for Plutonium-Bearing Zero-Power Reactor Fuel Elements, USAEC Report ANL-7313, Argonne National Laboratory, August 1967.
20. Argonne National Laboratory, Reactor Development Program Progress Report, December 1967, USAEC Report ANL-7403, pp. 3-8, Jan. 31, 1968.
21. Argonne National Laboratory, Reactor Development Program Progress Report, January 1968, USAEC Report ANL-7419, (*a*) p. 1, (*b*) pp. 107-110, Feb. 27, 1968.
22. Argonne National Laboratory, Reactor Development Program Progress Report, November 1967, USAEC Report ANL-7399, (*a*) pp. 1-5, (*b*) p. 8, Dec. 28, 1967.
23. R. A. Knight, B. R. Spicer, B. J. Ward, and J. S. White, Alpha-Phase Precipitation in Delta-Phase Plutonium, *J. Nucl. Mater.,* 24: 223-229 (July 31, 1967).
24. S. Beitscher, The Tensile Behavior of Pu–1 Wt.% Ga at −60, 30, and 77°C, *J. Nucl. Mater.,* 24: 113-117 (1967).
25. K. E. Spear and J. M. Leitnaker, Review and Analysis of Phase Behavior and Thermodynamic Properties of the Plutonium–Nitrogen System, USAEC Report ORNL-TM-2106, Oak Ridge National Laboratory, March 1968.
26. Nuclear Materials and Equipment Corp., Development and Testing of PuO_2–UO_2 Fast Reactor Fuels, 11th Quarterly Report, October–December 1967, USAEC Report NUMEC-3524-47, p. 4, January 1968.
27. F. J. Hetzler, T. E. Lannin, K. J. Perry, and E. L. Zebroski, The Thermal Conductivity of Uranium and Uranium–Plutonium Oxides, USAEC Report GEAP-4879, General Electric Company, Advanced Products Operation, August 1967.
28. E. H. Dewell (Comp.), Gel-Addition Process Chemical Studies. Quarterly Progress Report No. 5, July–October 1967, USAEC Report BAW-3714-5, pp. 32-33, The Babcock & Wilcox Co., February 1968.
29. R. G. Wymer (Coordinator), Thorium Fuel Cycle, Proceedings of Second International Symposium, Gatlinburg, Tennessee, May 3–6, 1966, USAEC Report CONF-660524, February 1968.
30. C. A. Javorsky and R. Benz, Phase Equilibria in the Thorium–Thorium Monophosphide System, *J. Nucl. Mater.,* 23: 192-198 (1967).
31. A. Y. Portnoff and D. Calais, Contribution A L'Etude du Systeme Plutonium–Thorium, *J. Nucl. Mater.,* 24: 158-163 (1967).
32. G. W. Gibson, The Development of Powdered Uranium–Aluminide Compounds for Use as Nuclear Reactor Fuels, USAEC Report IN-1133, Idaho Nuclear Corp., December 1967.
33. G. W. Gibson and M. J. Graber (Eds.), Annual Progress Report on Reactor Fuels and Materials Development for FY 1967, USAEC Report IN-1131, pp. 8-17, Idaho Nuclear Corp., February 1968.
34. R. A. Smith, E. O. Speidel, and D. E. Kizer, Factors Controlling the Growth of Cermets During Thermal Cycling, USAEC Report BMI-1824, Battelle Memorial Institute, Feb. 19, 1968.
35. J. H. Coobs and O. Sisman (Comps.), Coated Particle Fuels Development at Oak Ridge National Laboratory for Period January 15–October 15, 1967, USAEC Report ORNL-TM-2061, pp. 32-34, Oak Ridge National Laboratory, December 1967.
36. A. W. Savolainen (Comp. and Ed.), Gas-Cooled Reactor Program Semiannual Progress Report for Period Ending September 30, 1967, USAEC Report ORNL-4200, pp. 3-34, Oak Ridge National Laboratory, February 1968.
37. H. J. de Nordwall and J. B. Sayers, The Value of a Silicon Carbide Barrier in HTR Fuels, paper presented at the AIME Nuclear Metallurgy Symposium, Delevan, Wis., October 3–5, 1966.
38. H. S. Rosenburg, D. L. Morrison, C. W. Townley, and D. N. Sunderman, Postirradiation Fission-Product Release from Coated Fuel Particles, USAEC Report BMI-1734, Battelle Memorial Institute, July 7, 1965.
39. H. Furuya and S. Yajima, Lattice and Grain-Boundary Diffusions of Protactinium in ThO_2 and in a ThO_2–UO_2 Solid Solution, *J. Nucl. Mater.,* 25: 38-44 (1968).
40. G. L. Reynolds, The Surface Self-Diffusion of Uranium Dioxide, *J. Nucl. Mater.,* 24: 69-73 (1967).
41. A. B. Meservey, J. D. Sease, and R. B. Fitts, Method of Fabricating Ceramic Nuclear Fuel Product, U. S. Patent No. 3,356,776, to USAEC, Dec. 5, 1967.
42. F. T. Fitch and J. G. Smith, Process for the Preparation of Thorium Dioxide–Uranium Oxide Sols, British Patent No. 1,079,576, Aug. 16, 1967.
43. A. V. Protsenko, Production of Uranium-Compound Layers by Internal Electrolysis, *At. Energ. (USSR),* 23(1): 68-69 (January 1967).
44. H. G. Poole, Metallurgical Progress Report Number 37, October–December 1967, USAEC Report USBM-RC-1326, pp. 24-30, Bureau of Mines.
45. C. A. Alexander, private communication, Battelle Memorial Institute, Columbus Laboratories, May 1967.
46. J. T. Venard, Investigation of Certain Ternary Systems Containing Thorium and Uranium, USAEC Report ORNL-TM-2015, Oak Ridge National Laboratory, January 1968.
47. Los Alamos Scientific Laboratory, Quarterly Status Report on the Advanced Plutonium Fuels Program, October 1–December 31, 1967, USAEC Report LA-3880, p. 17-19, Feb. 20, 1968.
48. J. L. Bates, Thermal Conductivity of Uranium Oxycarbides, USAEC Report BNWL-SA-1494, Battelle–Northwest, Oct. 24, 1967.
49. A. W. Castleman, Jr., and H. R. Munkelwitz, Diffusion of Iodine in Uranium Monocarbide, USAEC Report

BNL-12212, Brookhaven National Laboratory, January 1968.
50. T. A. Golding and W. E. Krupp, Heavy Water Organic Cooled Reactor. Postirradiation Examination of the SAP–US Fuel Bundles of the NRU-305 Experiment, USAEC Report AI-CE-76, Atomics International and Combustion Engineering, Inc., Dec. 1, 1967.
51. L. P. Semenov, Theory of the Homogeneous Inception of Gas Pores in Metals, Soviet Report FEI-44, 1966.
52. R. Becker and W. Döring, Kinetische Behandlung der Keimbildung in Übersättigten Dämpfen, *Ann. Phys.*, 24: 719-752 (1935).
53. R. S. Nelson, The Influence of Irradiation on the Nucleation of Gas Bubbles in Reactor Fuels, *J. Nucl. Mater.*, 25: 227 (1968).
54. E. Ruedl, Evidence for Trapping of Bubbles by Alumina Particles in α-Bombarded Al–Al_2O_3 Alloys, *Mater. Res. Bull.*, 2(3): 369-374 (1967).
55. J. J. Cadwell, D. R. deHalas, R. E. Nightingale, and D. C. Worlton, Battelle–Northwest, unpublished, February 1968.
56. N. I. Tarantin, V. V. Gordeev, and A. V. Dem'yanov, Diffusion of Nuclear-Reaction Products in Various Materials, *At. Energ. (USSR)*, 22(4): 280-285 (April 1967).
57. B. L. Eyre and R. Bullough, The Formation and Behaviour of Fission Gas Bubbles in a Non-Uniform Temperature Environment, British Report AERE-R-5506, July 1967 (to be published in *J. Nucl. Mater.*).
58. L. A. Waldman, L. L. Lynn, and I. Goldberg, FIGRO (Addendum): A CDC-6600 Computer Program for the Analysis of Fuel Swelling and Calculation of Temperature in Bulk-Oxide Cylindrical Fuel Elements (LWBR-LSBR Development Program), USAEC Report WAPD-TM-618(Add. 1), Westinghouse Electric Corp., Bettis Atomic Power Laboratory, October 1967.
59. A. Schuerenkaemper and O. Gautsch, Release of Krypton Contained in a Thin Layer of Uranium Carbide, French Report EUR-3556f, September 1967.
60. T. S. Elleman, The Effect of Radiation and Gas Concentration on Rare Gas Diffusion in Solids, USAEC Report ORO-3508-3, North Carolina State University, Nov. 1, 1967.
61. J. J. Lipsett and J. F. Palmer, Locating Fuel Failures by Fission Product Deposition in CANDU–PHW Reactors, Canadian Report AECL-2786, November 1967.
62. S. Ferrari and G. J. Segre, Experiments on the Uranium Emission from Sintered Uranium Oxide Pellets, *J. Nucl. Mater.*, 24(2): 150-157 (November 1967).
63. D. G. Walker and B. S. Hickman, X-Ray Studies of the Radiation Damage in Beryllium Oxide Dispersion Fuels, *J. Nucl. Mater.*, 24(1): 60-68 (October 1967).
64. J. R. MacEwan, R. L. Stoute, and M. J. F. Notley, Effect of Porosity on the Thermal Conductivity of UO_2, *J. Nucl. Mater.*, 24(1): 109-112 (October 1967).
65. G. L. Reynolds, The Surface Self-Diffusion of Uranium Dioxide, *J. Nucl. Mater.*, 24(1): 69-73 (October 1967).
66. Various Abstracts of Papers on Gas Bubbles in Solids, presented at 97th AIME Annual Meeting, February 1968, *J. Metals*, 20(1): 13A, 29A-31A, 40A-44A (January 1968).

Section II

Reactor Materials

Moderator and Control Materials

Graphite

A second edition of the "Directory of Graphite Availability" is now available.[1] This is a revision and updating of the first directory published in 1963. A total of 262 graphite products, available from 19 suppliers, are characterized by type, manufacturing methods, analysis, and properties. For each of these products, supplier's availability on grades, sizes, shapes, price, rate or capacity of production, and delivery times are shown. An indexing system permits finding information on suppliers, sizes and shapes, unique characteristics, compositions, and properties.

The elastic constants of highly ordered pyrolytic graphite and the shear modulus of natural graphite crystals have been measured before and after irradiation in a study by Union Carbide.[2] Ultrasonic tests on the pyrolytic graphite yielded the elastic constants c_{11}, c_{12}, c_{33}, $c_{44} = 1/s_{44}$, and the stress derivative of c_{33}. The moduli $1/s_{11}$ and c_{44} were determined from the free flexural resonant vibrations of bars, and the shear modulus c_{44} also was determined from the fundamental torsional resonance of the bars and from the resonance of compound torsion oscillators composed of thin graphite disks with steel end pieces. Static tension, compression, and torsion tests on the pyrolytic graphite yielded a complete set of compliances (s_{11}, s_{12}, s_{33}, and s_{44}). The results are given below, where the c_{ij} and $1/s_{ij}$ are in units of 10^{11} dynes/cm^2 and the s_{ij} are in units of 10^{-11} cm^2/dyne:

$c_{11} = 106 \pm 2$ $\quad$ $1/s_{11} = 102 \pm 3$
$c_{12} = 18 \pm 2$ $\quad$ $1/s_{33} = 3.65 \pm 0.10$
$c_{13} = 1.5 \pm 0.5$ $\quad$ $s_{12} = -0.0016 \pm 0.0006$
$c_{33} = 3.65 \pm 0.10$ $\quad$ $s_{13} = -0.0033 \pm 0.0008$

$c_{44} = 0.018 - 0.035$ (pyrolytic graphite)
$c_{44} = 0.01 - 0.17$ (natural crystals)

The shear strength was found to be 25 to 76 g/mm^2 for the natural crystals and 90 to 250 g/mm^2 for the compression-annealed pyrolytic graphite.

Neutron irradiations were carried out at an exposure of 3 to 71×10^{17} neutrons/cm^2 at 50°C, at exposures of 3 to 8×10^{19} neutrons/cm^2 at 650°C, and at an exposure of 1.2×10^{20} neutrons/cm^2 at 1000°C. The shear modulus was the only elastic constant which changed significantly with irradiation. The natural crystals after irradiation had shear moduli in the range of 0.16 to 0.46×10^{11} dynes/cm^2, the modulus after irradiation showing no correlation with irradiation temperature, exposure, or modulus before irradiation. The average values of the shear modulus of the pyrolytic graphite after irradiation at 50, 650, and 1000°C were 0.22 to 0.40×10^{11}, 0.030 to 0.033×10^{11}, and 0.042×10^{11} dynes/cm^2, respectively; the modulus at the irradiation temperatures of 50 and 650°C increased as the neutron exposure increased. The shear modulus c_{44} of graphite when all dislocations are pinned was thus equal to or greater than 0.40×10^{11} dynes/cm^2. The changes in shear modulus upon irradiation for the pyrolytic graphite were interpreted in terms of the homogeneous nucleation theory of Reynolds and Thrower, which is based on electron-microscope observations on irradiated graphite crystals; the results for the natural crystals were interpreted in terms of the heterogeneous nucleation theory of the same authors.

The effective surface energy of graphite has been calculated by British investigators.[3] Two estimates of γ (the surface energy pertaining to the initiation of fracture) and one of γ_f (the work of fracture) were provided. These estimates were made from the same sets of load-deflection curves for notched bars deformed in bending. An estimate of $\gamma = 5 \times 10^4$ ergs/cm^2 may be applied to the Griffith-type flaw-size estimate to include a critical graphite flaw size of 0.2 mm. The authors estimated a value of $\gamma_f \approx 2 \times 10^5$ ergs/cm^2 using information published by Corum.* It is suggested that the reason for the high energy absorption during crack growth must lie in the tortuous crack path, and the secondary cracks that open up during fracture.

Phase equilibria between potassium vapor and graphite were examined by a Knudsen effusion-electrobalance technique of measuring vapor pressure.[4] The heats of reaction were calculated from the effusion data for three stages of reaction:

Stage 1 $\quad C_8K(\text{solid}) \rightleftharpoons C_{16}K(\text{solid}) + K(\text{gas})$

Stage 2 $\quad C_{16}K(\text{solid}) \rightleftharpoons C_{24}K(\text{solid}) + K(\text{gas})$

Stage 3 $\quad C_{24}K(\text{solid}) \rightleftharpoons C_{36}K(\text{solid}) + K(\text{gas})$

*J. M. Corum, ORNL-4030, 1966.

These calculated heats of reaction (in kcal/mole of alkali metal) are given below, together with those for rubidium and cesium:

Stage	K	Rb	Cs
1	31	33.9	43.8
2	22	25.3	29.6
3	23	27.2	32.7

Since the heats of reaction for all three stages decreased in the order cesium, rubidium, and potassium, it was suggested that the trend would continue with sodium. It was further noted this would account for the low stability of sodium graphite evidenced by the inability of sodium to form stages higher than $C_{64}Na$. (M. C. Brockway)

Beryllium and Beryllium Alloys

Fabrication

British patents[5,6] have been issued to Mallen and Weisz on processes for the manufacture of beryllium products, particularly fuel-element tubes. The process consists of extruding an ingot of beryllium, which is subjected to compression and then forged. If desired, the extrusion can be performed in a soft-steel can and may be followed by a second extrusion of the impact type. In the latter operation the metal is treated with a thin layer of silver.

A patent by Cadden and Friar[7] describes a process for preparing beryllium foil with a nominal thickness of about 0.0025 in. A $\frac{1}{4}$-in.-thick beryllium sheet is sealed in a mild-steel envelope and rolled to the desired thickness at 600 to 800°C. The sheet is then rapidly cooled to effect the release of the beryllium foil from the envelope material.

A method for the chemical vapor deposition of beryllium metal onto various substrates was developed by Wood and Frey.[8] Beryllium-metal coatings up to 10 mils thick were deposited by thermal decomposition of di-*tert*-butylberyllium. The best coatings were gray, adherent, coherent, and oriented. At a thickness of 1 mil, the coatings were superficially smooth, but as thickness increased they became nodular. Chemical analysis of the deposits showed the purity of the beryllium to be >97 wt.%, the principal impurities being carbon and hydrogen. The best coatings were obtained by operating over a narrow range of temperature (280 to 305°C) and pressure (< 1 torr). The use of various carrier gases was investigated, and these were generally found to have a detrimental effect on coating quality. Other plating compounds were employed, but these were found to give less satisfactory results than did di-*tert*-butylberyllium.

Corrosion Protection

The use of a beryllium fluoride coating as a corrosion retardant for beryllium has been studied by O'Donnell.[9] It was shown that a high-temperature modification of BeF_2, identified as a rhombic-tridymite type, is formed when beryllium is reacted with fluorine above 525°C. It has a glassy appearance and is insoluble in water. Beryllium strips treated with fluorine at 625°C and 200 torrs to form 2000 A fluoride films remained essentially unchanged in distilled water for about 3000 hr and showed less film buildup in tap water than did unfluorinated controls. Tests were also made in water with high chlorine-ion concentration, and the net weight changes were negative. Weight gain due to corrosion-film formation was not as prominent as weight loss due to crack formation, embrittlement, and loss of metal. A fluoride coating 2000 A thick was sufficient to retard corrosion; thicker coatings (12,000 A) gave poor corrosion resistance in dynamic tests, probably because of their nonadherence under high-flow conditions.

Powder Metallurgy

A British patent[10] describes a process for hot-pressing powder particles derived from cast beryllium into high-density compacts. The particles have an inert nonmetallic surface layer which prevents the formation of metal bonds between the beryllium particles. A valence imbalance in the surface layer is produced by adding sufficient silicon to promote beryllium diffusion through the layer, but not enough to form a compound or eutectic phase. Hot pressing is accomplished in a vacuum to produce compacts that exhibit high density and strength, no isolated grain growth, and little anisotropy in physical properties.

Mechanical Metallurgy

ANISOTROPY

Test techniques were developed at Lockheed[11] to determine the short-transverse mechanical properties of 0.077-in.-thick, cross-rolled, S-200 beryllium. A complete characterization of the anisotropic mechanical properties of the sheet was also performed. The short-transverse tensile specimens were fabricated by diffusion-bonding $\frac{1}{2}$-in.-diameter rods of vacuum-hot-pressed S-200 block to wafers of the cross-rolled beryllium sheet with copper foil as a bonding aid. Surfaces of the vacuum-hot-pressed block were given a 1-μ diamond polish, and the wafers of sheet were polished to 400 grit before bonding. The diffusion-bonding conditions were 1200°F (649°C) at 12,000 psi for 10 min in a vacuum of 10^{-5} torr. The property data obtained are summarized in Table II-1. The proportional limit, tensile strength, and elongation values were lower in the short-transverse

Table II-1 SUMMARY OF PROPERTIES FOR S-200 CROSS-ROLLED BERYLLIUM SHEET[11]

Strain direction	Loading direction: Longitudinal	Long transverse	Short transverse
Elastic Properties			
Stiffnesses, 10^6 psi			
Longitudinal	43.32	−561.9	(−3263)*
Long transverse	−561.9	42.58	(−2154)*
Short transverse	−3263	−2154	50.4
Young's moduli, 10^6 psi			
Same as loading direction	43.32	42.58	50.4
Poisson's ratio			
Longitudinal		0.0758	(0.0154)*
Long transverse	0.0771		(0.0234)*
Short transverse	0.0133	0.0198	
Shear moduli, 10^6 psi			
G_{xy} (in-plane)	19.85		
G_{xz} (through-thickness)	19.04		
$G_{yz} = G_{xz}$			
Plastic Properties			
Uniaxial tension			
Proportional limit, 1000 psi	13.0	14.5	2.8
Yield strength, 1000 psi	54.3	55.8	†
Tensile strength, 1000 psi	77.5	80.0	29.0
Elongation, %	15.9	16.5	0.051
Biaxial tension			
Tensile strength, 1000 psi		82.6	
4-point bends			
Max. moment, lb-in.	152‡	167‡	
Min. radius, in.	6.6	7.4	
Max. strain, longitudinal, μin./in.	7205	7550	
Max. strain, transverse, μin./in.	2226	2466	
3-point bends			
Max. moment, lb-in.	132	141	139
Bend angle at:			
Max. moment, deg.	4.5	4.5	
After failure, deg.	2.0	2.0	
Fracture toughness (K_{Ic}), 1000 psi $(in.)^{1/2}$	6		
Flexural fatigue			
Cycles to failure		$\sim 10^6$	Runout

*Not measured. Values assumed, considering stiffness matrix to have diagonal symmetry.

†Specimen did not attain 0.2% offset strain.

‡Data for bend specimens refer to specimen direction rather than loading direction.

direction than those predicted on the basis of mechanical metallurgical considerations. The metallurgical explanation of these low properties was not given because of the limited scope of the study. The development of this test technique is especially significant since a direct-test method may now be available for studying the metallurgical factors responsible for the lack of suitable short-transverse mechanical properties in beryllium sheet.

Physical Metallurgy

ALLOYING WITH COPPER

Solution strengthening of beryllium ingot sheet by the addition of copper has been investigated at The Beryllium Corp.[12] Beryllium alloys containing 0.008, 1.00, 2.79, and 4.65 wt.% copper were vacuum melted, cast, extruded into slabs, and converted into 50-mil-thick sheets. Extrusion was performed at 1850° F (1010° C), and it was noted that the extrusion force increased with increasing copper content. This indicated that there was an increase in the high-temperature yield strength because of solid-solution strengthening.

The extruded slabs were then rolled at temperatures of 1400, 1200, 1000, 800, 600, and 480° F (760, 649, 538, 427, 316, and 249° C) with a 5 to 10% reduction per pass. The 0.008 to 1.00 wt.% copper alloys were successfully rolled at all temperatures employed. The 2.79 and 4.65 wt.% copper alloys developed surface fissures and grooves at rolling temperatures below 1200° F. The strength of the as-rolled 0.008 and 1.00 wt.% copper-alloy sheets increased as the rolling temperature was reduced from 1400 to 600° F because of the increasing amounts of residual cold work. Annealing at 1200° F decreased the strengths of these materials to a common level, thereby eliminating the effect of rolling temperature. However, decreasing the rolling temperature from 1400 to 480° F decreased the annealed (recrystallized) grain size from 65 to 25 μ. Thus beryllium solid-solution strengthened with copper does not appear to follow the Petch-type relation that has been demonstrated with unalloyed beryllium-ingot sheet in this grain-size range. It was also observed that preferred orientation in copper-alloyed sheet was comparable to that noted in unalloyed ingot sheet.

Other studies at The Beryllium Corp. are devoted to further reductions in grain size of copper-alloy ingot sheet by pack rolling.[13] The method has been employed for beryllium and involved initial rolling of ingot sheet to a 60-mil thickness at the lowest possible rolling temperatures to obtain a fine grain size. The sheets were then stacked with an intermediate silver bonding agent and roll bonded to a final total thickness of 60 mils. An increase in strength and ductility of beryllium over conventionally rolled sheet was attributed to the grain refinement achieved in pack rolling to reduction ratios of 280 : 1. This rolling method will also be used for beryllium with alloying additions of 0.003, 0.005, and 1.0 wt.% copper.

ALLOYING WITH ALUMINUM

Techniques for the extrusion of thin Lockalloy (Be–38 wt.% Al) T-shapes have been developed at Nuclear Metals.[14] The extrusion speed for Lockalloy should be kept below 5.5 in./min, and the maximum extrusion temperature cannot be greater than 900° F (482° C). The most successful lubricating system consisted of a waterglass, tungsten disulfide, and graphite mixture sprayed on a Lockalloy billet that had a 20-mil-thick plated-copper coating. These low extrusion temperatures have resulted in high extrusion pressures. It was found that shortening the die approach cone reduced the high extrusion pressures. The extruded and annealed T-shapes exhibited de-

creased strength and increased ductility (see Table II-2) compared with the values obtained by others for extruded Lockalloy. The differences appear to have been caused by variations in time at temperature during annealing. Therefore it may be possible to heat-treat for maximum fabricability or optimum mechanical properties.

Table II-2 PROPERTIES OF EXTRUDED LOCKALLOY[14]

Material	Orientation	Yield strength (0.2% offset), 1000 psi	Ultimate tensile strength, 1000 psi	Elongation, %
Literature values for extruded and annealed bar	Longitudinal	46.3	56.5	6.7
	Transverse	42.5	46.3	1.5
Extruded and annealed web of the T-section	Longitudinal	38.3	55.4	13
	Transverse	34.7	37.7	2

Formability studies on the T-shape extrusions are in progress. The preliminary results indicate that they may be formed at a temperature of 500° F (260° C) into a 12-in.-radius circular shape and also joggled $\frac{1}{8}$ in.

A handbook containing information on the strength properties and design data for the Be–38 wt.% Al alloy was recently issued by Lockheed.[15] Included in the handbook are physical and mechanical properties, fracture toughness, creep, and fatigue data in addition to information on fabrication, joining, and design.

A British patent has been granted to Lockheed for a powder-metallurgical method to prepare Be–Al alloys with improved properties.[16] The alloys described are at least 50 wt.% beryllium with the remainder as aluminum, in the form of a beryllium-rich phase and an aluminum-rich phase. The beryllium-rich phase is an irregularly shaped network interspersed with the aluminum-rich phase. The alloy is prepared from fine aluminum-coated beryllium powder or small particles of Al–Be alloy. The material is compacted and pressed into the desired form and annealed at a temperature below 1193 and above 1150° F (649 and 621° C).

BERYLLIDES

A book by Samsonov[17] presents a complete review of the beryllides. Data on phase diagrams of the elements of the periodic table in combination with beryllium, methods of beryllide synthesis, beryllide structures, properties, and areas of application and on beryllium and complex beryllides are presented. The electronic structure and physiochemical properties of beryllides are also discussed. (F. T. Zurey)

Beryllium Oxide

Australian investigators achieved improved strength and lower iron impurity content in sintered BeO by modifications in mixing and extrusion.[18] BeO was produced which contained only 250 ppm iron and which, after extrusion (through BeO insert dies) and sintering 5 hr at 1400° C in nitrogen, had an average grain size of 6 μ, a mean modulus of rupture of 34,840 psi, and a density range of 2.86 to 2.90 g/cm^3. Sintering trials in nitrogen/6% hydrogen for 5 hr at 1400° C yielded lower densities than for dry nitrogen, which indicated that enhanced sinterability due to iron (even at the lowered content) was dependent on a nonreducing sintering atmosphere.

The literature since 1962 concerning the nature of radiation damage and the radiation-induced changes in the macroscopic properties of BeO, Al_2O_3, and MgO has been reviewed and reported by Wilks.[19]

(M. C. Brockway)

Solid Hydrides

Lithium Hydride

Slabs of LiH were used alone and in conjunction with heavy metals such as uranium and lead to determine neutron and gamma absorption, in experiments at Atomics International.[20] A fast-neutron flux of 2×10^8 neutrons/(cm^2)(sec) was reduced to 10^4 by a 60-cm thickness of LiH. A thermal-neutron flux of 4×10^{10} neutrons/(cm^2)(sec) was reduced to 8×10^5 by this material. When uranium or lead was used with the LiH, the neutron attenuation of the combination did not depend on which material was in front. However, for gamma attenuation, the sequence LiH–U was more efficient than U–LiH. The combination LiH–Pb was only slightly more efficient as a gamma absorber than was Pb–LiH.

The cohesive energy in LiH was calculated by Hatcher,[21] using a pairwise interaction model. A value of −195.2 kcal/mole was obtained, which compares favorably with a previous quantum mechanical calculation that resulted in a value of −199.1 kcal/mole. The activation energy for helium migration in LiH was determined to be 0.27 ev, which suggests that helium should begin to migrate at about 88° K.

Uranium Hydride

The U–H system was investigated for pressure–temperature–concentration equilibria up to 150 atm and 860° C by the French.[22] The hydrogen solubility in uranium was found to increase considerably with temperature. At 820° C and about 83 atm, the compositions of the U–H solid solution and of the hydride UH_{3-x} were found to be equal. Above this temperature the system formed only a continuous solid solution. The equilibrium diagram for the system was established for these results, and a temperature–composition plot of the data is shown in Fig. II-1. The integral molal enthalpy was found to change from about −1 to −8 kcal/gram atom of hydrogen

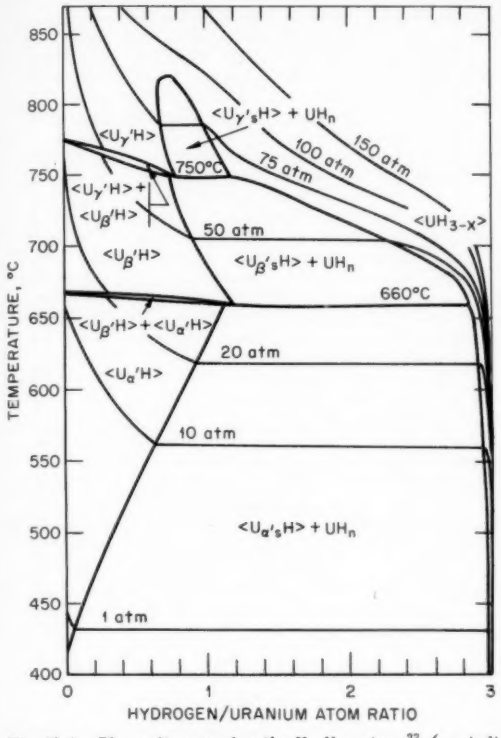

Fig. II-1 Phase diagram for the U–H system.[22] (< > indicates solid solution.)

as the hydrogen mole fraction increased from 0.1 to 0.75 at 650°C. The solid solutions of hydrogen in alpha, beta, and gamma uranium proved to be decreasingly exothermic, in that order. Further studies of these phase equilibria were carried out at the same laboratory,[23] and a series of pressure–composition, pressure–temperature, and temperature–composition diagrams were constructed. From these it was possible to deduce the three-dimensional pressure–temperature–composition equilibrium diagram.

Hydrided Zircaloys

Results of British studies[24] at Culcheth on Zircaloy-2 in solutions of LiOH at 300°C showed that the hydrogen produced by the corrosion reaction can hydride the Zircaloy-2 to concentrations well above the solubility limit, provided that a critical hydriding rate is not exceeded. This rate is increased by temperature cycling, and the optimum cycling conditions were to cool after each 60 ppm increment in hydrogen concentration. The amount of hydrogen absorbed by the specimen was approximately 65% of that generated by the corrosion reaction and was not influenced by the thickness of the oxide film or by the concentration of the LiOH solution.

The effects of hydrogen on the ductile–brittle behavior of Zircaloy have been noted by other workers at Culcheth.[25] As the temperature was reduced below 300°C, the crack-propagation-rate parameter of hydrided Zircaloy-2 gradually increased above that of the nonhydrided material until the condition was reached where self-propagating cracks occurred at maximum load. Hydrogen also reduced the bend angle at which the maximum load was reached. The impact strength of hydrogen-free Zircaloy was improved at high strain rates, whereas hydrided Zircaloy was considerably embrittled by increasing the strain rate. It was deduced that low temperatures and high strain rates which enhance twinning could be the cause of the increased brittleness in hydrided material, but attempts to verify this hypothesis were prevented by the presence of twins in the starting material.

An electron-microscope investigation of the orientation of ZrH on grain boundaries of Zircaloy-2 was conducted by the Swedish.[26] In spite of the stress relief afforded in the vicinity of grain boundaries, hydride precipitation was observed along the boundaries only when a habit plane properly oriented along the boundary was available; thus not all boundaries exhibited hydrides. No hydride precipitates were found on twin boundaries, but no less than four prism planes were found to operate as habit planes for the hydride.

The effects of alloy composition, grain size, and cold work on the terminal solubility and thermodynamic activity of hydrogen in the alpha phase of zirconium, Zircaloy-2, and Zircaloy-4 were determined at Westinghouse by a diffusion-sample method.[27] Minor differences in alloying elements between Zircaloy-2 and Zircaloy-4 caused no detectable difference in the terminal solubility in the alpha phase below 550°C. The solubility was nearly the same as that in unalloyed zirconium. The combined data for the pure metal and the two alloys are shown in Fig. II-2. The thermodynamic activity of hydrogen in the alpha solid solution of sponge zirconium, Zircaloy-2, and Zircaloy-4 differs only slightly from that in relatively pure iodide zirconium. Equilibrium partitioning of hydrogen in composites of these materials is not likely to exceed 10%. Hence the large differences in the pressure–composition–temperature relations previously reported were probably due to experimental error. Grain-size variations were found to have no effect on the properties studied, and the effects of residual cold work were minor.

The solubility of hydrogen in zirconium alloys was determined by the Canadians using a thermal-diffusion method.[28] Both Zircaloy-2 and Zr–2.5 wt.% Nb were hydrided and annealed in the alpha and $\alpha + \beta$ regions. A temperature gradient impressed on a uniformly hydrided specimen led to a solid solution + hydride region in the colder portion of the sample and an alpha solid solution in the warmer portion.

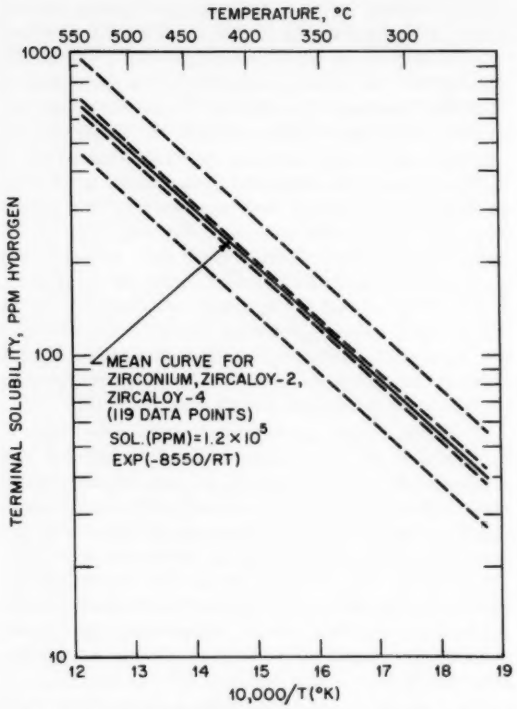

Fig. II-2 Combined data[8] for zirconium, Zircaloy-2, and Zircaloy-4. Inner and outer dashed lines represent, respectively, the 95% confidence band on the mean and the 95/99% tolerance band.[27]

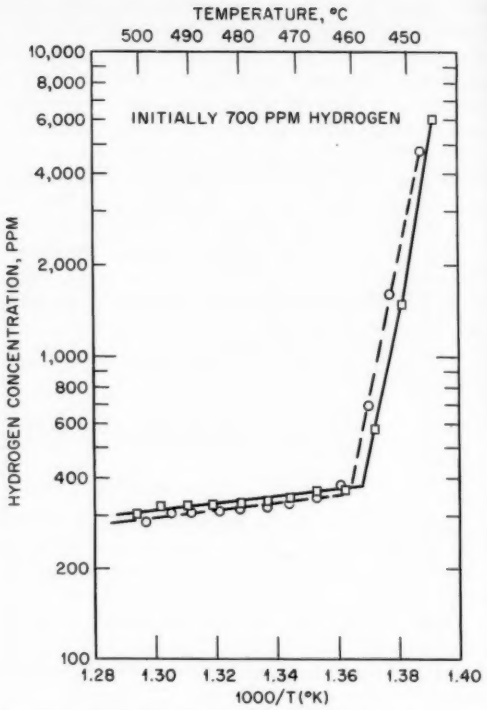

Fig. II-3 Hydrogen distribution in Zircaloy-2 under a temperature gradient.[28] —○—, 6 hr at 600°C and slow cooled; —□—, 6 hr at 600°C, slow cooled, heated in α + β, and quenched.

The terminal solid solubility of hydrogen was taken to be the hydrogen concentration in the alpha region at the $\alpha \rightarrow \alpha + \delta$ interface. Measurements were made in the temperature range 300 to 515°C. It was found that the terminal solid solubility in both alloys was given by

$$N \text{ (ppm)} = 1.99 \times 10^5 \exp(-9300/RT)$$

The hydrogen solubility was the same for samples slowly cooled from the alpha phase and those quenched from the $\alpha + \beta$ region. A typical hydrogen distribution found in Zircaloy-2 under the temperature gradient is shown in Fig. II-3. These terminal solubilities are for the stable hydrides because the specimens were initially hydrided, cooled to room temperature, and then reheated to the test temperature. Higher values reported by some investigators were obtained by hydriding at the test temperature and may correspond to the metastable hydrides postulated by Erickson.[29] (H. H. Krause)

References

1. J. Glasser and W. J. Glasser, Directory of Graphite Availability, Second Edition, Report AFML-TR-67-113, Chemical and Metallurgical Research, Inc., March 1967.
2. J. T. Meers, Effects of Neutron Damage on the Mechanical Properties of Pyrolytic and Single-Crystal Graphite, USAEC Report TID-24233, Sept. 6, 1967.
3. R. W. Davidge and G. Tappin, The Effective Surface Energy of Brittle Materials, *J. Mater. Sci.*, 3: 165-173 (1968).
4. J. R. Weeks (Comp.), Brookhaven National Laboratory, unpublished, 1967.
5. J. Mallen and M. Weisz, Process for the Manufacture of Beryllium Products, British Patent 1,085,034, Sept. 27, 1967.
6. J. Mallen and M. Weisz, Process for the Manufacture of Products of Beryllium or Beryllium Alloy, British Patent 1,085,804, Oct. 4, 1967.
7. J. L. Cadden and D. H. Friar, Beryllium Foil Fabrication, U. S. Patent 3,354,538, to USAEC, Nov. 28, 1967.
8. J. M. Wood and F. W. Frey, Chemical Vapor Deposition of Beryllium Metal, pp. 205-216 in Proceedings of the Conference on Chemical Vapor Deposition of Refractory Metals, Alloys, and Compounds, Sept. 12-14, 1967.
9. P. M. O'Donnell, Beryllium Fluoride Coating as a Corrosion Retardant for Beryllium, *Corros. Sci.*, 7: 717-718 (October 1967).
10. J. W. Butcher and R. L. Samuel, Improvements in or Relating to the Sintering of Beryllium, British Patent 1,088,049, Oct. 18, 1967.
11. R. W. Fenn, Jr., D. D. Crooks, W. C. Kinder, and B. M. Lempriere, Test Methods for Mechanical Properties of Anisotropic Materials (Beryllium Sheet), Report AD-

823194 (AFML-TR-67-212), Lockheed Missiles & Space Co., October 1967.

12. C. Carson and J. P. Denny, Solid Solution Strengthened Beryllium Alloy Ingot Sheet, Final Report, July 1966–July 1967, USAEC file No. NP-17171, The Beryllium Corp., November 1967.
13. C. Carson, Development of Solid Solution Strengthened High Purity Beryllium Alloy Sheet, Bi-Monthly Progress Report No. 2, October–November 1967, The Beryllium Corp. Nuclear Metals Division.
14. C. H. Zenuk and P. Lowenstein, Development of Improved Techniques for the Extrusion of Thin Lock-alloy Shapes, Interim Engineering Progress Report IR-9-146 (IV), September 15–December 15, 1967, Whittaker Corp., Nuclear Metals Division.
15. C. F. MacLean, Strength, Efficiency, and Design Data for Beryllium Alloy Structures. A Preliminary Handbook on Beryllium Aluminum (Be-38Al), Report SR/107-T/5523, Lockheed Missiles & Space Co., Oct. 17, 1967.
16. Beryllium–Aluminum Alloys and Method of Preparing Same, British Patent 1,094,269, Dec. 6, 1967.
17. G. V. Samsonov, Beryllides, Report JPRS-43479 (translated from pp. 1-106 of *Berillidy*, Kiev, 1966), Nov. 28, 1967.
18. J. Bardsley and A. Ridal, An Improved Method for Extruding and Sintering Beryllium Oxide, Australian Report AAEC/TM-401, August 1967.
19. R. S. Wilks, Radiation Effects in BeO, Al_2O_3, and MgO, British Report AERE-R-5596, November 1967.
20. A. W. Thiele, Lithium Hydride–Heavy Metal Shielding Experiments, USAEC Report NAA-SR-Memo-12440, Atomics International, Apr. 25, 1967.
21. R. D. Hatcher, Theoretical Research on Radiation Induced Defects in LiH, USAEC Report NYO-3657-2, Queens College, December 1967.
22. J. Chevallier, P. Desre, and J. Spitz, Study of the Uranium–Hydrogen System at Elevated Pressures, *J. Nucl. Mater.*, 23(3): 289-301 (September 1967).
23. Ph. Guinet, The Pressure–Temperature–Composition Diagram for the System Uranium–Hydrogen, *J. Nucl. Mater.*, 25(1): 24-37 (January 1968).
24. R. A. Murgatroyd and J. Winton, Hydriding Zircaloy-2 in Lithium Hydroxide Solutions, *J. Nucl. Mater.*, 23(3): 249-256 (September 1967).
25. G. D. Fearnehough and A. Cowan, The Effect of Hydrogen and Strain Rate on the "Ductile-Brittle" Behavior of Zircaloy, *J. Nucl. Mater.*, 22(1): 137-147 (April 1967).
26. V. S. Arunachalam, B. Lehtinen, and G. Östeberg, The Orientation of Zirconium Hydride on Grain Boundaries in Zircaloy-2, *J. Nucl. Mater.*, 21(3): 241-248 (March 1967).
27. J. J. Kearns, Terminal Solubility and Partitioning of Hydrogen in the Alpha Phase of Zirconium, Zircaloy-2, and Zircaloy-4, *J. Nucl. Mater.*, 22(3): 292-303 (June 1967).
28. A. Sawatzky and B. J. S. Wilkins, Hydrogen Solubility in Zirconium Alloys Determined by Thermal Diffusion, *J. Nucl. Mater.*, 22(3): 304-310 (June 1967).
29. W. H. Erickson, Hydrogen Solubility in Zirconium Alloys, *J. Electrochem. Technol.*, 4: 205-211 (1966).

Section III

Reactor Materials

Cladding and Structural Materials

Corrosion by Aqueous and Gaseous Media

Corrosion of Zirconium Alloys

OXIDATION

The oxidation behavior of a Zr–2.7 wt.% Nb alloy has been studied at McMaster University.[1] Martensitic and Widmanstätten-structured alloys were oxidized in 1 atm oxygen at 300 to 500°C. There was little difference in oxidation rates of the two types of alloy structures during early stages of oxidation at 300 and 400°C. During prolonged exposure the martensitic structure oxidized most rapidly, exhibiting first a decreasing oxidation rate and then a linear rate. Widmanstätten structures containing equilibrium amounts of proeutectoid alpha zirconium oxidized most slowly, attaining a linear oxidation rate after an initial decreasing rate. Specimens containing intermediate amounts of proeutectoid alpha zirconium oxidized at rates between these two limiting cases. At 500°C the initial oxidation rates of all structures were parabolic, with the reaction-rate constants being directly dependent on the volume fractions of martensite.

High-temperature X-ray diffraction has been used by Japanese scientists to study the mechanism of oxidation of zirconium and zirconium alloys.[2] Metastable tetragonal zirconium dioxide was found in the black oxide prior to breakaway oxidation. It was also noted that the color change of the oxide from black to white and transformation to monoclinic oxide occurred simultaneously at breakaway conditions. Larger contents of tetragonal oxide were found in the oxide scales on alloys containing titanium and tin than in those on unalloyed zirconium. This finding was correlated with observations that breakaway occurs at lower temperatures on these alloys and that these elements lower the transformation temperature of ZrO_2.

AQUEOUS CORROSION

The long-term (up to 500 days' exposure) aqueous corrosion behavior of Zr–Fe–Cr–Sn alloys has been studied by Bettis.[3] An alloy containing 0.5 wt.% iron and 1.0 wt.% chromium was superior to Zircaloy-2 with respect to lower pretransition and posttransition corrosion rates and total weight change. The addition of 0.5 wt.% tin to this alloy resulted in a hydrogen uptake lower than that in Zircaloy-4 in 680°F (360°C) water. At temperatures of 750 to 950°F (399 to 510°C), the tin-free alloy absorbed less hydrogen than did Zircaloy-4. An alloy containing 1.0 wt.% iron and 0.5 wt.% chromium, with and without 0.5 wt.% tin, also exhibited low corrosion rates but had higher hydriding rates than Zircaloy-4, particularly at the lower temperatures.

Bettis has also determined the corrosion, hydrogen absorption, and mechanical-property characteristics of Zircaloy-4 alloys containing 0.5 and 1.0 wt.% niobium additions.[4] In high-temperature water and steam, these alloys exhibited somewhat higher corrosion rates and approximately equivalent hydrogen pickup compared with Zircaloy-4.

Corrosion of Stainless Steels

Oxide formation and deposition on carbon steels and stainless steels in high-temperature water has been investigated by the Belgians.[5] Two oxide layers were found on chromium and chromium–nickel stainless steels. The inner layer was a spinel containing principally iron and chromium. The outer layer consisted of scattered crystals of magnetite which was shown to deposit from solution (presumably by decomposition of ferrous hydroxide). Iron solubility in neutral water was found to reach a maximum at about 250°C. This behavior was suggested as the probable cause of iron oxide precipitation on fuel-element surfaces where temperatures are greater than 300°C (and iron solubility is less).

The French[6] examined the stress-corrosion cracking behavior of high-purity 18/10 stainless steels in boiling $MgCl_2$. A beneficial effect of martensite in the steel's microstructure on prolonging time to failure was attributed to cathodic protection of the austenite by the martensite. Solution potential measurements revealed that the martensite was electronegative (anodic) to the austenite. Metallographic studies indicated that the martensite was corroded but the austenite was unattacked.

Corrosion of Nickel-Base Alloys

The degradation of oxides on superalloys as a source of oxygen contamination in gas loop environments has been demonstrated at Battelle–Northwest.[7] Oxides formed on superalloys at 1000°C were easily degraded in inert (10^{-4} torr vacuum) or reducing (0.02 torr hydrogen) atmospheres at 1100°C. Experiments with preoxidized Hastelloy X (13.8 mg oxygen total) and niobium in a container with 80 torrs hydrogen at 1100°C produced a weight gain of 26.9 mg for the niobium and a weight loss of 26.1 mg for the Hastelloy X. The weight gain for the niobium was attributed to pickup of contaminants in the system plus the oxygen from evaporation of the oxide on the Hastelloy.

Corrosion Studies with More Than One Alloy System

The accumulation of hydrogen within the internal space of a helium-filled bulb as the result of corrosion on the external surface has been studied at Westinghouse.[8] The corrodent was water at 575°F (302°C) and 1600 to 2000 psig, with *p*H 9.5 to 10.5 (NH_3) and dissolved hydrogen of 30 to 35 cm^3/kg of H_2O at STP. Surface area of the bulbs was 120 cm^2, and internal volume ranged from 13.7 to 29.4 cm^3. Hydrogen accumulations within the bulbs after exposure for 1700 to 1800 hr are summarized below. The hydrogen pickup in Inconel 600 was greater than could be accounted for on the basis of reported corrosion rates for this material in this environment. Hydrogen pickup in the other materials could be correlated with their corrosion rates, although hydrogen pickup in the 410 stainless steel virtually ceased during a short period of operation with no dissolved hydrogen in the water.

Bulb material	Cumulative hydrogen pickup, moles	Equivalent hydrogen internal pressure, torrs
347 stainless steel	47.8	122
Inconel 600	740	1110
410 stainless steel	1240	1480
Chromium-plated 410 stainless steel	855	1010
Nickel-plated 410 stainless steel	1550	1830
347 stainless steel with Zr–V getter	1.6	4

The effect of 10 to 50 ppm boron (as H_3BO_3) in the coolant on the corrosion behavior of Plutonium Recycle Test Reactor materials has been determined by Battelle–Northwest.[9] In-reactor exposure with occasional operational periods with boron did not cause accelerated corrosion of aluminum, Inconel 600, 304 stainless steel, or Zircaloy-2. Various pilot-plant tests with boron additions did not cause accelerated attack except on aluminum when coupled to Inconel or stainless steel. Continuous refreshment prevented pitting of 6061 aluminum when coupled to Inconel 600 in shim well tests designed to evaluate crevice effects.

Studies at Chalk River have shown that *p*H in the range of 7 to 10 has no effect on the wear characteristics of 10 metal combinations in room-temperature water.[10] Loaded journal-sleeve specimens were operated successfully for at least 2 million in. of travel. Materials in the wear combinations included 304, 416, and 440-C stainless steels and the nickel alloys Duranickel and Waukesha 23 and 28.

Other work at Chalk River[11] revealed that intergranular attack was initiated in carbon steel, Monel 400, and Inconel 600 when exposed to boiling-water-reactor environments in research-reactor loops at 520 to 550°F (271 to 288°C). Oxygen contents of the water ranged from 4 to 70 ppb. The addition of 11 ppm ammonia to the environments suppressed the oxygen content to less than 4 ppb and prevented initiation of the intergranular attack. It was concluded that the intergranular attack was prevented by the suppression of the oxidizing nature of the coolant.

(W. E. Berry)

Corrosion of Refractory Metals

UNCOATED REFRACTORY METALS

Oak Ridge[12] has studied the oxidation characteristics of tantalum at 500 to 625°C after anodizing in H_3PO_4. The anodic oxide films containing phosphorus were found to be considerably more effective in limiting oxygen access to the metal and in postponing breakaway oxidation than are phosphorus-free films of the same thickness. Thickness–voltage calibrations were obtained from anodization in 0.9*M* and 14*M* H_3PO_4. Oxygen permeation rates through films formed in the more concentrated acid were a factor of 5 lower than those found in the 0.9*M* solution.

The anodic oxidation of tantalum at 40 to 70°C in 70 μ oxygen was studied by Frankford Arsenal[13] using an electromagnetic ion cathode. The films were prepared at 1.0 and 2.0 ma/cm^2. The growth characteristics of anodic tantalum oxide films in the gas phase were found to be similar to those for films formed in liquid electrolytes. Growth of tantalum oxide was shown to be linearly dependent on the total charge passed in the anode circuit during the reaction, up to 200 volts.

The potential difference between various interfaces during the oxidation of niobium and tantalum in air at 400 to 1200°C has been measured at Lewis.[14] The polarity of the oxide–gas interface was found to be electrically positive with respect to the oxide–metal interface. This polarity had a retarding effect on oxidation and contradicted Hauffe's oxidation theory which predicts the reverse polarity. The magnitude of the potential was in the 1-volt range and did not depend on oxide thickness. Breaks in the tempera-

ture-dependence curve corresponded to significant changes in oxidation rate.

Addition of up to 40 at.% niobium increased the hardness, density, and electrical conductivity of V–Nb alloys.[15] Corrosion resistance of the alloys in H_2SO_4, HCl, and HNO_3 increased with increasing niobium content. Alloys containing 30 at.% niobium were stable in 10 and 57 vol.% HNO_3 up to 100°C. Niobium delayed the anodic solution of vanadium in H_2SO_4.

The oxidation of chromium alloys[16] containing up to 24 wt.% zirconium was carried out in oxygen at 1100 and 1200°C. For compositions up to 5 wt.% zirconium, oxidation was parabolic and independent of zirconium content. With higher zirconium contents, oxidation was linear, and the increase in rate was proportional to the zirconium content. Both ZrO_2 and alpha Cr_2O_3 were detected in the scale. The zirconium content in the scale increased with increasing zirconium in the alloy. At high zirconium contents, ZrO_2 with anion defects promoted the diffusion of oxygen and thus increased the oxidation rate.

COATED REFRACTORY METALS

The French[17] have investigated improvement of self-regenerative coatings for niobium. One approach was to add a third element (aluminum or nickel) to lower the vapor pressure of zinc coating and increase the temperature limit for oxidation resistance about 150°F (83°C). Replacement of zinc by magnesium and addition of a third element (Co, Ni, Fe, Si, or Sb) were unsuccessful. Formation of $NbSi_2$ in a molten Zn–Al bath in the presence of SiO_2 resulted in oxidation protection of 50 hr at 2500°F (1371°C). Binary alloying of the substrate with up to 15 wt.% vanadium, 5 wt.% chromium, or 5 wt.% zirconium offered no improvement. However, addition of 10 to 15 wt.% titanium not only increased oxidation life about 10% but also eliminated the "silicide pest" behavior at 1100 to 1650°F (593 to 900°C).

Chromalloy[18] has investigated a variety of pack-cementation aluminum-base coatings for the protection of Cr–5 wt.% W–0.1 wt.% Y sheet.[19] Of the systems studied, a simple aluminum coating (Cr_5Al_8 type) and Fe–Al coating [$(Fe-Cr)_x Al_y$ type] gave the best results. Under cyclic air oxidation these systems survived over 600 hr at 2100°F (1149°C), compared with 100 hr for the uncoated alloy. Oxidation life was about 200 hr at 2400°F (1316°C). Under dynamic conditions of a Mach-0.5 flame and 350-rpm rotation, the systems tended to fail in about 100 hr at 2100°F. Protectiveness of the systems was closely related to $AlCr_2O_4$ and $FeO \cdot Al \cdot Cr_2O_4$-type spinel formation that also limited nitrogen penetration. By causing substrate recrystallization, the coating process increased the bend ductile–brittle transition temperature (no cracks produced in a 90 to 105° bend) from about 500 to 800°F (260 to 427°C). However, the oxidation exposures raised the transition to above 1600°F (871°C), primarily because of aluminum diffusion into the substrate and secondarily because of atmosphere contamination of the coating.

Protection of the Cr–5 wt.% W–0.1 wt.% Y alloy using gas-pressure-bonded alloy foils was studied by Battelle–Columbus.[20] The outer 5- to 10-mil-thick layer consisted of Ni–20 wt.% Cr or Ni–20 wt.% Cr–20 wt.% W which was modified with 3 to 5 wt.% aluminum in some cases. The study also included barrier layers of Mo, W–1 wt.% ThO_2, W–25 wt.% Re, and W, with the latter being the most useful in preventing interdiffusion of nickel and chromium. Compatibility layers of platinum or vanadium between the outer and barrier layers were not beneficial. The outer cladding layers gave cyclic oxidation resistance of over 600 hr at 2100°F (1149°C) and about 100 hr at 2300°F (1260°C), with the aluminized Ni–20 wt.% Cr–20 wt.% W giving the best performance. Rapid oxidation occurred at 2400°F (1316°C). After exposure for 100 hr at 2100°F, the bend ductile–brittle transition temperature was a minimum of about 1000°F (538°C). After exposure at 2300°F, edge cracking was observed and the transition was over 1600°F (871°C). The embrittlement mechanism included metallic interdiffusion at 2100°F and involved both interdiffusion and nitrogen contamination at 2300°F. (B. C. Allen)

Corrosion by Nonaqueous Liquids

Corrosion by Sodium

Biaxial stress-rupture tests by Atomics International described in an earlier issue of *Reactor Materials* were unlike previous investigations, in that a marked decrease was noted in stress-rupture life of 304 and 316 stainless steels tested in zirconium-gettered sodium as compared with the results of tests in helium. Subsequently, it was found[21] that the zirconium foil, in addition to its intended function of gettering oxygen from the sodium, was decarburizing the stainless-steel specimens. This decarburization (30 to 50% reduction in carbon content in <1000 hr at 705 and 760°C) reduced the creep-rupture strength of the 304 stainless steel by about 25% and that of the 316 stainless steel somewhat less, whereas the sodium itself had no apparent effect. In the range of test conditions employed, the stress-rupture behavior was sensitive to cold working, as indicated by the difference in slopes of the stress-rupture curves for annealed material and cold-worked material (Fig. III-1).

Uniaxial stress-rupture tests at 700°C by Böhm and Schneider at Karlsruhe[22] on an austenitic stainless steel designated X8CrNiMoVNb 1613 and on

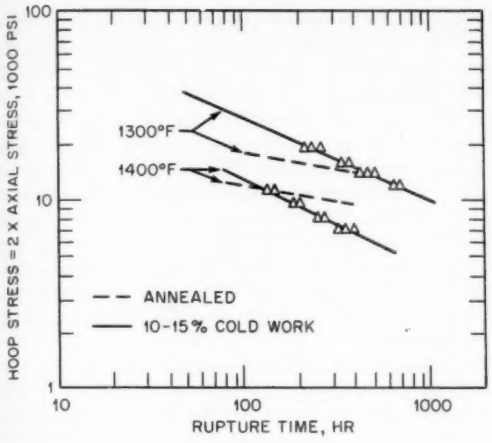

Fig. III-1 Biaxial stress-rupture data for 304 stainless-steel tubing (0.295 in. in outside diameter by 10 mils in wall thickness).[21]

Incoloy 800 showed that the second-stage creep rate of both alloys is not influenced by the presence of sodium (<50 ppm oxygen). However, the specimens tested in sodium showed strains at fracture significantly lower than those for specimens tested without sodium. As with the Atomics International studies discussed above, there was no significant difference in time to rupture for the austenitic stainless steel with and without sodium present. The rupture life of the Incoloy 800, on the other hand, was reduced by the sodium, particularly at the lower stresses. These effects are shown in Figs. III-2 and III-3.

A comparison of 304 and 316 stainless steels for use in sodium systems was presented by MSA Research.[23] Bases for comparison were metallurgy, mechanical properties, and ease of fabrication. The conclusions do not lead to a clear-cut superiority of one steel over the other. Rather, they follow the stated purpose of the report — "... not to choose but to present what knowledge is available in a useful manner." In general, the findings indicate that the effect of impurities in the sodium is more pronounced on 304 than on 316 stainless steel and that, although 316 is somewhat more difficult to machine than 304 stainless steel, the difference is not great. Mechanical-property comparisons are somewhat confusing, in view of the fact that there are two materials, five environments (air, helium, "clean" sodium, high-oxygen sodium, and high-carbon sodium), two temperatures, and seven properties. Furthermore, the differences in comparable properties are usually not too pronounced, and there is no consistent favoring of one material or the other.

In the Brookhaven program[24] for testing a variety of materials in liquid sodium for application as fuel claddings in a fast breeder, the following observations have been gleaned from thermal-convection loop tests at temperatures to 760°C:

1. Maximum weight losses for the alloys containing Fe–Ni–Cr were < 1 mg/cm^2 in 1000 hr.
2. Alloys containing the highest percentage of nickel (Incoloy 800 and Multimet) underwent the greatest weight loss.
3. Nickel was leached from the surface of all test specimens, the greatest depletion occurring in the hottest regions.
4. Chromium was leached from the higher temperature zones only and was apparently deposited in lower temperature regions.
5. The cobalt-base alloys showed weight losses equal to or lower than those exhibited by 316 stainless steel.

United States Steel researchers[25] compared some characteristics of a sample of welded 304 stainless-steel pipe that had been exposed to liquid sodium at 300 to 800°C for ~ 7800 hr with those of an unexposed sample of pipe from the same heat. Except for an increase in nitrogen, no marked changes in composition of the pipe occurred. A greater amount of nitrogen was absorbed by the inside surface that had been exposed to the liquid sodium, which likely contained calcium nitride as an impurity, than by the outside surface that had been exposed to air. There was no marked deleterious change in strength or ductility.

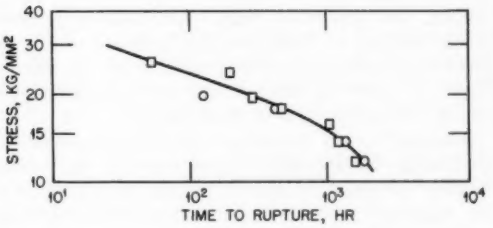

Fig. III-2 Stress-rupture behavior[22] *of 16 wt.% Cr–13 wt.% Ni–MoVNb steel at 700°C in contact with sodium (○) and in air (□).*

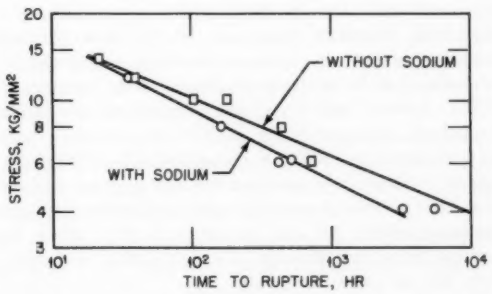

Fig. III-3 Stress-rupture behavior[22] *of Incoloy 800 at 700°C in contact with sodium (○) and in air (□).*

Metallography revealed a sensitized structure throughout and a lamellar phase (probably from nitrogen absorption) on the inside surface. It was recommended that any sodium to be used in contact with 304 stainless steel be stripped of nitrogen-bearing impurities to minimize nitriding of the steel.

Samples of 304 stainless steel, Inconel 600, Incoloy 800, and Hastelloy X, which had been subjected to a fluence of 7.2×10^{20} neutrons/cm^2 ($4.7 \times 10^{19} > 1.35$ Mev) in Experimental Breeder Reactor II (EBR-II) flowing sodium at 510 and 530°C, suffered no measurable weight or dimensional changes and exhibited no metallographic evidence of attack by the sodium. Microprobe traverses of the surfaces[26] showed no compositional gradients in the 304 stainless steel or the Hastelloy X—a surprising result in view of the fact that similar ex-reactor exposures leave such surfaces rich in iron. The Inconel 600 surfaces lost both nickel and chromium and picked up iron, whereas the Incoloy 800 lost both chromium and iron, with no change in nickel content.

In the same experiment a sample of unalloyed vanadium was severely pitted and lost about half its weight, whereas samples of V–20 wt.% Ti and V–40 wt.% Ti experienced small weight losses (equivalent to ~0.5 mil in the 7-month exposure).[27] Microscopic examination of the two alloys showed that there was no hardened surface layer of the type normally observed in all ex-reactor experiments under comparable conditions of sodium temperature, oxygen content, and exposure time. The Argonne workers are attempting to track down the reason for this important difference between in-reactor and ex-reactor behavior, since the brittle layer can degrade stress-rupture properties if it is thick enough.

Holcomb[28] used microhardness scans across test specimens to determine quantitatively the carburization potential of molten sodium in contact with 304 stainless steel. He found that the microhardness data at 565, 605, and 650°C correlated well with the carbon content of the liquid sodium to which the stainless steel had been exposed. Carbonaceous compounds intentionally added to the liquid sodium provided a source of carbon for carburization of the stainless-steel tab specimens. The quantitative picture was confused, however, by the fact that the surfaces of the test capsules were also carburized.

Cavitation in sodium systems was induced at NASA–Lewis[29] with a vibratory apparatus to promote cavitation damage on samples of 316 stainless steel, L-605 alloy, and Stellite 6B at 800°F (700°K). Damage at various pressures of the argon cover gas was assessed metallographically and by volume-loss-rate measurements. As can be seen in Fig. III-4, the volume loss rate increased exponentially with pressure for all three materials.

A sodium thermal-convection loop constructed of Nb–1 wt.% Zr was operated in a vacuum environment by General Electric[30] for 1000 hr at a peak temperature of 3480°F (1300°C) and a ΔT of 980°F (545°C) to check out components in preparation for subsequent tests on forced-convection systems. Posttest metallographic examination of Nb–1 wt.% Zr tubing specimens from all regions of the loop revealed no evidence of corrosion of either the base material or weldments. Chemical analyses of the tubing indicated that the nitrogen and carbon contents were unaffected by the exposure but that the oxygen level had dropped in the hottest regions of the loop and increased in the cooler zones. An unexpectedly high hydrogen level and consequent embrittlement of tubing was traced to the posttest alcohol-cleaning technique used.

Encouraged by these results, General Electric workers constructed a forced-circulation Nb–1 wt.% Zr loop[31] and ran it for 2650 hr with a maximum temperature of 2065°F (1180°C) and a ΔT of 100°F (55°C). As with the thermal-convection loop, detailed chemical and metallurgical examinations of the loop tubing revealed no evidence of significant contamination or corrosion from either the sodium or the vacuum-chamber environment. Again, however, there was a transfer of oxygen from the high- to the low-temperature sections of the loop tubing.

Refractory metals are being considered for use in high-temperature sodium systems. It is known that impurities can have an important effect on the corrosion and mechanical properties of the refractory metals, but the mechanisms have not been defined. Results of studies of the kinetics in the Ta–O–Na and Nb–O–Na systems carried out by Argonne[32]

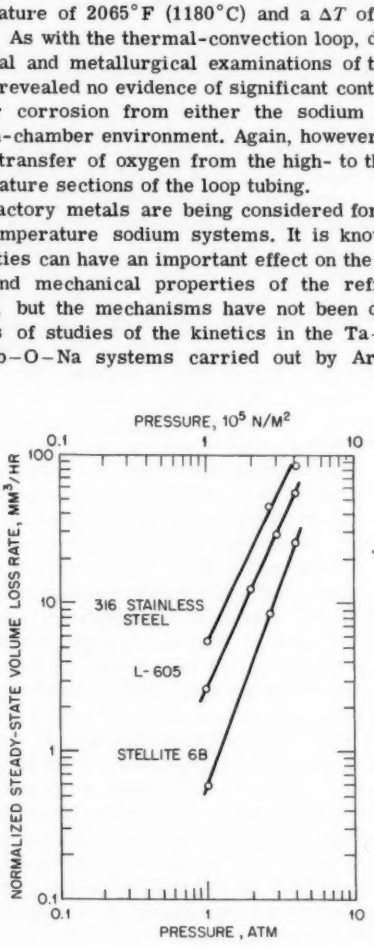

Fig. III-4 Relation of cavitation damage, normalized to area basis, to ambient pressure for materials tested in 800°F (700°K) sodium.[29]

should be very useful in establishing a predictive capability. Starting with literature values for the solubilities of oxygen in sodium, tantalum, and niobium, the investigators derived the parabolic rate constants for oxygen solution in tantalum and niobium in the presence of low-oxygen (1 to 20 ppm) sodium. They also predicted the conditions of temperature and oxygen content of sodium over which the phases tantalum and Ta_2O_5, and niobium, NbO, and NbO_2 are thermodynamically stable in sodium. Calculated distribution coefficients (equilibrium ratio of oxygen concentration in the refractory metal to oxygen concentration in sodium) are shown in Fig. III-5. Apparently, tantalum does not give up its oxygen to sodium nearly as readily as it does to potassium, according to the NASA–Lewis observations[33] discussed in the subsection "Corrosion by Potassium" below.

Work done at Oak Ridge on NaK-to-air radiators for the Aircraft Nuclear Propulsion Project during the years 1955 through 1957, reported previously in only limited-distribution documents, has now been summarized in a 1968 report.[34] Eighteen Inconel fin-and-tube radiators were tested at NaK temperatures from 1200 to 1600°F (650 to 870°C). Problems uncovered in the course of these tests are described in some detail. These include failures stemming from stress concentrations and thermal cycling, and plugging of tubes by sodium oxide, foreign materials, or mass-transfer deposits. Background Inconel–NaK corrosion-loop data and extensive mechanical-property data on Inconel are also presented.

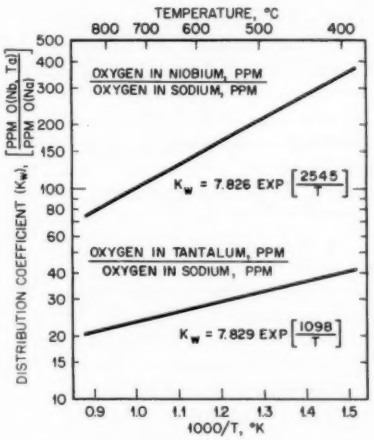
TEMPERATURE, °C
800 700 600 500 400
500 400 300 200 150 100 80 60 40 30 20 15 10
DISTRIBUTION COEFFICIENT (K_w), [PPM O(Nb, Ta) / PPM O(Na)]
OXYGEN IN NIOBIUM, PPM / OXYGEN IN SODIUM, PPM
K_w = 7.826 EXP [2545/T]
OXYGEN IN TANTALUM, PPM / OXYGEN IN SODIUM, PPM
K_w = 7.829 EXP [1098/T]
0.9 1.0 1.1 1.2 1.3 1.4 1.5
1000/T, °K

Fig. III-5 Distribution coefficients of oxygen between tantalum and sodium, and niobium and sodium.[32]

Corrosion by Potassium

Workers at NASA–Lewis[33] succeeded in isolating and identifying the hygroscopic crystalline solid resulting from a 96-hr treatment at 1800°F (980°C) of a 1-g coil of oxygen-doped (3800 ppm) 0.025-cm tantalum wire in a tantalum capsule containing 0.9 g of potassium. The tantalum wire was completely deoxidized, and the corrosion product was found by X-ray and chemical analyses to be K_3TaO_4. The dissolution appears to be governed by the equation

$$3K + Ta + 4O_{(Ta)} \rightarrow K_3TaO_{4(K)}$$

which suggests that the extent of corrosion in the Ta–O–K system can be predicted if the total amount of interstitial oxygen in the tantalum is known. This is consistent with results reported in *Reactor Materials*, Vol. 11, No. 2, wherein Oak Ridge studies[35a] showed that tantalum would give up oxygen to potassium at 600°C, even when the initial oxygen in the potassium was very high (to 3300 ppm) and that in the tantalum was quite low (50 ppm).

A 316 stainless-steel, gas-fired loop and potassium-vapor-turbine test facility was constructed by General Electric. Testing of candidate refractory turbine alloys was done by inserting sample blades and stationary inserts in the turbine second stage and running a 2100-hr endurance test with turbine-inlet potassium vapor at 1500°F (815°C).[36] Minimal deterioration of the stainless-steel turbine parts and the sample rotor blades of U-700 (Ni–17 to 20 Co–13 to 17 Cr–4.5 to 5.75 Mo–3.75 to 4.75 Al–3 to 4 Ti–1.0 Fe–0.15 C, by weight), TZM (Mo–0.5 Ti–0.08 Zr, by weight), and TZC (Mo–1.2 Ti–0.25 Zr–0.15 C, by weight) occurred. Average weight losses of the U-700 blades after the 2100-hr run were 0.3% (stage 1) and 0.02% (stage 2), and the TZM and TZC blades in stage 2 lost about 0.1% in weight.

In view of these encouraging results, the turbine was tested for an additional 3000 hr, with the following conclusions:[37]

1. The oxygen and carbon levels in the potassium, which were low at the outset, were reduced even further as the test progressed. This may be part of the reason that blade corrosion was less in the 3000-hr test than in the 2100-hr test.

2. The room-temperature ductility of the U-700 blades in the first stage was reduced because of sigma-phase formation, and the room-temperature ductilities of the refractory alloys were in some instances likewise lowered.

3. Some erosion of the René 41 blade clips and of the 316 stainless-steel shrouds in both stages was noted, although even the worst erosion (second stage) was not considered serious.

4. The observed mass-transfer and alloy-depletion effects were also not considered serious, being generally less than 1 mil deep.

5. There was no damage to the turbine which compromised its safety or reliability.

Corrosion by Lithium

Figure III-6 shows the results of short-time tensile tests of Soviet-developed experimental alloys for service in molten lithium.[38] Sheet tensile specimens were encapsulated in a niobium tube containing filtered lithium (100 ppm oxygen and 190 ppm nitrogen), soaked at 1000°C for the times shown, then tensile tested in an argon atmosphere. The results (solid curves) were compared with those for identical control specimens (dashed curves) which had been given similar heat-treatments in argon without lithium present. It is apparent that the lithium had a negligible influence on the strength and ductility of PH-3, PH-5, and PH-6, and only a slight weakening effect on PH-2.

Reactor Materials, Vol. 11, No. 2, mentioned a study at the Jet Propulsion Laboratory of a magnetohydrodynamic (MHD) power system in which liquid lithium is accelerated by cesium vapor in a two-phase nozzle, separated from the cesium, decelerated in an MHD generator, and finally forced by its remaining dynamic head through a heat source and back to the nozzle. There were indications that materials which had withstood static lithium at 1090°C were badly eroded after 100 hr under a 150 ft/sec 1090°C lithium jet. The alloy Nb–1 wt.% Zr was least affected.

Follow-up experiments[39] corroborated these observations quantitatively. Two materials, Nb–1 wt.% Zr alloy and yttrium oxide, were subjected to the lithium stream. After 109 hr at 1143°C, the yttria specimens were completely dissolved. The maximum depth of material removed from the niobium alloy after an additional 391 hr at 1093°C was 7 μ. This value corresponds to the depth calculated from turbulent mass-transfer relations for simple dissolution if the temperature coefficient of solubility is taken to be 1.2×10^{-9} g Nb/(g Li) (°C). As shown in Fig. III-7, the measured variation of material loss with lith-

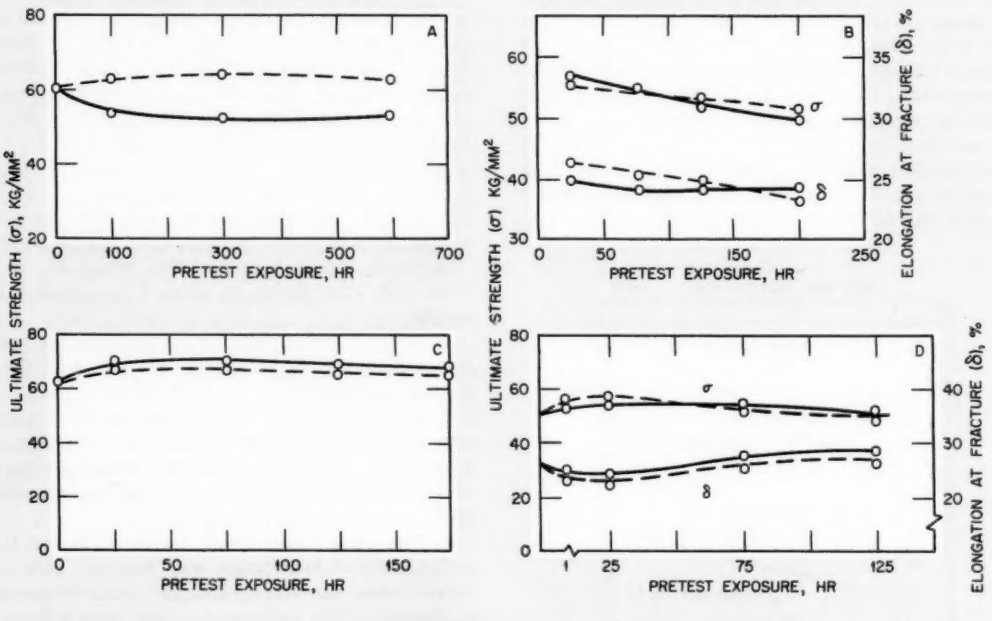

Curve	Alloy	Nominal composition, wt.% (balance Nb) W	Mo	Zr	Interstitials, wt.% O	N	C
A	PH-2	7 to 10			0.033	0.03	0.04
B	PH-3	4.5 to 6		1 to 1.5	0.03	0.012	0.020
C	PH-5	9 to 11		1 to 1.5	0.025		0.034
D	PH-6	4.5 to 6	4.5 to 6	1 to 1.5	0.028		0.026

Fig. III-6 Effect of exposure to molten lithium on the 1000°C tensile properties of experimental niobium-base alloys.[38] Solid curves: specimens soaked in lithium at 1000°C; dashed curves: specimens heated in argon at 1000°C.

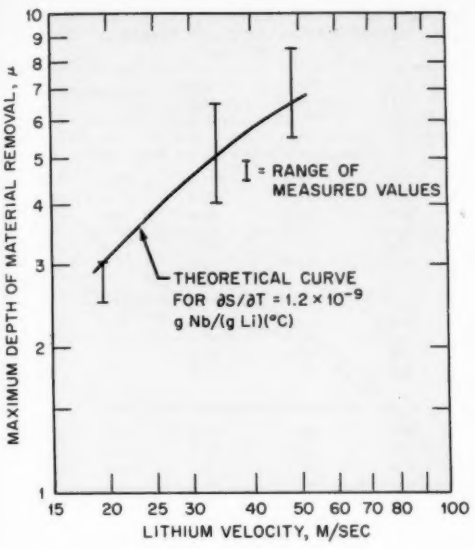
MAXIMUM DEPTH OF MATERIAL REMOVAL, μ
LITHIUM VELOCITY, M/SEC
I = RANGE OF MEASURED VALUES
THEORETICAL CURVE FOR ∂S/∂T = 1.2 × 10⁻⁹ g Nb/(g Li)(°C)

Fig. III-7 Depth of material removal[39] from Nb–1 wt.% Zr vs. lithium velocity, 500 hr at 1073 to 1143°C.

ium velocity agrees very well with the dependency predicted by these relations, which indicates that the dissolution is a diffusion-limited process.

As reported previously,[40] Argonne has been experimenting with soluble corrosion inhibitors for lithium–refractory metal systems. Corrosion of tantalum by lithium has been found[41,42] to be inhibited by additions of silicon or iridium. In the case of silicon, the protective layer was identified as Ta_2Si. With 1.0 and 1.5 at.% iridium additions to lithium in high-purity tantalum capsules, a 50-μ protective layer was found after a 9-day exposure at 1200°C. The layer consisted of three phases: Ta_3Ir next to the tantalum, $TaIr_3$ on the outside, and TaIr in-between.

High-density molybdenum-cemented tungsten and niobium carbides were unattacked by 1100°F (595°C) lithium after 7000 hr in Nb–1 wt.% Zr rocking capsules. Also, they showed excellent wear resistance in a rotating disk–static shoe assembly with 1000°F (540°C) lithium or NaK as the lubricant.[43] These results were obtained by Pratt & Whitney in a study of bearing materials for advanced Rankine-cycle space systems. Carbides bonded with 8 to 25 wt.% cobalt or with 4.5 to 25 wt.% nickel suffered solution attack in 1100°F lithium. Carburized Nb–1 wt.% Zr surfaces gave wear characteristics that were sensitive to the processing technique and coating thickness. Plasma-sprayed coatings of WC and WC–Co gave encouraging wear results in NaK, but the process control requires considerable development to avoid problems from poor adhesion, porosity, and impurities.

Corrosion by Electrolytes

Corrosion of electrodes by electrolytes at elevated temperatures limits the life and output of batteries, fuel cells, and other energy-storage devices. Workers at TRW Systems[44] developed a technique for evaluating candidate electrode materials by measuring progressive corrosion in terms of differential electrical-resistance changes of a unique temperature-compensated sensing probe. Probes of 316 stainless steel gave fairly reproducible corrosion rates when tested in KCl at 820°C and in KCl–NaCl at 700°C. Tantalum and Ta–10 wt.% W alloy were attacked by hot concentrated H_3PO_4 at rates less than 1 mil/year. Pure tungsten, W–25 wt.% Re, and W–30 wt.% Re–40 wt.% Mo were also resistant to hot H_3PO_4 and showed corrosion rates between 1 and 6 mils/year.

In the course of this work, it became apparent that considerable improvement in corrosion resistance might be achieved by appropriate alloying. To circumvent the lengthy and expensive alloy-preparation and testing program required to find the optimum alloy for a given electrolyte, the TRW researchers developed the "diffusion-block" concept. This consists of stacking rectangular-cross-section specimens of different metals in such an order that binary, ternary, and quaternary alloys form and grow according to Fick's laws at the interfaces as the assembly is held at a high temperature.

In the TRW work a wide range of solid-solution and intermetallic phases was obtained from a five-element (Cr, Co, Mo, Ni, and W) diffusion block by slicing off sections after 60, 150, and 250 hr at 1100°C. After metallographic examination, these sections could be evaluated by exposure to the corrosive media of interest and scrutinized to see which phases were most resistant.

Liquid-Metal Literature Reviews

A critical review of the literature on the solubilities of transition metals in molten alkali and alkaline-earth metals has been published by Lawrence Radiation Laboratory.[45] This valuable compilation summarizes the data graphically on each of the numerous systems studied. Solvents covered are Li, Na, K, Rb, Cs, Mg, Ca, La, and Ce. Solutes include Fe, Ni, Cr, Co, Mn, Ti, Ta, Mo, V, W, U, and Zr. The report is available from CFSTI for $3.00.

A detailed review[46] of liquid-metal embrittlement phenomena has been published by Martin Marietta. The reviewers believe that chemisorption of the liquid metal reduces the atomic bond strength at regions of stress concentration in the solid metal. They disagree with Robertson's concept[47] that embrittlement results from stress-enhanced dissolution and subsequent diffusion of the liquid metal at a crack tip. The review discusses the effects of chemical composition, temperature, prestrain, and rate

of loading on severity of embrittlement, and concludes that there are still substantial gaps in our understanding of the phenomena. (E. M. Simons)

Radiation Effects in Structural Materials

Component failures due to accelerated corrosion and radiation-induced embrittlement of metals in nuclear reactors are among those described in a compilation by Battelle–Northwest.[48] The basic phenomena of radiation damage and radiation effects on the engineering properties of materials has been reviewed by the Russians.[49] A considerable part of the discussion on engineering properties, which is mostly concerned with pressure-vessel steels and stainless steels, pertains to original Russian research. A thorough summary of effects of neutron radiation on structural materials has been issued by the Radiation Effects Information Center.[50] Data are presented for aluminum alloys, magnesium alloys, beryllium, zirconium alloys, mild steels, stainless steels, nickel alloys, and refractory metals. The effects of radiation on the mechanical properties of selected materials at cryogenic temperatures are also described.

Zirconium and Aluminum Alloys

In-pile creep studies[7] of Zr–2.5 wt.% Nb have shown that, at 350°C and above, the in-pile creep rates are similar to out-of-pile creep rates, but that, below 350°C, the in-pile creep rates are higher.

Results of studies[51a] on as-received SAP alloys after a fluence of 2.3×10^{20} neutrons/cm^2 ($E > 1$ Mev) and flash-welded SAP alloys after a fluence of 4.0×10^{20} neutrons/cm^2 ($E > 1$ Mev) indicate that irradiation does not significantly alter their tensile properties.

Stainless Steels and Nickel-Base Alloys

Results of postirradiation tensile tests[7] on 304 and 348 stainless steels are given in Table III-1. These specimens were irradiated in EBR-II to a total fluence of 1.7×10^{22} neutrons/cm^2 at about 530°C. Little difference was observed between the preirradiation and postirradiation tensile properties of the 25% cold-worked stainless steels. Irradiation influenced the tensile properties of annealed stainless steel by significantly increasing the yield strength, slightly increasing the ultimate strength, and reducing the uniform elongation. The radiation-induced trends in both 304 and 348 stainless steels were similar. In another series of tests, specimens of 316 stainless steel were irradiated in contact with sodium at 600°C in the Engineering Test Reactor (ETR) to a fast fluence of 1.4×10^{21} neutrons/cm^2. The postirradiation tensile properties of these specimens indicate that the irradiation at high temperature did not significantly alter the strength properties but both uniform and total elongation are reduced at all testing temperatures (Fig. III-8).

German investigators have irradiated stainless steel (16 wt.% chromium and 13 wt.% nickel) specimens that contained 15, 60, and 85 ppm boron.[52] These tests were undertaken to study the effect of helium generation from ^{10}B by (n,α) reaction on the tensile properties. Irradiated specimens tested at 750°C indicate that the postirradiation elongation is reduced by increasing thermal fluence as shown in

Table III-1 POSTIRRADIATION TENSILE PROPERTIES OF IRRADIATED 304 AND 348 STAINLESS STEELS[7]

Test temp., °C	Yield strength, 1000 psi	Ultimate strength, 1000 psi	Elongation, % Uniform	Elongation, % Total
Annealed AISI 304 Stainless Steel, TD*				
25	75.4	102.9	36.8	45.7
300	52.9	75.6	16.4	19.8
500	47.0	66.5	18.8	21.9
600	46.9	60.0	20.6	25.9
650	27.6	37.8	17.6	20.0
750	14.2	19.5	9.9	18.1
25% Cold-Worked 304 Stainless Steel, TD				
300	88.0	100.5	5.3	7.4
500	79.2	87.2	3.7	5.9
650	54.9	62.3	1.7	3.3
750	27.7	35.1	1.3	2.5
Annealed 348 Stainless Steel, RD†				
RT	68.5	110.5	32.9	40.0
300	52.5	76.5	14.1	17.6
500	55.8	68.8	9.4	13.0
650	36.3	44.3	5.6	6.1
750	16.2	23.2	2.1	7.2
Annealed 348 Stainless Steel, TD				
RT	69.9	102.9	31.2	37.2
300	58.0	77.6	15.1	18.0
500	23.4	61.4	33.5	36.6
550	49.0	63.2	16.6	21.5
600	45.6	55.5	13.6	17.0
650	21.2	44.9	16.4	16.5
700	29.0	32.6	5.4	9.5
871	7.2	9.2	4.3	14.5
25% Cold-Worked 348 Stainless Steel, RD				
RT	115.8	135.9	13.7	18.6
300	107.8	117.2	3.6	6.9
500	87.9	94.1	3.2	4.8
600	70.5	79.6	2.0	3.2
650	58.2	69.3	1.9	4.2
750	24.3	32.3	2.3	5.6
25% Cold-Worked 348 Stainless Steel, TD				
RT	126.2	141.8	12.9	20.4
300	105.6	114.1	4.5	9.5
500	100.9	106.1	2.9	4.5
650	66.0	72.9	1.7	2.4
750	23.6	34.3	2.1	4.2

*TD = specimens cut transverse to the rolling direction.

†RD = specimens cut parallel to the rolling direction.

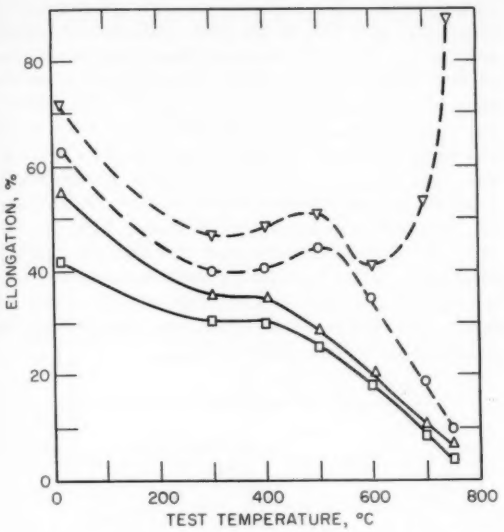

Fig. III-8 Effect of test temperature on the ductility of 316 stainless steel irradiated in a sodium environment at 600°C.[7] □ ○, uniform elongation; ▽ △, total elongation;----, as-fabricated controls; ——, irradiated.

Fig. III-9. This effect does not appear to depend on the helium that is generated from the boron by (n,α) reactions. The nondependence of the postirradiation ductility on helium content was attributed to the dual role of boron in the neutron-induced embrittlement phenomenon. The presence of boron improves the high-temperature ductility of stainless steel and promotes transgranular fracture at the expense of intergranular fracture when the steel is tested at elevated temperatures. Consequently the beneficial effects of increasing boron content tend to counterbalance the detrimental effects of the higher helium generation.

Figure III-10 illustrates the effect of carbon content on the postirradiation ductility of stainless steel at high temperatures. These results show that the post-

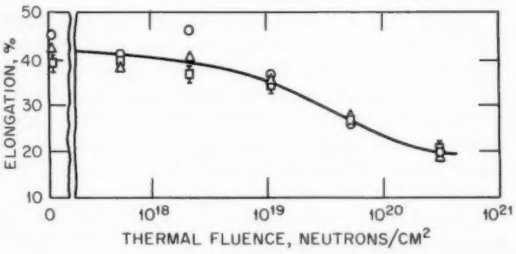

Fig. III-9 Effect of boron content on postirradiation elongation of 16/13 chromium–nickel stainless steel at 750°C.[52] □, 15 ppm boron; △, 60 ppm boron; ○, 85 ppm boron.

irradiation behavior is not influenced by carbon which is in solution. However, by aging the stainless steel that contains 0.1 wt.% carbon for 100 hr at 800°C, fine carbide particles are developed near the grain boundaries. These carbide particles are believed to improve the postirradiation ductility by containing the cracking within the interparticle spacing.

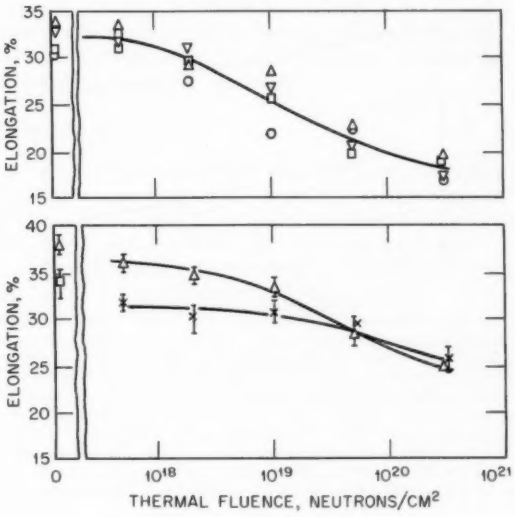

Carbon content, %	1 hr at 1050°C	1 hr at 1050°C + 100 hr at 800°C
0.004	□	○
0.028	▽	△
0.1	△	×

Fig. III-10 Effect of carbon on the postirradiation elongation of 16/13 chromium–nickel stainless steel at 750°C.[52]

The postirradiation creep ductility of 304 stainless steel at 704°C was determined as a function of calculated helium content.[35b] As shown in Fig. III-11, 304 stainless steel modified with 0.2 wt.% titanium has considerably higher postirradiation ductility than the unmodified 304 stainless steel even though it has a larger grain size. These results indicate that the modification of 304 stainless steel has a beneficial effect on postirradiation creep properties, since previous studies have shown that material with smaller grain size is more resistant to radiation-induced embrittlement.

The effect of irradiation on the stress-rupture properties of Incoloy 800 at 705°C has been investigated by General Electric.[53] The specimens were irradiated in a predominantly fast flux in EBR-II at 540°C to a fast fluence of 2.8×10^{20} neutrons/cm^2. Although the elongation at rupture is reduced by

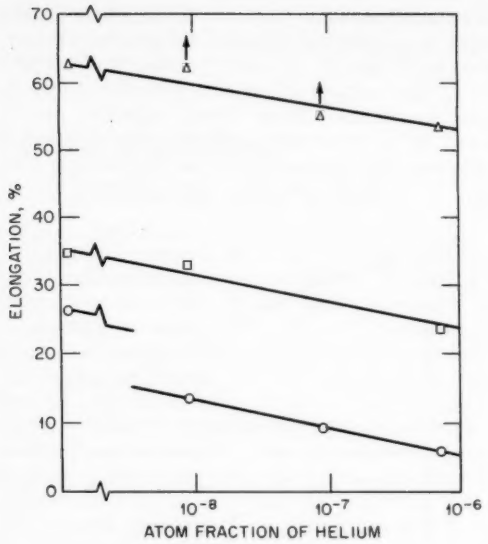

Fig. III-11 Effect of helium on the stress-rupture ductility of 304 and modified 304L stainless steel irradiated at 50°C, tested at 704°C and 15,000 psi. Arrows on points indicate that the ductility plotted was reached without failure of the specimen.[35b] ○, 304 stainless steel annealed 1 hr at 1038°C, ASTM 5 to 6 grain size; □, 304 stainless steel annealed 1 hr at 900°C, ASTM 8 to 10 grain size; △, 304L + 0.2% Ti annealed 1 hr at 925°C, ASTM 7 to 8 grain size.

irradiation, the rupture life is somewhat increased as shown in Fig. III-12. The increased rupture life of irradiated Incoloy 800 is caused by lengthening of the second-stage creep and by increased elongation in the third-stage creep.

Effect of irradiation on the stress-rupture properties of Hastelloy X at 650°C is illustrated in Fig. III-13. The rupture life at all stresses was decreased by irradiation, the decrease being less at lower

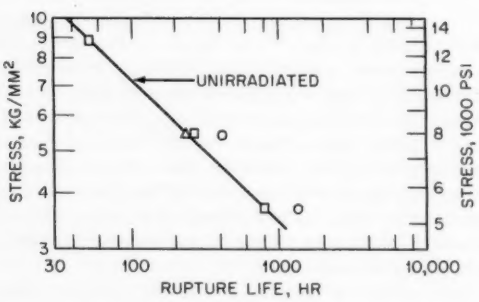

Fig. III-12 Stress-rupture properties of irradiated and unirradiated Incoloy 800 at 705°C.[53] Pretest treatment: △, mill anneal plus 214 hr at 540°C; □, mill anneal; ○, EBR-II irradiated at 540°C to a fast fluence of 2.8 × 10²⁰ neutrons/cm² (Eₙ > 1 Mev).

stress levels. Material that was irradiated in a predominantly fast flux in the EBR-II appears to behave similarly to material irradiated to a lower fast fluence in the ETR. A detrimental effect of helium on the stress-rupture properties of Hastelloy R-235 at 870°C was also noted. In these specimens the ^{10}B content was varied although the total boron content ($^{10}B + ^{11}B$) was held constant. These variations resulted in a different helium generation than in the ^{10}B-containing specimens at equivalent fluences. The test results at 870°C indicated that the rupture life was shortened by the increasing helium content. Post-irradiation re-solution annealing and aging did not result in recovery of preirradiation rupture life, but it further shortened rupture life.

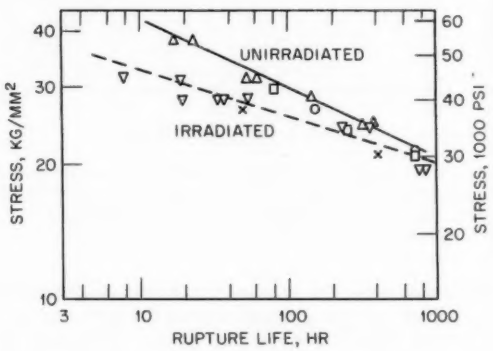

Fig. III-13 Stress-rupture properties of irradiated and unirradiated Hastelloy X at 650°C.[53] Pretest treatment: △, 100 hr at 650°C; □, solution treated; ○, solution treated plus 223 hr at 540°C; ▽, ETR irradiated at 650°C to fast and thermal fluences of 6 × 10¹⁹ and 4 × 10¹⁹ neutrons/cm², respectively; ×, EBR-II irradiated at 540°C to a fast fluence of 3.2 × 10²⁰ neutrons/cm²; ⎓ determined by least-squares fit through ▽ and △ only.

The effects[54] of irradiating to a thermal fluence of 2.3×10^{20} neutrons/cm² on the stress-rupture properties of Hastelloy N at 650 and 760°C are illustrated in Fig. III-14. The large decrease in rupture life was attributed to helium, which is generated from boron by (n,α) reactions.

Preirradiation thermomechanical treatments result in improved postirradiation tensile ductility of Hastelloy X-280 and Inconel 600.[7] Tables III-2 and III-3 illustrate the comparative postirradiation tensile properties of these alloys at 1350°F (732°C) after standard and experimental heat-treatments. These alloys were irradiated at 1250°F (677°C) to a fast fluence of 1×10^{20} neutrons/cm².

Pressure-Vessel Steels

A complete review of the effects of irradiation on pressure-vessel steels has been published.[55] The

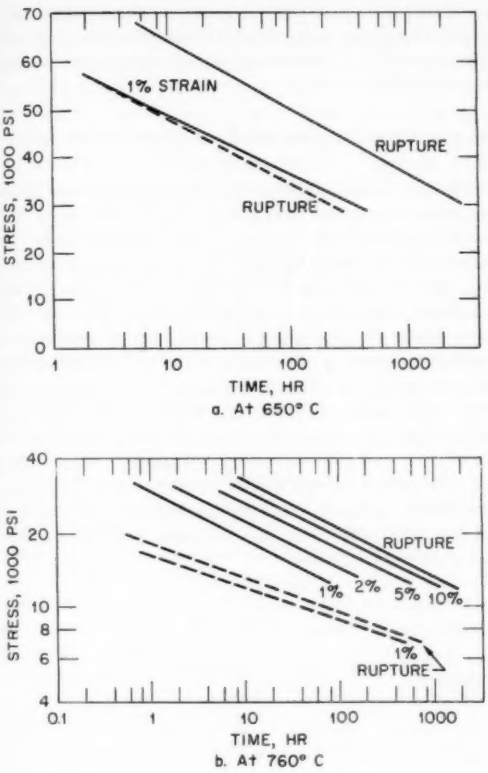

Fig. III-14 Preirradiation and postirradiation creep properties[54] of Hastelloy N. ——, unirradiated; – – –, irradiated to a thermal fluence of 2.3×10^{20} neutrons/cm².

Table III-2 IMPROVED POSTIRRADIATION TENSILE PROPERTIES[7] AT 1350°F RESULTING FROM EXPERIMENTAL TREATMENTS OF HASTELLOY X-280

Treatments	Yield strength, 1000 psi	Tensile strength, 1000 psi	Elongation, % Uniform	Elongation, % Total
Standard: 2150°F for 1 hr, air cooled	41.5	57.5	1.8	2.2
Experimental: 2150°F for 1 hr, air cooled; 1500°F for 24 hr, air cooled	38.0	63.5	5.5	6.0
Experimental: 2150°F for 1 hr, air cooled; 10% cold worked; 1500°F for 24 hr, air cooled	51.5	56.2	5.7	7.0

major emphasis was placed on the radiation-induced shift in the nil ductility temperature. The variables that affected the shift in nil ductility temperature were separated into two categories: (1) material variables, including chemical impurities, grain size, and metallurgical structure associated with welding and (2) radiation variables, including instantaneous flux, fluence, neutron spectra, and irradiation temperature. A complete section on radiation effects in pressure-vessel steels is provided in a Nuclear Safety Information Center (NSIC) report, which discusses the technology of steel pressure vessels for water-cooled nuclear reactors.[56]

Refractory Metals

The effect of irradiation on the high-temperature mechanical properties of vanadium alloys is being studied at Argonne.[57,58] Figure III-15 illustrates the tangential rupture strength of V–15 wt.% Ti–7.5 wt.% Cr alloy tubes that were irradiated in EBR-II at 550°C to a fluence of 5×10^{21} neutrons/cm². These results show that, as the testing temperature increases, the rupture strengths of the unirradiated and irradiated tubes approach each other, which indicates that some radiation damage is being annealed out at

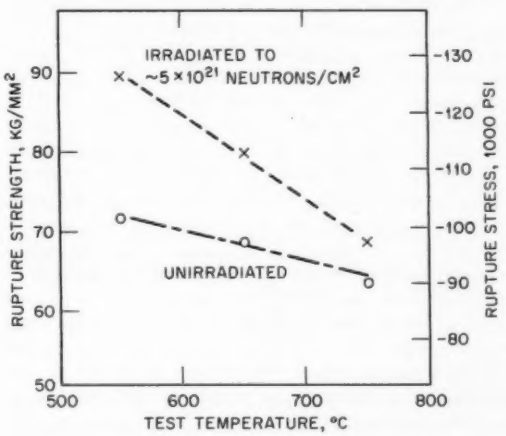

Fig. III-15 Effect of test temperature and irradiation on the tangential rupture strength of V–15 wt.% Ti–7.5 wt.% Cr alloy.[57]

Table III-3 EFFECT OF 1250°F IRRADIATION[7] ON THE 1350°F TENSILE PROPERTIES OF PRETREATED INCONEL 600

Treatments	Condition	Yield strength, 1000 psi	Ultimate Tensile strength, 1000 psi	Elongation, % Uniform	Elongation, % Nonuniform	Elongation, % Total
Standard: 2050°F for 2 hr, air cooled	Control	23.1	34.5	6.0	43.5	49.6
	Irradiated	19.1	25.0	1.2	1.7	2.9
Experimental: 2150°F for 2 hr, air cooled; 1550°F for 24 hr, air cooled; 1600°F for 20 hr, air cooled	Control	19.7	33.4	9.7	9.7	28.7
	Irradiated	12.2	24.6	6.8	2.6	9.4

the higher testing temperatures. It was also observed that no saturation of radiation-induced changes in rupture strength was reached after a fluence of 5×10^{21} neutrons/cm^2 at test temperatures of 550, 650, and 750°C. Postirradiation tensile properties of V–20 wt.% Ti and V–15 wt.% Ti–7.5 wt.% Cr alloys at 650°C are given in Table III-4. These specimens were irradiated in the EBR-II at 600°C to a fluence of 5×10^{21} neutrons/cm^2 to determine the effect of grain size on postirradiation tensile properties. The postirradiation tensile properties of V–20 wt.% Ti do not appear to depend on the grain size. Increasing the grain size of V–15 wt.% Ti–7.5 wt.% Cr alloy results in decreased strength, although the ductility is not affected.

Table III-4 TENSILE PROPERTIES AT 650°C OF VANADIUM-BASE ALLOYS IRRADIATED[58] IN EBR-II TO A NOMINAL FLUENCE OF 5×10^{21} NEUTRONS/CM^2 AT 600 ± 100°C

Composition, wt.%	Average grain diameter, μ	Yield strength (0.2% offset), 1000 psi	Tensile strength, 1000 psi	Elongation, %	
				Uniform	Total
V–20 Ti	10	71.6	98.8	17.7	24.0
	20	77.6	103	17.3	23.2
	20	74.6	97.8	16.9	22.0
	35	76.5	101	15.5	20.7
V–15 Ti–7.5 Cr	10	88.8	114	11.1	16.0
	10	92.0	117	10.7	14.8
	25	83.1	97.5	10.5	18.3
	25	85.1	103	10.5	18.4
	35	78.7	97.4	10.4	17.0
	35	80.3	97.2	10.2	16.6

Tensile properties of niobium after irradiation to a fast fluence of 2.1×10^{20} neutrons/cm^2 at 70°C reveal a significant increase in yield strength and a reduction in uniform elongation from 24.4 to 0.5% (see Table III-5).[53] Annealing of the irradiated niobium for 1 hr at 300 or 650°C results in minor recovery of preirradiation tensile properties at room temperature. However, annealing for 1 hr at 1000°C results in complete recovery of preirradiation room-temperature tensile properties. Irradiation also increases the strength and decreases the ductility of niobium in tests at 300 and 650°C.

Table III-5 TENSILE PROPERTIES OF IRRADIATED AND UNIRRADIATED NIOBIUM[53]

Condition	Postirradiation anneal	Test temperature, °C	Yield strength (0.2% offset), 1000 psi	Ultimate strength, 1000 psi	Elongation, %	
					Uniform	Total
Control	None	25	18.7	31.6	24.4	35.5
*	None	25	39.2	40.1	0.5	18.6
*	†	25	41.8	44.2	2.5	15.9
*	‡	25	33.2	41.2	5.4	13.5
Control	§	25	20.1	30.6	25.3	35.3
*	§	25	19.6	31.5	28.3	43.0
Control	†	300	21.6	28.7	9.2	13.4
*	†	300	32.7	33.0	0.4	5.9
Control	‡	650	9.8	15.3	9.0	14.7
*	‡	650	17.5	17.5	1.0	12.6

*Irradiated at reactor ambient temperature (~70°C) to fluences of 2.1×10^{20} neutrons/cm^2 ($E_n \geq 1$ Mev) and 4.7×10^{20} neutrons/cm^2 (thermal).
†1 hr at 300°C.
‡1 hr at 650°C.
§1 hr at 1000°C.

Basic Mechanisms of Radiation Damage

Transmission electron microscopy was performed on copper single crystals that had been irradiated to a fast fluence of 1.1×10^{18} neutrons/cm^2 and plastically strain fatigued at room temperature.[59] The stress necessary to produce a given strain was increased significantly by irradiation. However, beyond about 25 strain cycles, the stress required to produce a given glide strain in the irradiated crystal was found to decrease, the rate of decrease being very slow after 100 cycles. Transmission electron microscopy revealed that progressive cycling of the irradiated metal resulted in "channels" from which the radiation-induced defect clusters were swept out. The width of these channels increased with increasing number of cycles, but the rate of width increase was found to decrease.

Enhanced stress relaxation occurred in various metals and alloys under irradiation.[60] For this study, helical springs of Ni, Ti, Mo, 316 stainless steel, Nimonic 80A, and Nimonic PE16 were loaded in tension at 100°C and irradiated to a fast fluence of 3×10^{20} neutrons/cm^2. Periodic measurements were made on the springs to determine how much extension had occurred. It was found that the pure metals of titanium, nickel, and molybdenum exhibited more extension than the alloys. Saturation in the extension values occurred earlier in the annealed stainless steel than in the cold-worked stainless steel. Similar behavior was experienced by the Nimonic alloys in which the weaker solution-treated alloy reached saturation in extension earlier than the stronger heat-treated spring.

Defect clusters in irradiated tungsten were revealed by transmission electron microscopy.[61] These clusters were not observable for material which had received a fast fluence of less than 6×10^{18} neutrons/cm^2. The defect clusters, which grew into dislocation loops on annealing, are believed to account for the radiation-induced embrittlement that occurrs when tungsten is tested in tension at 400°C. Field-ion microscopic observations[62] have been made on tungsten irradiated to a fast fluence of 10^{18} neutrons/cm^2. Annealing of the irradiated tungsten indicated that excess vacancies are removed at 870°C (0.31 T_m), and the activation energy for migration of these vacancies was found to be 3.3 ev. It was further noted that vacancies do not serve as permanent sinks for defects migrating in stage III (0.15 T_m) recovery. The stage III recovery is believed to take place with a mechanism of impurity migration to dislocation loops.

Transmission-electron-microscopy examination of polycrystalline sheets of pure niobium irradiated to a fast fluence of 2×10^{18} neutrons/cm^2 revealed defects that were identified as dislocation loops.[63] The size of these defects ranged from 30 to 170 A, and their density was 5×10^{15}/cm^3. Deformation of the irradiated niobium resulted in defect-free channels that were swept clean by the moving dislocations.

Field-ion microscopy examination[64] of pure platinum irradiated to fast fluences ranging from 10^{16} to 10^{18} neutrons/cm^2 at 65°C revealed that the irradiation causes depleted zones which range from 10 to 40 A, and the concentration of these depleted zones is linearly dependent on fast fluence. No change in microstructure is noted after annealing in the stage III recovery range (50 to 100°C) for platinum. The room-temperature yield strength of irradiated platinum recovers in two distinct stages. The stage IV recovery occurs at 200 to 300°C and takes place by vacancy migration. The stage V recovery occurs by self-diffusion and takes place at 500 to 600°C. On annealing, the zones larger than 40 A collapse to form dislocation loops.

A method has been developed for predicting ductile-to-brittle transition temperatures of irradiated steels by utilizing the attenuation of stress waves.[65] Small samples (~0.2 cm^3) of irradiated material are subjected to a stress-time endurance test. The energy absorption of the unirradiated and irradiated specimens is measured at different temperatures, and curves are obtained. The higher energy absorption by irradiated materials allows correlations with increase in transition temperature to be made. Another approach has been developed where the radiation-induced shift of nil ductility temperature of pressure-vessel steels can be predicted by ultrasonic nondestructive testing techniques.[66]

A method has been developed for predicting the long-time, creep-rupture properties of alloys in a nuclear environment.[67] This method is based on dividing the rupture process into different components and predicting the effect of neutron irradiation on each component. Correlation of the proposed models to actual postirradiation stress-rupture data has resulted in reasonable agreement with predicted values. (M. Kangilaski)

Metallurgy of Refractory Metals

Niobium

Researchers at Ames Laboratory[68] showed that in the presence of liquid-metal coolants containing up to 2000 ppm oxygen, Nb–1 wt.% Zr alloy becomes contaminated with oxygen, especially at temperatures above 1000°C. The oxygen contaminant in the alloy occurs in the form of a ZrO_2 dispersion. Data are tabulated to show the effects of such oxide dispersions on various tensile properties as functions of temperature and oxygen content.

A method was developed at General Dynamics[69] for obtaining stress–dislocation–strain curves from internal-friction and modulus-defect measurements. The stress–temperature dependence showed that separate, distinctly discrete processes are operative. The activation energy for the low-temperature process (α') obtained from a separate experiment and the slope of the stress–temperature dependence led to a stress-coupling factor (activation volume) of about 1.5 cu barns. The α' process appears to be stress-assisted diffusion of individual kinks. The tendency of the slopes to approach zero as the temperature approaches zero for temperatures below 4°K is to be expected from theoretical thermodynamics.

Tensile and bending properties of niobium containing up to 8 at.% hydrogen have been determined by the Japanese.[70] The Nb–H alloys were made by heating niobium in purified hydrogen at 1 atm pressure and 450°C for several hours. Platelike and lenticular hydrides were observed in all specimens used for the experiments. The yield stress and elongation of specimens were measured at room temperature, −75°C, and −195°C. The yield stress increased gradually with increasing hydrogen content. Elongation decreased with increasing hydrogen to about half the original value in a Nb–2.05 at.% H alloy. The bend angle decreased abruptly to zero in alloys containing more than 2 05 at.% hydrogen, and alloys containing less than 1.63 at.% hydrogen showed ductile deformation in the bend test.

The Russians[71] have studied the effects of up to 10 wt.% W, Mo, Ta, Ti, Re, Pd, Zr, Cr, and Ir on the properties of niobium. Alloying in the region of the solid solutions increased the tensile strength and reduced elongation at room temperature. Additions

of Cr, Re, Zr, and Ti were the most effective. The tensile strength and elongation of the Nb–2.3 wt.% Cr alloy were about 57 kg/mm^2 and 80%, respectively. With increased concentration of Ta, W, Re, Mo, Ir, and Zr, the coefficient of linear expansion decreased, and elasticity increased. This was indicative of an increase in the forces of interatomic interaction. At 1100°C the Nb–2.3 wt.% Cr alloy was somewhat superior to the Nb–10 wt.% Mo alloy on the basis of tensile strength and elongation.

To study the effect of nitride precipitation in niobium and Nb–Zr alloys, the University of Illinois[72] equilibrated wires of the two materials with pure nitrogen at high temperatures. Room-temperature hardness was correlated with the alloy composition, heat-treatment, and microstructure. Hardness was found to be most sensitive to the amount of nitrogen in solution; however, a significant hardening up to 500 DPH took place upon aging of quenched alloys. A coarse dispersion of nitride did not significantly increase the hardness of the material though the nitride was found to have a hardness of 1400 KHN. High-nitrogen alloys cleaved on (1 0 0) planes and had negligible ductility. Precipitation occurred in either a discontinuous or a continuous fashion, depending on the composition and cooling rates. Upon cooling, the precipitation first proceeded discontinuously by the nucleation of nitride needles at subboundaries and subsequent growth of a two-phase microconstituent. At lower temperatures, continuous precipitation occurred in the subgrain interior ahead of the discontinuous precipitation interface.

Tantalum

At the University of Liverpool,[73] high-purity tantalum single crystals were deformed in compression at various temperatures and strain rates. The shape of the stress–strain curve was strongly dependent on orientation but, for certain orientations over a narrow range of temperatures and strain rates, the curve could be divided into three stages. The work-hardening rates for the various stages were determined and compared with those obtained by other workers. Strain-rate-change and temperature-change experiments were evaluated to yield values of activation energy and activation volume. The values obtained were comparable with those obtained in other investigations on polycrystalline tantalum or on single crystals where three-stage hardening was not observed.

Molybdenum

High-frequency fatigue tests were conducted at TRW Inc.[74] in a high-vacuum environment on the recrystallized molybdenum-base alloy TZC at 1800 to 2200°F (982 to 1204°C). The results indicated that no well-defined endurance limit existed in this temperature range. Fatigue strengths at 2200°F and 10^9 cycles were as low as 16,000 psi. The application of a cyclic load to a statically loaded specimen produced a marked acceleration in the degree of specimen extension. This increase was characterized by a relatively rapid extension during the first 30 min of testing followed by a period of steady-state creep that was approximately two orders of magnitude greater than the creep rate observed under a comparable static peak stress.

The creep properties of molybdenum have been investigated by the British.[75] Pure molybdenum sheets, 0.04 in. thick, prepared from both arc-cast ingot and sintered slab, were creep tested at 650 and 750°C in both the recrystallized and stress-relieved conditions. Sheet made from sintered stock had a better creep resistance than that made from arc-melted material.

So that dislocations could be observed, molybdenum crystals deformed in direct shear on the $(1\bar{1}0)$ [1 1 1] system were examined by transmission electron microscopy at Rice University.[76] The dislocation structures and dislocation and jog densities were determined as a function of shear strain and deformation temperature at 78 to 373°K. The mobility of edge dislocations was greater than that of screw dislocations, but this difference was diminished with increased temperatures and strains. Motion of screw dislocations was impeded by jogs, and conservative motion of these jogs at higher temperatures helped to relieve this immobility. The flow stress was a linear function of the square root of the dislocation density. Though no cells tended to form, tangling was pronounced at all temperatures, and it appeared that the tangles originated at small precipitates and at the grown-in dislocation network.

Tungsten

Workers at Cornell University[77] showed that the mechanical properties of tungsten are sensitive to the grain structure and composition as well as to the temperature and strain rate during testing. The effect of the degree of misorientation (mosaic spread) between grains on the resolved shear stress at the proportional limit was studied. The stress increased with mosaic spread in the range of misorientation where the grain-boundary structure changed from low angles (2°), where it is best described by simple dislocation models, to high angles (10°) where it is characterized by high atomic misfit. The Petch slope calculated from the experimental data using a $\sqrt{\theta}$ dependence of the Petch slope on the misfit angle θ agreed to within an order of magnitude with those predicted theoretically. Deviations from the theoretical were attributed to stabilization of the boundary by interstitial impurity elements.

The addition of 3 wt.% rhenium to tungsten decreased the shear modulus from 19.6 to 16.1 × 10^6

psi. Carbon additions did not change the modulus of the pure tungsten, but 70 ppm carbon increased that of the alloy to 18.7×10^6 psi. These changes in modulus were attributed to changes in the electronic structure of the metal upon alloying. Differences in the behavior of carbon in the pure tungsten and the alloy were related to an increased carbon solubility in the alloy which in turn is a function of the electronic structure of the metal.

The Matsushita Electronics Corporation[78] conducted X-ray diffractometer studies of the deformation texture in drawn tungsten wires. Experimental results showed that the diffraction intensities were equal to those predicted from the (1 1 0) fiber texture, but the angular spreads of diffraction peaks in the pole distribution curves were different for different diffraction planes and directions. For this reason a modified (1 1 0) fiber-texture model, in which a kind of anisotropy is assumed, was proposed to explain the results. According to this model, the poles lying on a line directing from the $(1\,\bar{1}\,0)$ to the $(\bar{1}\,1\,0)$ poles in the (1 1 0) standard stereographic projection should show spreads which are different from those lying on a line directing from the (0 0 1) to the $(0\,0\,\bar{1})$ poles, which is confirmed by the experiments. The anisotropy and the spreads of the pole positions were large at the outer part of the wire but decreased gradually toward the inside of the wire. The possibility of the occurrence of such anisotropy in metals with fcc structures was discussed.

An electron fractographic technique was used to study grain-boundary cavities formed in tungsten under creep conditions.[79] At low temperatures and high stresses, the cavities were shallow and irregularly shaped, whereas at low stresses and high temperatures, they acquired regular, polyhedral shapes. Growth by slip, grain-boundary sliding or stress-induced vacancy diffusion, and internal rearrangement by surface diffusion were mechanisms contributing to these structures. Triple grain junctions were not preferred sites of cavity nucleation.

The shapes of grain-boundary gas bubbles and creep voids in tungsten were studied by stereo electron fractography.[80] Bubbles and voids were polyhedral, being bounded by (1 0 0), (1 1 0), (1 1 2) and (1 0 2) faces with the (1 0 0) and (1 1 2) faces being smooth but terraced, the (1 0 2) faces stepped, and the (1 1 0) faces rough. No terracing, stepping, or roughness was observed on creep cavities. Relative surface tensions measured on small bubbles were approximately $\gamma(1\,0\,0):\gamma(1\,1\,2):\gamma(1\,1\,0) = 1.00:1.05:1.08$. The discrepancies between these values and the predictions of theoretical models may be due to absorption of the unidentified gas phase in the bubbles. Other features of the bubbles can be explained by considering the kinetic processes involved in changing the size and shape of the bubbles and by postulating that the (1 1 0) faces are not real crystallographic planes. (J. Lombard)

Metallurgy of Common Cladding and Structural Materials

Aluminum and Magnesium Alloys

Considerable interest has been shown in Al–Al_2O_3 alloys (SAP) as possible cladding materials for heavy-water-moderated reactors. A summary describing fabrication, mechanical properties, corrosion and compatibility, joining, forming, and in-pile behavior of SAP alloys has been issued by the Danish.[81] Also discussed are attempts to improve the performance of SAP alloys by further alloying and by changing the Al_2O_3 particle distributions. A bibliography on dispersion-strengthened materials, with special emphasis on SAP alloys, has also been issued.[82] Abstracts of 445 different papers that became available during 1965 are contained in this reference.

The stress-rupture properties[51b] of Al–6 wt.% Al_2O_3 which was fabricated from 4-μ aluminum powder have been determined at 400°C. In an attempt to improve the elongation at rupture, particles of 22-μ aluminum powder were incorporated into some specimens. Incorporation of the large aluminum-powder particles resulted in reduced rupture life and reduced elongation. The low ductility of Al–Al_2O_3 alloys at high temperatures was attributed to the presence of fine Al_2O_3 in the matrix and was independent of grain size.[83]

Testing atmosphere has shown a marked influence on the creep strength of heat-treated Magnox ZR-55 (Mg–0.5 wt.% Zr) at high stresses.[84] Hydrogen pickup originating from water vapor in air resulted in the formation of zirconium hydrides that strengthened the material and reduced the creep rate compared with the usual creep rates of the alloy in CO_2. However, at low stresses, no atmospheric effect was observed and the data suggest that diffusion creep is the predominant mode of deformation. The creep rates of Magnox ZR-55 in air and dry CO_2 are illustrated in Fig. III-16.

Zirconium Alloys

Stress orientation of zirconium hydride platelets in Zircaloy tubing was found to be greatest in the directions in which the major fabrication strain had been contractile.[85] Conversely, very little stress orientation was exhibited in directions in which the major strain had been tensile. Thus the stress-orientation effect should be most prevalent in the circumferential and radial directions of reduced tubing, in the longitudinal and radial directions in expanded tubing, and in the thickness direction in rolled plate. The stress required to orient the hydrides was considerably less for hot-reduced tubing

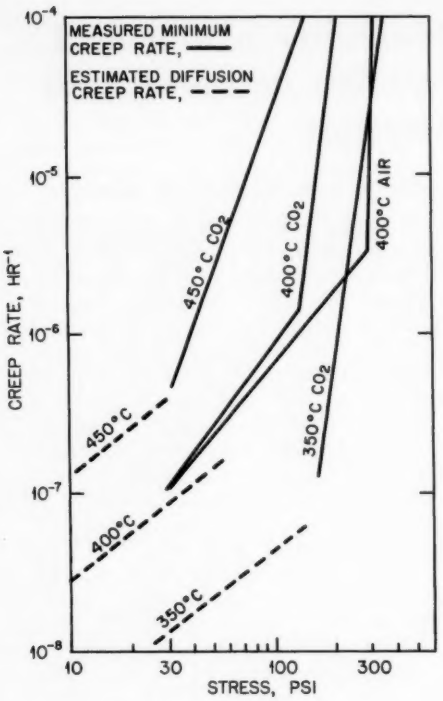

Fig. III-16 Effect of stress and atmosphere on creep rates of Magnox ZR-55 at various temperatures.[84]

than for cold-worked tubing as shown in Fig. III-17. The texture in cold-worked tubes was found to have no measurable effect on the hydride orientations.

A dependency of the distribution of hydride-platelet orientation in Zircaloy on the sign and magnitude of the three-dimensional strain history prior to platelet formation was observed.[86] It was suggested that the orientation of hydride platelets was controlled primarily by a critical dislocation structure produced by compressive deformation of the zirconium matrix by basal slip. Figure III-18 illustrates the degree of hydride orientation that is expected from the various fabrication processes.

The effect of circumferentially aligned hydrides (100 ppm) on the failure of 25-mil-thick Zircaloy-2 tubing has been investigated.[87] The hoop stress at failure was not affected by hydrogen, but the ductility at failure was significantly reduced at test temperatures below about 150°C.

Attempts have been made to improve the properties of Zr–1 wt.% Cu by small additions (0.5 wt.%) of numerous elements.[88] Specifically, Be, Ti, Cr, Fe, Ni, Co, misch metal, Al, Si, As, Ag, Cd, Sb, and Te were added to the alloy. Specimens were cast, hot worked at about 850°C, solution annealed at about 880 to 890°C for 40 min, quenched, and finally cold rolled about 80% into 20-mil-thick sheet. Properties of the specimens in various stages of fabrication were examined. Hardness and tensile strength were generally increased and the ductility was decreased, with the maximum effect being obtained by additions of Ti, Cr, Co, and Si. Decreases in hardness and strength were caused by additions of antimony and misch metal. Oxidation was improved by all elemental additions with the exception of tellurium. The optimum properties of high strength and improved heat resistance were obtained by additions of chromium, cobalt, and silicon.

A British patent has been issued for a ternary zirconium alloy suitable for use in pressurized CO_2-cooled reactors.[89] The composition of the alloy is 0.5 to 6 wt.% copper and a total of 0.1 to 5 wt.% of at least one of the following elements: Mg, Ce, Pt, and Mn.

The hardening characteristics of Zr–0.5 wt.% Nb–1.0 wt.% Cr have been determined.[90] Alloy specimens were quenched from 850, 900, and 950°C and then tempered between 400 and 700°C. Quenching from the highest temperature resulted in the largest hardenability, whereas tempering at the highest temperature (700°C) resulted in the most softening. The hardening was attributed to the martensitic transformation accompanied by solute hardening of the

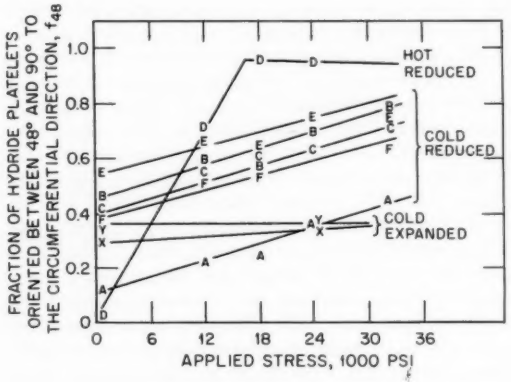
FRACTION OF HYDRIDE PLATELETS ORIENTED BETWEEN 48° AND 90° TO THE CIRCUMFERENTIAL DIRECTION, f48
APPLIED STRESS, 1000 PSI
HOT REDUCED
COLD REDUCED
COLD EXPANDED

Tubing designation	Fabrication processes
A	Tube reduced, then roll formed
B	Tube reduced*
C	Tube reduced*
D	As extruded (no cold work)
E	Mandrel drawn
F	Swaged, then tube reduced
X	Tube reduced, annealed, then cold expanded
Y	Tube reduced, annealed, then cold expanded

*Different manufacturers.

Fig. III-17 Effect of applied stress in circumferential tubing direction on hydride orientation.[85]

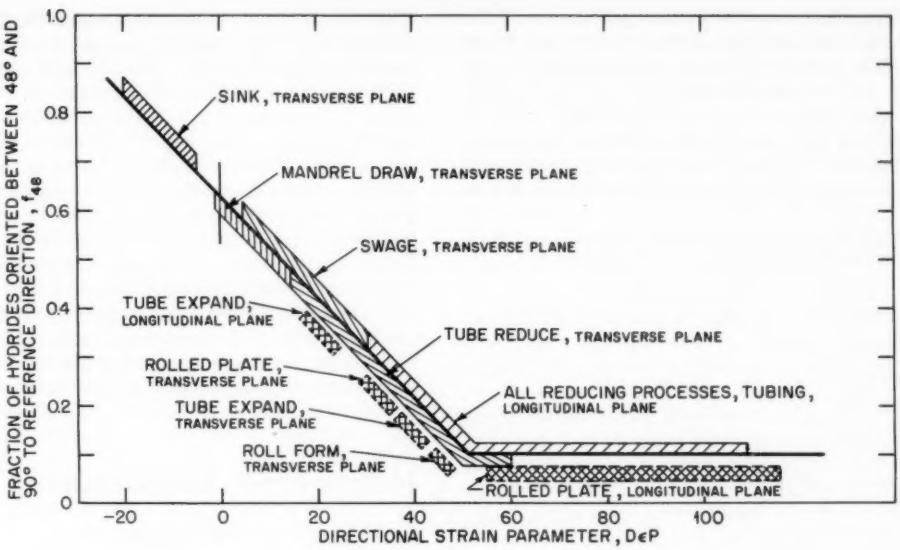

Fig. III-18 Hydride orientations predicted for Zircaloy fabrication processes.[86]

chromium. The softening of the material upon tempering was due to the precipitation of $ZrCr_2$ particles. Figure III-19 illustrates the tensile properties of specimens that were water quenched from 900°C and tempered for 24 hr at 500°C before testing.

Pressure-Vessel Steels

All aspects of pressure-vessel technology for water-cooled reactors have been reviewed by the Nuclear Safety Information Center (NSIC) at Oak Ridge.[56] Pressure-vessel features, environmental and service conditions, materials, and effects of corrosion, temperature, hydrogen embrittlement, and radiation on the materials are discussed, along with basic aspects of crack growth and fracture. Also included are details of design, fabrication, testing conditions, and quality-assurance procedures for pressure-vessel fabrication.

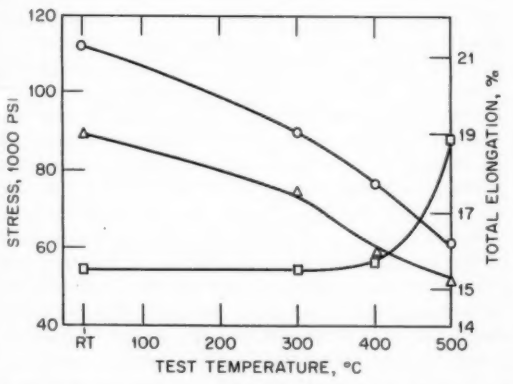

Fig. III-19 Tensile properties[90] *of Zr−1 wt.% Cr−0.5 wt.% Nb alloy water quenched from 900°C and tempered for 24 hr at 500°C. ○, ultimate tensile strength; ◇, 0.2% offset yield strength; □, % elongation.*

Stainless Steels

The effect of $\gamma'(Ni_3Ti)$ particle size on the creep rate of A-286 stainless steel has been investigated by the British.[91] The minimum creep rate at 650°C under a stress of 36,000 psi was obtained with a particle radius of 50 to 60 A. The decreasing creep rate with increasing particle size (for particle sizes less than 50 A) was predicted by assuming that the dislocations push the particles ahead of them. Increasing creep rate with increasing particle size (above 50 to 60 A) occurs when the particles are sufficiently large that dislocations are no longer pinned.

Attempts were made to develop a stainless-steel dispersion containing fine (0.1 to 0.5 μ) Al_2O_3, ZrO_2, TiO_2, or MgO particles to eliminate or minimize the radiation-induced embrittlement at high temperatures.[92] Both direct sintering of the mixed powders and internal oxidation of an Fe−Cr alloy containing aluminum, titanium, and zirconium were examined. A ferritic matrix of Fe−Cr alloy was employed because of its tendency to fracture transgranularly instead of intergranularly as do austenitic stainless steels at high temperatures. Difficulties were encountered with chromium additions, and therefore the

oxides were dispersed in a pure-iron matrix. Table III-6 shows the tensile properties of the various iron dispersions at 700°C. These results indicate that, although the strongest dispersions are significantly weaker than austenitic stainless steel, they are stronger than pure iron produced by powder metallurgy. Further improvements in strength can be expected by incorporating chromium into the dispersion.

Table III-6 TENSILE TESTS AT 700°C ON IRON COMPACTS CONTAINING VARIOUS DISPERSIONS[92]

Dispersion	Ultimate tensile strength, psi	Elongation, %
2 vol.% Al_2O_3	7,400	12
4 vol.% Al_2O_3	9,300	12
2 vol.% ZrO_2	4,300	12
4 vol.% ZrO_2	5,700	11
2 vol.% TiO_2	6,800	25
4 vol.% TiO_2	6,100	31
2 vol.% MgO	7,600	22
None	3,800	16
304 stainless steel	35,000	35

Nickel-Base Alloys

Improved resistance to radiation-induced embrittlement in Hastelloy N has been achieved by additions of about 0.5 wt.% titanium.[93] Aging the titanium-modified alloy for 500 hr at 1200 and 1400°F (649 and 760°C) had a minor effect on the tensile properties at 1200°F. The only consistent change was an increase in ultimate tensile strength for all cases. Optical metallography showed the alloy to be free of precipitates; however, electron microscopy revealed the presence of a very thin and fine precipitate at the grain boundaries. Electron-diffraction studies indicated that these precipitates consisted of two distinct phases, one of the phases being Ti_2O. Lattice-parameter measurements indicated that the second phase was either TiN or TiB, but chemical analysis showed the boron and nitrogen contents to be too low for significant precipitate formation.

Additions of about 0.5 wt.% zirconium to Hastelloy N also improve the postirradiation ductility, but the presence of zirconium caused weld-metal cracking during cooling of the heat-affected zone (HAZ). Reduction of the molybdenum content from 16 to 12 wt.% yielded significant improvements in weldability. It was possible to predict the creep behavior of Hastelloy N in the temperature range of 600 to 1050°C by use of stress-relaxation data.[94] The agreement of the predicted data with experimental creep data indicate that this method can be used for design if adequate experimental data are not available.

The effect of adding 0.005, 0.010, 0.05, and 0.1 wt.% boron on the tensile behavior of pure nickel has been determined.[95] Tests on vacuum-melted alloys at 20 to 700°C showed that boron enhances the interatomic bonding forces in the lattice and reduces the diffusion mobility of atoms and vacancies. Boron additions were also found to increase resistance to plastic deformation, especially to creep deformation. The recrystallization temperature and rate of grain growth were significantly increased by boron additions. It was noted that boron collects at the grain boundaries of nickel, where it enhances the strength of the grain boundaries by neutralizing the harmful effect of other impurities. The strengthening of the grain boundaries was believed to be the reason why boron-containing nickel exhibits ductile transgranular fractures in creep, whereas the nonboron-containing nickel alloys fail by brittle intergranular fracture. The highest plasticity was displayed by nickel that contained 0.01 wt.% boron. Increasing the boron content to higher levels resulted in embrittlement, which was caused by intermetallic boride particles.

(M. Kangilaski)

Nonfueled Refractories

Fabrication and Properties

The fabrication and characterization of hot-pressed TaC were studied by Leipold and Becher.[96] Carbide compacts from several commercially available powders were vacuum hot pressed at temperatures to 2420°C and at pressures to 10,000 psi. Densification did not appear to be diffusion controlled, and some evidence suggested plastic deformation as a possible controlling process. An impurity grain-boundary phase of Ta_2O_3 was observed, as were variations in the Ta/C ratio within a given compact.

Three British patents[97-99] were issued describing methods of preparing refractory powders and fabricating refractory materials. A process for producing finely powdered nonpyrophoric carbides of B, Si, Ti, Zr, Hf, Nb, Ta, Mo, W, Th, and V by subjecting gaseous halides of the elements to hydrocarbon reactions at 2000 to 5000°C is the subject of one patent.[98] Another patent[99] concerns a method for sintering refractory nonfissile metal carbides or nitrides by compacting in an inert-gas atmosphere containing less than 20 ppm and 10 ppm each of oxygen and water vapor. A process is also described[99] for the production of refractory compounds consisting of a metallic portion and a nonmetallic portion in which the metallic portion is V, Ti, Th, Nb, Zr, Hf, W, Mo, Ta, U, Pu, or Si and the nonmetallic portion is a nitride, boride, phosphide, silicide, or sulfide. Oxide particles of the metallic portion of the compound are reacted with carbon or with a carbon-containing material in a fluidized-bed reactor to form the carbide, which is then reacted in a fluidized-bed reactor with a substance consisting of or containing the nonmetallic portion of the refractory compound.

Riley[100] developed characterization techniques for selecting and procuring carbide powders. The purity,

density, particle shape, particle size, and specific surface area of various carbide powders were examined. The morphological types of structures observed in commercial NbC, TaC, and ZrC powders are discussed.

Keilholtz and Moore[101] have studied the behavior of various refractory nonfissile materials under irradiation. The volume expansions of several carbide materials at both low and high temperatures are plotted in Fig. III-20 as a function of fast-neutron fluence (>1 Mev). The very large shrinkage of TaC was suggested to be a consequence of the transmutation of tantalum to tungsten by slow neutrons. There was virtually no gross damage to the specimens irradiated at high temperature. In previous irradiations at low temperature, the carbides of zirconium, tantalum, and niobium sustained minor to severe fracturing after irradiation to fluences greater than $\sim 2 \times 10^{21}$ neutrons/cm^2. The volume expansion was much less in these high-temperature irradiations, and some shrinkage was observed. Despite the fact that the irradiation temperature (~1000°C) was relatively low compared with the melting points of the carbides, it is suggested that in-reactor annealing out of gross damage and dimensional changes occurs. Rapid diffusion within the specimens, as indicated by bonding of adjoining specimens in some cases, would anneal out some of the point defects as they were being produced by fast-neutron irradiation. Shrinkage during irradiation has also been observed in graphite.

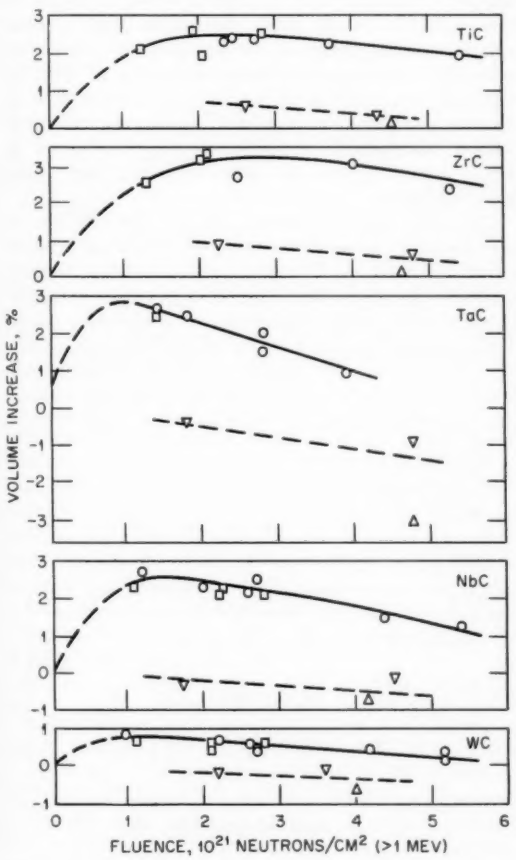

Fig. III-20 Gross volume increase of monocarbides of Ti, Zr, Ta, Nb, and W as a function of the fast-neutron fluence.[101] Hot pressed: ○, 300 to 700°C, △, 1000°C. Slip cast: □, 300 to 700°C, ▽, 1000°C.

Nitrides of Zr, Ti, Ta, and Nb irradiated at ~150°C to fast fluences ranging from 0.7 to 4.9×10^{21} neutrons/cm^2 did not show a volume dependence on fluence. The specimens of TiN and NbN expanded in volume 2 to 3%, and those specimens of ZrN which could be measured expanded by 3%. The nitrides of titanium and niobium generally withstood the fast-neutron irradiation up to $\sim 3.8 \times 10^{21}$ neutrons/cm^2 without fracturing. Severe fracturing occurred in most of the specimens of these nitrides at the higher fluences. All the nitride specimens of tantalum and zirconium fractured during irradiation.

Disilicides of Zr, Ti, Ta, and W were irradiated to fluences of 0.4 to 2.7×10^{21} neutrons/cm^2. Dimensional changes were much smaller than those observed in the corresponding monocarbides. Zirconium disilicide expanded in volume by ~0.7% over the entire range of fluences. The expansion of titanium disilicide was ~0.8% at the low fluence, but above 1.5×10^{21} neutrons/cm^2 the expansion was not so great, being only 0.3% at 2.6×10^{21} neutrons/cm^2. Tantalum disilicide specimens expanded in volume by approximately 1% over the range of the experimental conditions. The disilicides of zirconium and titanium were generally undamaged at fluences up to about 2×10^{21} neutrons/cm^2, but nearly all specimens receiving higher fluences were severely fractured.

At low temperatures (300 to 600°C) and at a fast fluence of approximately 2.3×10^{21} neutrons/cm^2, grain-boundary separation occurred in Al_2O_3. The volume increases for irradiated Al_2O_3 samples are reported in Fig. III-21.

Researchers at Los Alamos[102] investigated the effect of stoichiometry on the thermal expansion of TaC_x. The X-ray thermal expansion of TaC_x was measured over the composition range from $TaC_{0.789}$ to $TaC_{0.997}$ at temperatures to 1000°C. The average thermal-expansion coefficient increased with increasing formula weight: e.g., from 25 to 1000°C, the values were 6.04, 6.37, and 6.96×10^{-6}/°C for $TaC_{0.789}$, $TaC_{0.912}$, and $TaC_{0.997}$, respectively.

Leipold and Nielson[103] studied the mechanical behavior of tantalum carbide and magnesium oxide. Data for $TaC_{0.93}$ indicated a fracture stress of approximately 25 kg/mm^2 (35,000 psi) and a Young's modulus of 2.8×10^4 to 2.9×10^4 kg/mm^2 (39×10^6 psi). Numerous failures in the end section of hot-

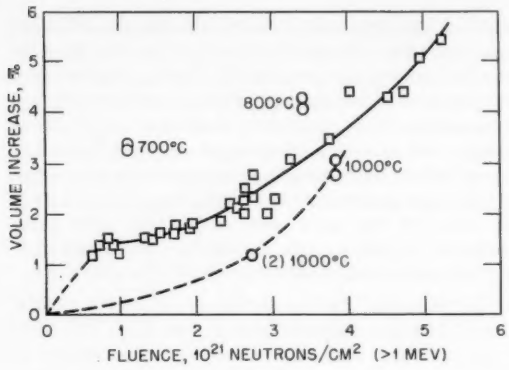

Fig. III-21 Volume increase of irradiated specimens of translucent alpha Al_2O_3 (99.8% of theoretical density) as a function of fluence.[101] □, low temperature (300 to 600°C); ○, high temperature (as indicated).

press welded MgO test samples indicated a need for improved fabrication techniques.

Several Russian investigators[104] measured the thermal and electrical conductivity of hot-pressed ZrC, HfC, NbC, and TaC at 1370 to 3270°K. In all carbides, apart from NbC, the increase in thermal conductivity with temperature was linear. The electric resistivity also increased with temperature, but the values were somewhat higher than published data. This apparently can be explained by the deviation from stoichiometric composition. (W. C. Chard)

Structure and Phase Relations

McDaniel and Schneider[105] investigated the phase relations between PdO and the rare-earth sesquioxides in air by X-ray diffraction techniques after various heat-treatments. The results indicate that palladium oxidizes in air at moderate temperatures and dissociates reversibly at 800 ± 5°C at 1 atm pressure. The pseudobinary system Nd_2O_3–PdO that exemplified the typical reaction is shown in Fig. III-22. Three compounds $2Nd_2O_3 \cdot PdO$, $Nd_2O_3 \cdot PdO$ (metastable), and $Nd_2O_3 \cdot 2PdO$ occur in the system. The 2:1, 1:1, and 1:2 compounds, of unknown symmetry, dissociate or decompose at 1135, 860, and 1085°C, respectively. Above 1135°C the system corresponds to the Nd_2O_3–Pd binary system. No further reaction appears to take place between Nd_2O_3 and Pd up to 1300°C. Similar-type compounds were found to exist in other rare-earth sesquioxide–palladium oxide systems. Other systems investigated included Sm_2O_3–PdO, Eu_2O_3–PdO, La_2O_3–PdO, Gd_2O_3–PdO, Dy_2O_3–PdO, Ho_2O_3–PdO, Y_2O_3–PdO, Er_2O_3–PdO, Tm_2O_3–PdO, and Yb_2O_3–PdO.

The solid-phase reactions among borides, refractory metals, and ZrO_2 were investigated by Samsonov and Strashinskaya.[106] Metallographic analysis and microhardness measurements were used to evaluate the interaction between compacted Nb, Ta, Mo, and W and TiB_2, ZrB_2, TaB_2, Mo_2B_5, and W_2B_5 powders at 1000 to 2000°C in a vacuum of 5×10^{-2} mm Hg. The ZrB_2 interacted with metals at 1200°C, TaB_2 at 1400 to 1500°C, and Mo_2B_5 and W_2B_5 at 1300 to 1800°C. The TiB_2 was the most resistant boride in contact with the metals, with interactions occurring from 1400 to 1800°C.

Morgenthal[107] reviewed the elevated-temperature properties of intermediate compounds of the transition elements of Groups IV, V, and VI with C, B, N, and Si. The oxidation resistances of titanium carbides, chromium carbides, and zirconium carbides, nitrides, borides, and silicides under various conditions and various temperatures, with different percentages of binder metals, were determined. The experiments showed that sintered parts of CrC with nickel as the binder may be used to 1100°C and with short-time exposures to 1200°C. If specimens annealed at 1000°C are quenched in ice water, the oxide layer formed adheres permanently as no changes are observed after 100 cycles of alternating exposure to 1000°C, followed by a cold-air blast. Oxidation resistances of commercial compositions were tabulated, together with a comparison of the corrosion resistances in acids and NaOH of chromium carbides and other hard materials.

The X-ray line broadening measurements by Gillies and Lewis[108] have shown that ionic materials, such as alkali halides and metal oxides, may be heavily strained by ball milling. This work has been extended to compounds containing atoms in interstitial sites. These studies included some of the carbides of Ti, Zr, Ta, U, Nb, Mo, and W. Ball milling produced strain comparable to that observed after ball-milling the parent metal, and, in some instances, the induced

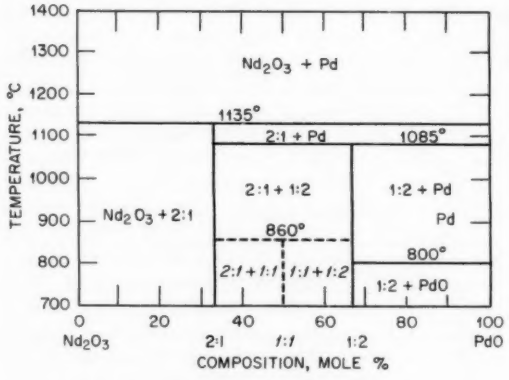

Fig. III-22 Phase equilibrium diagram for the Nd_2O_3–PdO system in air.[105] Dotted lines indicate metastable 1:1 compound and decomposition temperature. Italic lettering indicates metastable phase assemblages.

strain was removed by annealing. The induced strain has been compared with the free energy of formation as a parameter of bond strength. The presence of oxygen in the lattice causes some carbides to lose cubic symmetry.

The structures of the orthorhombic beta-prime phase of Nb_2C and V_2C and conditions for stabilizing them were defined by Aliamovskii et al.[109] The introduction of small impurities of nitrogen and oxygen promotes the rearrangement of the hexagonal lattice of the lower carbides into the orthorhombic phase.

The vaporization behavior of Mo_2C, reported by Fries[110] was investigated over the temperature range 2125 to 2550°K, by Langmuir experiments using an induction-heated, ultrahigh-vacuum microbalance. As shown in Fig. III-23, a congruently vaporizing composition of $MoC_{0.49}$ was found at temperatures from 2250 to 2300°C. It was found that the total evaporation rate increases and the heat of vaporization decreases as the C/Mo ratio decreases from 0.49 to 0.44. A mass-spectrometric examination of the evaporate from $MoC_{0.49}$ did not show any Mo_xC_y molecules; therefore evaporation by decomposition is assumed. If monatomic gaseous species and unit evaporation coefficients are also assumed, the pressures over $MoC_{0.49}$ are:

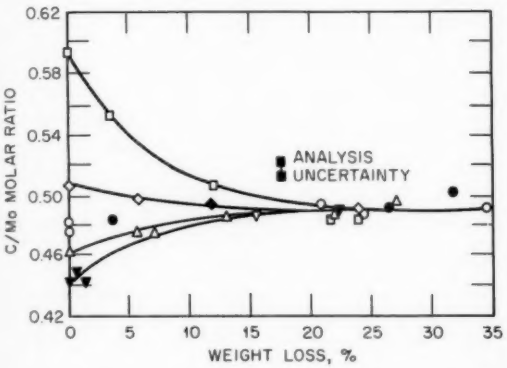

Fig. III-23 Composition of Mo_2C as a function of initial composition and amount of material evaporated.[110] Open points, 2300°C; solid points, 2250°C.

$$\log P_{Mo}\ (atm) = 7.112 \pm 0.139 - (3.420 \pm 0.333)(10^4/T)$$

$$\log P_{C}\ (atm) = 6.351 \pm 0.139 - (3.420 \pm 0.033)(10^4/T)$$

The errors quoted are standard deviations. The heat of formation at 298°K of $MoC_{0.49}$ is −4.9 kcal/mole from third-law calculations, which is in good agreement with the −5.5 kcal/mole measured calorimetrically.

The effects of carbon activity on alloying Mo_2C with iron and nickel were studied from 600 to 900°C by the Russians.[111] Partial free energies, enthalpies, and entropies for various carbon contents were determined. It was shown that the thermodynamic properties of carbon in Mo_2C change on alloying even at concentrations less than 1 at.%.

Bartlett[112] observed the growth parameters of mixed solid-solution boules grown with 40 wt.% HfC−60 wt.% TaC and 20 wt.% HfC−80 wt.% TaC starting powders. These boules were polycrystalline, with little change in metal ratio for the 20/80 composition; however, the hafnium content of the 40/60 composition reduced the total metal content to 35%. A few long HfC boules were grown with large single-crystal sections, as determined by X-ray diffraction. These boules were grown at 5 to 10 cm/hr and contained subgrain boundaries.

(J. D. Weyand)

Ceramic Technology

The control of grain size independent of density has received major effort in ceramic-materials development because their mechanical strength, creep resistance, and stability under neutron irradiation depend critically upon microstructure. It has been possible, by special preparation of starting material, control of forming conditions, or firing schedules and atmospheres, to achieve adequate control for some ceramics. However, a more general approach to control is through the use of additives. The additive may enter into solid solution in the matrix and, by segregation at grain boundaries, influence grain growth, or it may exist as discrete, dispersed particles that impede grain-boundary movement (grain growth). The latter has received relatively little experimental effort and attention.

An excellent review and analytical discussion of grain growth in ceramics was presented by Woolfrey.[113] Conditions for grain-size stabilization of normal grain growth were derived using a Zener-type analysis for random dispersions and for the case in which all dispersed particles are located at specific sites upon a grain boundary. The results of this analysis give the following relations for stabilization:

Random dispersion:

$$V_f = 0.3\ (d/D)$$

All particles located at grain boundaries:

$$V_f = 0.6\ (d_2/D_2)$$

All particles located at triple grain edges:

$$V_f = 1.86\ (d_3/D_3)$$

Here V_f is the volume fraction of dispersed spherical particles, d = is the diameter of dispersed spherical particles, and D is the grain diameter. It was concluded that discontinuous grain growth cannot be stabilized by second-phase particles, but nucleation

(of discontinuous growth) may be prevented by stable second-phase particles. The second-phase particles must either be relatively large or be present in a large quantity.

Maximum stability of dispersed-phase particles is needed for stabilization of normal grain growth. Instability may (1) permit discontinuous grain growth to develop, (2) result in solution of cation or anion components of the particles in the vicinity of pores and grain boundaries, which affects the vacancy concentration gradient, and (3) yield a liquid phase and result in liquid-phase sintering. The chief factors given for promoting stability of the dispersed phase are high free energy of formation, large particle radius, high density of the dispersed phase, low values of the diffusion coefficients of the components of the dispersed phase in the matrix, low interfacial energy between the dispersed phase and matrix, and increased complexity of the crystal structure of the dispersed phase.

The specific case of grain-size stabilization in the BeO matrix of a dispersion-type fuel element was cited. Considering both the dispersed-phase grain-refinement criteria and the nuclear requirements, the most applicable materials for dispersion were silicon carbide, oxide sols, and colloidal platinum.

Jorgensen and Anderson[114] studied the densification of yttria by conventional means. They found that a thoria addition inhibited grain growth during sintering and permitted the sintering process to proceed to near-zero porosity. The inhibition was accomplished by the segregation of ThO_2 at the grain boundaries, causing a decrease in grain-boundary mobility. Specimens were pressed isostatically at 50,000 psi, and sintered in hydrogen at 2000°C.

Sandia[115] described a process for preparing transparent (i.e., theoretically dense) yttrium oxide polycrystalline ceramics. The powder was doped with 3 to 5 wt.% lithium fluoride, then vacuum hot forged at 950°C and 10,000 to 12,000 psi.

A review of research on fiber-reinforced ceramics and a critical assessment of opportunities that might exist was made by Krochmal.[116] Despite a number of virtues of fiber-reinforced ceramics, as demonstrated with model materials, the present technology has been unable to capitalize on this approach to achieve more thermal-shock-resistant ceramics with predictable mechanical integrity. This inability to extrapolate theoretical-model behavior to real or technologically interesting materials is attributed to such factors as thermochemical interactions, cracking, and reinforcement oxidation. The present status indicates that studies of the micromechanics of reinforced ceramics and the subsolidus kinetics in some systems are needed. Filaments of chromium, transition-metal borides, and beryllides are potential solutions to the presently indicated problems.

The concept of internally prestressing chemically consolidated zirconia with tungsten cable to increase flexural and tensile-load-carrying ability of the ceramic at room and elevated temperatures has been demonstrated by workers at Lockheed.[117] Stress at failure was increased fourfold in flexure and eightfold in tension. A theory for predicting the strength of the composite from the properties of the constituents was developed for estimating the initial and ultimate strengths of the composites.

Chvatal[118] also has reported some interesting research on metal-fiber-reinforced phosphate-bonded alumina. The material was rammed with helical filaments of Kanthal A or Nicrothal. As little as 1 vol.% of reinforcing improved the room-temperature flexural and tensile strengths significantly.

Air Force investigators[119] have examined 258 refractory materials existing in solid form above 2000°C and considered their potential as coating materials, with the qualifying requirement that they (1) do not undergo catastrophic oxidation in still air below 1700°C and (2) do not react observably with water vapor. The nine materials meeting these criteria were, in order of decreasing melting point: ThO_2, HfO_2, ZrO_2, $ZrSiO_4$ (zircon),* Cr_2O_3,† WSi_2, $CaCr_2O_4$, Ti_2O_3,‡ and Al_2O_3 (corundum). Data were thought to be questionable for an additional 34 materials.

AVCO[120] observed the effects of thermal conductivity and plastic strain on the flow and fracture of polycrystalline alumina. Yielding and fracture characteristics of dense, pure, fine-grained aluminum oxide were analyzed using stress–strain curves obtained from four-point bend tests by means of a bent-beam plastic stress analysis. Transitions from brittleness to ductility in bending were shown to occur at temperatures from 1200 to 1400°C. Yielding was found to be a thermally activated process with an an apparent activation energy of 59,000 cal/mole, which is similar to that for oxygen-ion diffusion in alumina. The mechanism of plastic deformation was attributed primarily to stress-enhanced diffusion, rather than to slip, in which the small grain size of the experimental material promoted ductility. Observations of grain-boundary sliding and separation were also made.

The effect of strain on the brittle-fracture stress was investigated by prestraining specimens above the transition temperature and unloading, cooling, and testing to fracture below the transition temperature. For strains up to about 0.4%, there was no significant effect on the fracture stress, but for higher prestrains, up to 1.5%, reduction of the brittle-fracture stress averaging about 30% was observed. This weakening was believed to be due to intergranular sepa-

*Dissociates above about 1550°C.
†High vapor pressure above 1650°C.
‡Dissociates.

ration. The brittle-fracture strength also appeared to decrease with increased porosity. Addition of 0.25% MgO to ultrafine-grained alumina had no significant effect on flow and fracture near the T_{BD}.

Davidge and Tappin[121] studied the thermal-shock resistance of a variety of high-density ceramic materials. The technique involved water quenching from a series of gradually increasing temperatures. Resistance could be estimated (1) by reporting the temperature drop for which half the specimens showed some cracking, (2) by comparing the degree of cracking by measurements on photographs following dye penetration after a given shock, and (3) by measurements of strength reductions. It was concluded that, if cracking must be avoided, the material of highest strength for a given elastic modulus should be chosen. For the case in which cracking can be tolerated without spalling, the degree of cracking after a standard shock or a series of shocks would be the desired measurement. This measurement would be based on the area of new surface formed or on the depth of cracking. (H. D. Sheets)

References

1. M. G. Cowgill and W. W. Smeltzer, The Oxidation Properties of a Zr–2.7 Wt.% Nb Alloy in the Temperature Range 300 to 500°C, *J. Electrochem. Soc.*, 114(11): 1089-1095 (November 1967).
2. T. Nakayama and T. Koizumi, On the Polymorphic Transformation of Zirconium Dioxide Associated with the Breakaway During High-Temperature Oxidation of Zirconium and Some Zirconium Alloys, *Nippon Kinzoku Gakkaishi*, 31: 839-845 (1967).
3. S. Kass, The Corrosion and Hydrogen Absorption Characteristics of Zirconium Alloys Containing Iron and Chromium in High-Temperature Water and Steam, USAEC Report WAPD-TM-517, Westinghouse Electric Corporation, Bettis Atomic Power Laboratory, February 1968.
4. S. Kass, The Corrosion and Hydrogen Absorption Properties of Zircaloy-4 Alloys Containing Additions of Niobium, USAEC Report WAPD-TM-647, Westinghouse Electric Corporation, Bettis Atomic Power Laboratory, December 1967.
5. M. Warzee, C. Sonnen, and Ph. Berge, Corrosion of Carbon Steels and Stainless Steels in Pressurized Water at High Temperatures, USAEC–Euratom Report EURAEC-1896, Société d'Etudes, de Recherches et d'Applications pour l'Industrie, July 6, 1967.
6. G. Chaudron, Quarterly Report No. 18 (On Stress Corrosion of Stainless Steels) April 1–June 30, 1967, USAEC–Euratom Report EURAEC-1932, Centre National de la Recherche Scientifique, Jan. 18, 1968.
7. J. J. Cadwell, D. R. de Halas, R. E. Nightingale, and D. C. Worlton, unpublished, Battelle–Northwest, February 1968.
8. F. W. Pement, Hydrogen Accumulation Rates Within Thick-Walled Tubes of Fe–Cr and Fe–Cr–Ni Alloys During Exposure to High-*p*H, High-Temperature, Pressurized Water Containing Dissolved Hydrogen, USAEC Report WERL-1114-3, Westinghouse Research Laboratories, June 1967.
9. G. R. Bloom and T. F. Demmitt, Corrosion and Boron Deposition in Boric Acid Solutions, USAEC Report BNWL-520, Battelle–Northwest, December 1967.
10. O. Ogunlade, Effect of *p*H on the Wear Characteristics in Water of Ten Metal Combinations, Canadian Report AECL-2784, October 1967.
11. P. E. C. Bryant and J. E. LeSurf, Some Observations of Intergranular Corrosion on Iron and Nickel Alloys in High Purity Water, paper presented at the NACE Conference in Cleveland, Ohio, March 18, 1968.
12. R. E. Pawel, The Effect of Anodic Films on the Gaseous Oxidation of Tantalum. II. Films Formed in Phosphoric Acid Solutions, *J. Electrochem. Soc.*, 114: 1222-1227 (December 1967).
13. W. McNeill and R. E. Salomon, Gas-Phase Anodization of Tantalum, *J. Electrochem. Soc.*, 114: 1134-1137 (November 1967).
14. I. Zaplatynsky, Determination of Electric Potential Across the Oxide Scale During Oxidation of Tantalum, Niobium, and Magnesium, Report NASA-TN-D-4240 (N68-10498), National Aeronautics and Space Administration, Lewis Research Center, November 1967.
15. I. I. Druzhinina, V. V. Andreeva, T. P. Stepanova, and E. I. Semenova, Corrosion Resistance, Physico-Mechanical, and Electrochemical Properties of V–Nb Alloys, *Zashc. Metal.*, 3: 672-675 (September–October 1967).
16. A. V. Guts and A. S. Tumarev, High-Temperature Corrosion Resistance of Chromium Alloys with Zirconium, *Tr. Leningrad. Politekh. Inst.*, 251: 76-81 (1965).
17. N. Perlhefter and B. Lux, Contribution to the Study of Protective Coatings for Columbium Based on Intermetallic Phases, *Publ. Sci. Tech. Min. Air*, n° B.S.T. 131 (November 1967).
18. M. Negrin and A. Block, Protective Coatings for Chromium Alloys, Report NASA-CR-54538, Chromalloy-American Corp., July 1967.
19. L. J. Goetz, J. R. Hughs, and W. F. Moore, The Pilot Production and Evaluation of Chromium Alloy Sheet and Plate, Report NASA-CR-72184, General Electric Company, March 1967.
20. D. N. Williams, R. H. Ernst, C. A. MacMillan, J. J. English, and E. S. Bartlett, Development of Protective Coatings for Chromium-Base Alloys, Report NASA-CR-54619, Battelle Memorial Institute, Columbus Laboratories, March 1968.
21. W. T. Lee, Biaxial Stress-Rupture Properties of Austenitic Stainless Steels in Zirconium-Gettered Sodium, USAEC Report NAA-SR-12353, Atomics International, Oct. 1, 1967.
22. H. Böhm and H. Schneider, Creep and Stress-Rupture Behavior of Austenitic Steels in the Presence of Sodium (in German), *J. Nucl. Mater.*, 24: 188-197 (1967).
23. R. C. Andrews, R. H. Hiltz, L. H. Kirschler, and R. J. Udavcak, A Limited Comparison of the Relative Merits of 304 vs. 316 Stainless Steel for Liquid Metal Service, Topical Report No. 10, USAEC Report MSAR-67-216, MSA Research Corporation, December 1967.
24. Brookhaven National Laboratory, Nuclear Engineering Department Annual Report, USAEC Report BNL-50082, pp. 94, 95, 128-130, Dec. 31, 1967.
25. G. A. Ratz and K. G. Brickner, Effect of Liquid Sodium on Welded AISI Type-304 Stainless-Steel Pipe, *Nucl. Appl.*, 4(3): 154-158 (March 1968).
26. Argonne National Laboratory, Reactor Development Program, Progress Report, January 1968, USAEC Report ANL-7419, p. 4, Feb. 27, 1968.
27. S. Greenberg, C. F. Cheng, and W. E. Ruther, In-Reactor Sodium Corrosion of Vanadium and Vanadium–Titanium Alloys, *Nucl. Appl.*, 4(3): 170-172 (March 1968).
28. W. F. Holcomb, Carburization of Type 304 Stainless Steel in Liquid Sodium, *Nucl. Eng. Design*, 6(3): 264-272 (October 1967).
29. S. G. Young and J. R. Johnston, Effect of Cover Gas Pressure on Accelerated Cavitation Damage in Sodium, Report NASA-TN-D-4235 (or N68-10104), Na-

tional Aeronautics and Space Administration, Lewis Research Center, November 1967.
30. E. E. Hoffman and J. Holowach, Cb–1 Zr Sodium Thermal Convection Loop, Potassium Corrosion Test Loop Development, Topical Report No. 5, Report R67SD3014, General Electric Company, June 15, 1967.
31. E. E. Hoffman and J. Holowach, Cb–1 Zr Pumped Sodium Loop, Potassium Corrosion Test Loop Development, Topical Report No. 6, Report R67SD3015, General Electric Company, Dec. 20, 1967.
32. T. F. Kassner and D. L. Smith, Calculations on the Kinetics of Oxygen Solution in Tantalum and Niobium in a Liquid-Sodium Environment, USAEC Report ANL-7335, Argonne National Laboratory, September 1967.
33. C. W. Hickman, Jr., Corrosion Product of the Tantalum–Interstitial Oxygen–Potassium System at 1800° F (1255° K), Report NASA-TN-D-4213 (N68-11511), National Aeronautics and Space Administration, Lewis Research Center, December 1967.
34. R. E. MacPherson and R. J. Gray (Comps.), Development of a 500-kw NaK-to-Air Radiator, USAEC Report ORNL-4159, Oak Ridge National Laboratory, January 1968.
35. S. Peterson (Comp. and Ed.), Metals and Ceramics Division Annual Progress Report for Period Ending June 30, 1967, USAEC Report ORNL-4170, *a*, pp. 93-96; *b*, pp. 17-18, Oak Ridge National Laboratory, November 1967.
36. H. E. Nichols and R. W. Fink, Two-Stage Potassium Test Turbine, Volume II, Mechanical Design and Development, Report NASA-CR-923, General Electric Company, February 1968.
37. E. Schnetzer (Ed.), 3000 Hour Test—Two Stage Potassium Turbine, Final Report, NASA-CR-72273, General Electric Company, July 1967.
38. Ye. M. Savitskiy, V. V. Baron, and K. N. Ivanova, Niobium-Based Alloys and Their Properties, Report JPRS-4317 [from *At. Energ. (USSR)*, 23(7): 32-37 (July 1967)].
39. L. G. Hays, Corrosion of Nb–1% Zr Alloy and Yttria by Lithium at High Flow Velocities, Report JPL-TR-32-1233 (N68-11617), Jet Propulsion Laboratory, Dec. 1, 1967.
40. E. M. Simons, Corrosion by Liquid Metals and Fused Salts, *Reactor Mater.*, *a*, 9(4): 224-225 (Winter 1966–1967); *b*, 10(1): 30 (Spring 1967).
41. Argonne National Laboratory, Reactor Development Program, Progress Report, October 1967, USAEC Report ANL-7391, pp. 132-134, Nov. 30, 1967.
42. Argonne National Laboratory, Reactor Development Program, Progress Report, February 1968, USAEC Report ANL-7427, pp. 100-101, Mar. 26, 1968.
43. M. J. Wallace, Wear and Compatibility Behavior of Liquid-Metal Bearing Materials, *J. Lubric. Technol.*, 89: 466-472 (October 1967).
44. TRW Systems Group, Research Investigation of Corrosion-Resistant Materials for Electrochemical Cells, Final Report 05660-6002-R000 (AD-654807) for January 1966–January 1967.
45. D. F. Anthrop, The Solubilities of Transition Metals in Liquid Alkali and Alkaline Earth Metals, Lanthanum and Cerium: A Critical Review of the Literature, USAEC Report UCRL-50315, University of California, Lawrence Radiation Laboratory, Sept. 20, 1967.
46. A. R. C. Westwood, C. M. Preece, and M. H. Kamdar, Adsorption-Induced Brittle Fracture in Liquid Metal Environments, First Annual Report, Report RIAS-TR-67-8C (AD-658210), Research Institute for Advanced Studies, Martin Marietta Corp., May 1967.
47. E. M. Simons, Corrosion by Nonaqueous Liquids, *Reactor Mater.*, 10(3): 166 (Fall 1967).
48. S. H. Bush, unpublished, Battelle–Northwest, 1967.
49. S. T. Konobeyevskiy, *Effects of Irradiation on Materials*, Atomizdat, Moscow, 1967.
50. M. Kangilaski, The Effects of Neutron Radiation on Structural Materials, USAEC Report REIC-45, Battelle Memorial Institute, Radiation Effects Information Center, June 30, 1967.
51. Metallurgy Department Annual Progress Report for the Period Ending March 31, 1967, Danish Report RISO-151, *a*, pp. 21-23; *b*, pp. 31-32, July 1967.
52. H. Böhm, H. Hauck, and G. Hess, Untersuchungen Über Die Hochtemperaturversprödung Nach Neutronenbestrahlung Von 16/13–CrNi–Stählen, *J. Nucl. Mater.*, 24(2): 198-209 (November 1967).
53. General Electric Company, Nuclear Materials and Propulsion Operation, AEC Fuels and Materials Development Program Progress Report No. 71, USAEC Report GEMP-1002, pp. 39-41, Dec. 29, 1967.
54. H. E. McCoy, Jr., Effects of Irradiation on the Mechanical Properties of Two Vacuum-Melted Heats of Hastelloy N, USAEC Report ORNL-TM-2043, Oak Ridge National Laboratory, January 1968.
55. M. S. Wechsler, Radiation Damage to Pressure Vessel Steels, *Nucl. Safety*, 8(5): 461-469 (Sept.–Oct. 1967).
56. G. D. Whitman, G. C. Robinson, Jr., and A. W. Savolainen (Eds.), Technology of Steel Pressure Vessels for Water-Cooled Nuclear Reactors. A Review of Current Practice in Design, Analysis, Materials, Fabrication, Inspection, and Test, USAEC Report ORNL-NSIC-21, Oak Ridge National Laboratory, December 1967.
57. Argonne National Laboratory, Reactor Development Program, Progress Report, November 1967, USAEC Report ANL-7399, pp. 13-14, Dec. 28, 1967.
58. Argonne National Laboratory, Reactor Development Program, Progress Report, December 1967, USAEC Report ANL-7403, pp. 11-13, Jan. 31, 1968.
59. R. B. Adamson, Cyclic Deformation of Neutron Irradiated Copper, *Phil. Mag.*, 17: 681 (1968).
60. G. W. Lewthwaite, D. Mosedale, and I. R. Ward, Irradiation Creep in Several Metals and Alloys at 100°C, *Nature*, 216: 472-473 (Nov. 4, 1967).
61. R. C. Rau, J. Moteff, and R. L. Ladd, Comparison of Microstructure with Mechanical Properties of Irradiated Tungsten, *J. Nucl. Mater.*, 24(2): 164-173, (November 1967).
62. D. A. Jeannotte, Vacancy Annealing in Irradiated Tungsten, USAEC Report CU-3551-8, Columbia University, February 1967.
63. R. P. Tucker and S. M. Ohr, Direct Observation of Neutron Irradiation Damage in Niobium, *Phil. Mag.*, 16: 643-646 (September 1967).
64. M. Attardo, Radiation Damage in Platinum. Final Progress Report (Part 1), USAEC Report CU-3551-7, Columbia University, February 1967.
65. H. C. van Elst, A New Determination of Embrittlement in Steel Using Small Specimens (approximately 0.2 cm^3) in Particular with Respect to Irradiation, USAEC–Euratom Report EURAEC-1857, Metaalinstituut TNO, Apr. 28, 1967.
66. D. O. Hunter, Ultrasonic Method for Nondestructively Detecting Radiation-Induced Embrittlement in Pressure Vessel Steels, USAEC Report BNWL-SA-1467, Battelle–Northwest, Oct. 16, 1967.
67. W. Siegfried and S. Zimering, Research to Determine the Long-Term Mechanical Properties of Metals Subjected to Mechanical Stress at Elevated Temperatures and Neutron Irradiation, USAEC–Euratom Report EURAEC-1921, Battelle–Geneva, July 1967.
68. C. C. Foune, The Effect of Oxygen on the Mechanical Properties of the Nb–1% Zr Alloy, Thesis, Ames Laboratory, November 1966.
69. T. E. Firle and R. H. Chambers, Microstrain Measurements in Nb from 1.8 to 300°K, USAEC Report CONF-660327-13, General Dynamics Corp., February 1967.
70. Y. Sasaki, H. Kimuar, and S. Uehara, Mechanical Properties of Nb–H Alloys, *Nippon Kinzoku Gakkaishi*, 31: 401-405 (April 1967).
71. E. de Lamotte, Y. Huang, and C. Altstetter, Precipitation of Nitride in Niobium (Columbium) and Nb–Zr

Alloys, *Trans. Met. Soc. AIME*, 239: 1625-1630 (October 1967).

72. N. D. Tarasov, R. A. Ul'yanov, Ya. D. Mikhailov, Effect of Alloying on the Nature of the Interatomic Interaction in Niobium-Base Solid Solutions, in *Vysokotemperaturnye Neorganichiskie Soedineniya*, pp. 55-62, Nauk Dumka, Kiev, 1965.
73. B. L. Mordike and G. Rudolph, Three-Stage Hardening in Tantalum Deformed in Compression, *J. Mater. Sci.*, 2: 332-338 (July 1967).
74. C. R. Honeycutt, T. F. Martin, J. C. Sawyer, and E. A. Steigerwald, Elevated-Temperature Fatigue of TZC Molybdenum Alloy Under High-Frequency and High-Vacuum Conditions, *Amer. Soc. Metals, Trans. Quart.*, 60: 450-458 (September 1967).
75. J. E. Bowers, R. D. S. Lushey, and P. W. J. Sanson, Final Report on the Creep Properties of Molybdenum at 650 to 750°C, British Report TRG-Report-1550, January 1967.
76. H. W. Loesch, Jr., and F. R. Brotzen, Observation of Dislocations in Deformed Molybdenum Crystals, *J. Less-Common Metals*, 13: 565-578 (December 1967).
77. D. R. Hay, Parameters Affecting the Mechanical Behavior of Tungsten: Grain Boundary Structure and Alloy Additions of Carbon and Rhenium, Thesis, Cornell University, 1966.
78. S. Nakajima and H. Okazaki, Fiber Texture in Drawn Tungsten Wires, *Trans. Met. Soc. AIME*, 239: 1060-1065 (July 1967).
79. J. O. Stiegler, K. Farrell, B. T. M. Loh, and H. E. McCoy, Nature of Creep Cavities in Tungsten, *Amer. Soc. Metals, Trans. Quart.*, 60: 494-503 (September 1967).
80. K. Farrell, T. M. Loh, and J. O. Steigler, Morphologies of Bubbles and Voids in Tungsten, *Amer. Soc. Metals, Trans. Quart.*, 60: 485-493 (September 1967).
81. N. Hansen, Dispersion Strengthened Aluminum Powder Products for Nuclear Application, *Powder Met.*, 10: 94-115 (Autumn 1967).
82. H. Lilholt, J. C. Balling-Jensen, and U. Jensen, Bibliography on Dispersion-Strengthened Materials, 1965, Danish Report RISO-48, Supplement 3, August 1967.
83. T. M. Nilsson, Influence of Grain Size on the High-Temperature Ductility of an Aluminum–Al_2O_3 Alloy, *J. Nucl. Mater.*, 24: 343-346 (December 1967).
84. B. W. Pickles, The Creep Behavior of Heat-Treated Magnox ZR-55 in the Temperature Range 350 to 450°C, *J. Inst. Metals*, 95: 333-337 (1967).
85. R. P. Marshall, Influence of Fabrication History on Stress-Oriented Hydrides in Zircaloy Tubing, *J. Nucl. Mater.*, 24(1): 34-48 (October 1967).
86. R. P. Marshall, Control of Hydride Orientation in Zircaloy by Fabrication Practice, *J. Nucl. Mater.*, 24(1): 49-59 (October 1967).
87. E. D. Hindle, Effect of Circumferentially Aligned Hydride on the Ductility of Zircaloy-2 Tubing Under Biaxial Stress, *J. Inst. Metals*, 95: 359-363 (1967).
88. H. Suzuki, I. Kawakatsu, H. Kitano, and A. Murase, Influences of the Additional Elements on Some Properties of High Zirconium Cu–Zr Alloys, *Nippon Kinzoku Gakkaishi*, 31: 14-19 (1967).
89. P. Baque and R. Darras, Zirconium Alloy, British Patent No. 1,083,057, Sept. 13, 1967.
90. S. Ray, J. L. Mukherjee, and M. L. Mehta, Effect of Thermal Treatment on Hardness and Tensile Properties of Zr–0.5 Wt.% Nb–1.0 Wt.% Cr Alloy, Indian Report BARC-295, 1967.
91. L. K. Singhal and J. W. Martin, The Effect of $\gamma'(Ni_3Ti)$ Particle Size upon the Creep Deformation at 650°C of an Austenitic Stainless Steel, *Scripta Metallurgica*, 1(3): 181-183 (December 1967).
92. J. J. Huet, Possible Fast-Reactor Canning Materials Strengthened and Stabilized by Dispersion, *Powder Met.*, 10: 208-215 (Autumn 1967).
93. Oak Ridge National Laboratory, Molten-Salt Reactor Program, Semiannual Progress Report for Period Ending August 31, 1967, USAEC Report ORNL-4191, pp. 200-207, December 1967.
94. A. W. Dalcher, Computed Stress-Relaxation Curves for Hastelloy Alloy N, USAEC Report NAA-SR-Memo-12590, Atomics International, Nov. 1, 1967.
95. V. M. Amonenko, V. M. Azhazha, I. S. Bolgov, M. P. Zeidlits, B. I. Shapoval, and N. D. Rybal'chenko, Effect of Boron on the Structure and Mechanical Properties of Nickel, *Izv. Akad. Nauk SSSR, Metal.*, No. 4: 140-146 (July–August 1967).
96. M. H. Leipold and P. F. Becher, Fabrication and Characterization of Hot-Pressed Tantalum Carbide, Report NASA-CR-90036 (N68-10078), Jet Propulsion Laboratory, Oct. 1, 1967.
97. Finely Divided Carbides and Process for Their Production, British Patent No. 1,069,748, May 24, 1967.
98. J. D. L. Harrison and W. G. Roberts, Improvements in or Relating to Sintering, British Patent No. 1,088,724, Oct. 25, 1967.
99. J. M. Fletcher, K. R. Hyde, and F. Roberts, Improvements in or Relating to the Manufacture of Refractory Compounds, British Patent No. 1,084,338, Sept. 20, 1967.
100. R. E. Riley, Characterization of Commercial Carbide Powders, USAEC Report LA-3653, Los Alamos Scientific Laboratory, Dec. 15, 1966.
101. Oak Ridge National Laboratory, Reactor Chemistry Division Annual Progress Report for Period Ending December 31, 1967, USAEC Report ORNL-4229, pp. 142-144, March 1968.
102. R. J. Fries and L. A. Wahman, Effect of Stoichiometry on the Thermal Expansion of TaC_x, *J. Amer. Ceram. Soc.*, 50: 475-477 (Sept. 21, 1967).
103. M. H. Leipold and T. H. Nielson, The Mechanical Behavior of Tantalum Carbide and Magnesium Oxide, Report JPL-TR-32-1201, Jet Propulsion Laboratory, Dec. 1, 1967.
104. Yu B. Paderno, I. G. Barantseus, and V. L. Yupko, Measurement of the Thermal Conductivity and Electrical Conductivity of HfC, ZrC, NbC, and TaC at High Temperatures, *Vysokotemperaturnye Neorganichskie Soedineniya*, pp. 199-204, Nauk Dumka, Kiev, 1965.
105. C. L. McDaniel and S. J. Schneider, Phase Relations Between Palladium Oxide and the Rare-Earth Sesquioxides in Air, *J. Res. Nat. Bur. Stand., A*, 72A: 27-37 (Aug. 22, 1967).
106. G. V. Samsonov and L. V. Strashinskaya, Solid-Phase Surface Reactions Between Borides, Refractory Metals, and ZrO_2, in *Vysokotemperaturnye Neorganicheskie Soedineniya*, pp. 437-444, Nauk Dumka, Kiev, 1965.
107. J. Morgenthal, Oxidation-Resistant Hard Materials, *Neue Huette*, 11: 484-490 (August 1966).
108. D. C. Gillies and D. Lewis, Strain in Metal Carbides, *J. Less-Common Metals*, 13: 179-185 (August 1967).
109. S. I. Aliamovskii, G. P. Shveikin, P. V. Gel'd, and N. M. Volkova, Orthorhombic β'-Phases of Niobium and Vanadium Carbides, *Zh. Neorg. Khim.*, 12: 579-582 (1967).
110. R. J. Fries, Vaporization of Dimolybdenum Carbide, *J. Chem. Phys.*, 46: 4463-4469 (June 7, 1967).
111. V. I. Alekseev, Yu. N. Surovoi, and L. A. Shvartsman, Determination of Thermodynamic Activity of Carbon in Alloyed Molybdenum Carbide, *Porosh. Met., Akad. Nauk Ukr. SSR*, No. 9: 64-70 (September 1967).
112. R. W. Bartlett, Study of Growth Parameters for Refractory Carbide Single Crystals, Quarterly Status Report, September 1–December 1, 1966, Report NASA-CR-82466 (N67-18983), Stanford Research Institute, Jan. 9, 1967.
113. J. L. Woolfrey, Feasibility of Dispersed Phase Grain Refinement in Ceramics, Australian Report AAEC/E-170, February 1967.
114. P. J. Jorgensen and R. C. Anderson, Grain-Boundary

Segregation and Final Stage Sintering of Y_2O_3, *J. Amer. Ceram. Soc.*, 50(11): 553-558 (1967).
115. R. A. Lefever and J. Matsko, Transparent Yttrium Oxide Ceramics, *Mater. Res. Bull.*, 2: 865-869 (September 1967).
116. J. J. Krochmal, Fiber Reinforced Ceramics: A Review and Assessment of Their Potential, Report AFML-TR-67-207, Air Force Materials Laboratory, July 1967.
117. L. B. Greszczuk and H. Leggett, Development of a System for Prestressing Brittle Materials, Report NASA-CR-89607, Douglas Aircraft Co., Inc., August 1967.
118. T. Chvatal, Metallic-Fiber-Reinforced Heat-Resistant Ceramic Materials, *Sprechsaal*, 100(5): 181-185(1967).
119. L. C. Long and J. R. Joiner, Refractories in a Reactive Atmosphere, Report AFFDL-FDTR-TM-67-1, Air Force Flight Dynamics Laboratory, April 1967.
120. E. M. Passmore, A. Moschetti, P. Burnett, and D. Sellers, Effect of Thermal Conditioning and Strain on the Microstructure and Mechanical Properties of Alumina, Report AMMRC67-16(F), AVCO Corp., November 1967.
121. R. W. Davidge and G. Tappin, Thermal Shock and Fracture in Ceramics, *Trans. Brit. Ceram. Soc.*, 66: 405-422 (1967).

Section IV

Reactor Materials

Special Fabrication Techniques

Cast and Wrought Materials

Melting and Casting Processes

Hueston and Barclay[1] studied the melting and casting of uranium and uranium alloys and found that in some applications zirconia, fused magnesia, and graphite were the most suitable crucible materials. Graphite was found best for alloy castings with cross sections of 4 in. or greater; ceramic molds were superior to machined graphite molds from an economic standpoint for small sections and for shaped castings. Melting procedures and conditions for these materials were also investigated.

Battelle–Northwest[2] has published a handbook that includes summaries of melting and casting, machining, and mechanical-working methods for unalloyed plutonium and plutonium-base alloys. Fabrication methods used for plutonium are often determined by available facilities and are generally batch operations applied to a few kilograms at a time, because of critical mass limitations. Unalloyed plutonium is usually fabricated by casting and machining because of the brittle alpha phase, which is the stable form at ordinary temperatures. Plutonium can be fabricated in the beta phase at higher temperatures by rolling, extrusion, or forging.

Fabrication procedures that have been employed in the past are also described for aluminum-base plutonium, plutonium-base aluminum, and plutonium-base iron alloys for use as nuclear fuels. Aluminum-base plutonium alloys have been used on a large scale in thermal reactors, e.g., in the plutonium loading for the MTR, the spike enrichment of the PRTR, and the transplutonium fuel elements. Metallic plutonium stabilized in the delta phase by alloying with aluminum or calcium has been used as a fast reactor fuel in the Los Alamos reactor Clementine and Argonne's EBR-I. Plutonium–iron eutectic alloy was selected for Core I and Core II of the LAMPRE because of its low melting point and limited corrosive attack on tantalum.

Single crystals of nickel are being prepared at Ames Laboratory[3] by the Czochralski crystal-pulling technique. Crystals ranging in size from 0.06 in. in diameter and 0.5 in. long to 1.5 in. in diameter and 9.0 in. long were grown from the melt using an NRC crystal-pulling unit.

Researchers at NASA[4] examined the application of directional solidification to the preparation of castings of a nickel-base alloy, TAZ-8B. Castings of this material prepared by directional solidification were found to possess strength properties at high temperature that compared favorably with those of other high-strength nickel-base alloys. Grain boundaries transverse to the major stress axis (as might be encountered in turbine-blade applications) were largely eliminated. Substantial increases in ductility, ultimate tensile strength, and stress-rupture life were obtained with the alloy in the directional polycrystalline condition over those obtained in the random polycrystalline condition.

Procedures were developed at Battelle–Columbus[5] for sound castings of hypereutectic ZrC–carbon and HfC–carbon alloys by skull arc melting and drop casting. Good-quality castings 13 in. long and $1\frac{1}{2}$ in. in diameter were prepared. Over 200 castings were produced to provide specimens for specific-heat, thermal-conductivity, thermal-expansion, tensile, compression, dynamic-modulus, and environmental tests.

The Bureau of Mines[6] is conducting a project to develop equipment and techniques for producing high-melting-point metal–carbon alloys by spin casting. Approximately one hundred $\frac{1}{4}$- by $\frac{1}{2}$- by $3\frac{1}{2}$-in. specimens of NbC alloys were satisfactorily prepared and are being evaluated in bend-rupture, thermal-expansion, electrical-resistivity, hardness, and air-oxidation tests.

The alloying behavior of elements in the Nd–Pr, Gd–Y, Gd–Sm, and Sm–Y systems was studied at Denver Research Institute.[7] The deviation from solution ideality, free energies, and enthalpies and entropies of mixing were determined. Variables considered were atomic diameter, crystal structure, electronegativity, electronic structure, and valence. It was found that the Nd–Pr system was thermodynamically ideal and that no variables were introduced. Crystal structure, on the other hand, was the variable introduced in the Gd–Sm system. Excess enthalpy and entropy caused strain in these alloys. The variable in the Gd–Y system was electronic structure, but ideality of the complete solid solution existed. In the Sm–Y system the variables were crystal and electronic structure, but the thermodynamics were similar to those of the Gd–Sm system.

The difference in electronic structure was negligible in the Gd–Y system, whereas the crystal-structure variable in the Gd–Sm system caused a large negative deviation from an ideal solution.

A Japanese patent[8] describes an improved method of casting Al–U alloys. Normally these alloys are cast as ingots of 20 to 30 mm thickness, rolled to a thickness of several millimeters, and then clad on both sides with aluminum plate. In cast alloys with 14 to 50 wt.% uranium, the presence of large compound particles results in extrusion cracking and nonuniform uranium distribution in the final product. In the Japanese process, alloys with 14 to 50 wt.% uranium are cast into a mold, heated at 150 to 350°C, and vibrated at an amplitude of 0.1 to 0.4 mm in order to minimize the Al–U compound grain size and to promote uniform distribution in the material.

The French[9] have applied vertical zone melting in the purification of zirconium and determined the influence of various metallic and nonmetallic impurities on the recrystallization temperature and the resistivity ratio (ratio of resistivities of a given specimen at the boiling point of liquid helium and at room temperature). The zirconium bar in a static ultravacuum was isolated from the pumping equipment; thus the progressive contamination of metal by carbon from oils in the diffusion pumps was prevented. Mechanisms of purification noted were (1) segregation of Cd, Ag, Au, Ni, Fe, and Cr; (2) inverse segregation of mercury (as expected) and copper (abnormal); (3) an anomaly in the segregation of hafnium; and (4) elimination of certain impurities by a distillation effect superimposed on segregation and most pronounced with respect to Cu, Ag, Fe, Mn, Cr, and Al. An apparent absence of this last effect was noted in the case of certain extremely volatile impurities such as zinc and especially cadmium, which indicated that a coefficient of activity must be considered in addition to the vapor-pressure ratio. The zone-melted bars comprised very large alpha crystals elongated in the direction of the axis of the bar, some being more than 3 cm long.

The Russians[10] have conducted basic studies on the solidification of metals melted by electric arc. The crystallization front in electric-arc zone melting was of a complicated form and was influenced by impurities in the sample. An equation was developed for determining the impurity-transfer velocity associated with the motion in the molten zone. Crystallization pulses were also studied by the use of autoradiographs that showed the shape of the crystallization front during melting and solidification.

Methods of purifying beryllium are also being examined by the Russians.[11] Specimens of beryllium containing impurities in amounts varying from 0.99 wt.% for lead to 0.1 wt.% for iron were purified by zone refining or by pulling crystals from the melt. In zone refining, three passes lowered the Fe, Cu, Cr, Mg, and Al contents, but the specimens remained polycrystalline even after six passes. When zone refining was combined with direct or alternating current applied to the specimens, single crystals were obtained after one or two passes, and higher purity was achieved. Refining by the crystal-pulling method in vacuum or in an inert-gas atmosphere produced specimens consisting of several large crystals with a purity comparable to that achieved by zone refining with one or two passes.

In zone refining, yttrium and iron were found to have no negative effect on the elimination of other impurities. However, yttrium had a modifying effect on the structure of beryllium and prevented the formation of single crystals. In contrast, beryllium single crystals containing 0.1 wt.% molybdenum were successfully grown. Carbon was eliminated not only by the zonal effect but also by migration to the surface of the specimen. The latter phenomenon was especially marked when zone refining was combined with an applied alternating current.

The engineering properties of W–25 wt.% Re produced by both arc-melting and powder-metallurgy methods were determined at the Bureau of Mines.[12] Creep-rupture tests showed that arc-melted sheet had a greater rupture life at a given stress and temperature than did powder-metallurgy sheet. Also, the ductility at rupture was very low for the powder-metallurgy material, as compared with that of the arc-melted sheet, possibly because of microporosity in the powder-metallurgy material. In weldments of the two materials, a heavier concentration of macroporosity occurred in powder-metallurgy materials than in arc-melted materials. The arc-melted materials also showed a lower ductile-to-brittle transition temperature. Data obtained in ductile-to-brittle transition-temperature measurements are plotted in Fig. IV-1.

Fabrication of Cast Products

An excellent bibliography on the hydrostatic and fluid-to-fluid extrusion of metals and the effects of pressure on certain metals has been compiled at the Lawrence Radiation Laboratory.[13] In fluid-to-fluid extrusion, a liquid under high pressure forces a billet through a die into a liquid at a lower pressure. Because the system is pressurized on both sides of the die, both total pressure and pressure differential can be adjusted to values at which plastic flow can occur without billet failure. The bibliography provided background information for extrusion and forming experiments on beryllium, tungsten, molybdenum, or alloys of these metals to be performed at the Lawrence Radiation Laboratory.

Techniques for the extrusion of tungsten and tungsten-alloy tubing from arc-cast and powder-metallurgically prepared billets by the floating-mandrel method were developed at Oak Ridge.[14] Naturally forming tungsten oxide served as a lubri-

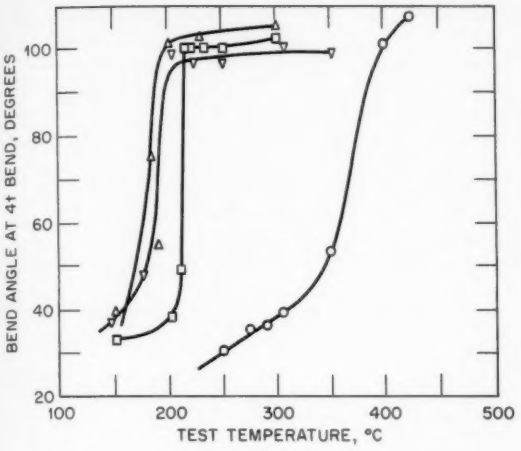

Fig. IV-1 Ductile-to-brittle transition-temperature comparisons for W–25 wt.% Re sheet.[12] ○, powder-metallurgy sheet recrystallized; □, powder-metallurgy sheet stress relieved; △, arc-melted sheet recrystallized; ▽, arc-melted sheet stress relieved.

cant. Extrusion temperatures ranged between 1650 and 2250°C, and extrusion ratios ranged between 4 and 9. Satisfactory service was obtained from zirconia-protected dies and mandrels, but surface melting of the container sleeve began when billet temperatures exceeded 1850°C. Rapid extrusion speeds were necessary to minimize heat loss and to reduce contact time with the tooling. Thin-walled tungsten tubing was produced with the floating-mandrel technique by reextruding a section of the tube shell in a duplex billet. Figure IV-2 shows a schematic drawing of the general process developed for extrusion and drawing of tungsten and tungsten-alloy tubing.

The shear-spinning process for the fabrication of difficult alloys has been described.[15] In particular, the use of the process for the fabrication of TZM–Mo alloy (molybdenum with 1 wt.% titanium and zirconium) into a hemispherical shape with a 13.7-in. nose radius for a missile nose tip was noted. The shear-spinning process was selected over die forming and hydroforming because with shear spinning it is possible to control the required variable wall thickness, the mandrel and workpiece are easily heated with controlled gas flames, and only a male die is needed. The four machining stages for the nose tip were (1) cutting the TZM plate to size, (2) preforming by hand spinning, (3) final forming by shear spinning, and (4) trimming to length. Following trimming the nose tip was polished to a finish suitable for plating and was inspected for cracks and conformance with specifications.

Special machining techniques were required to fabricate tungsten jet pipes for France's SEPR plant.[16] Slow turning, milling, and boring at 3-rpm average speed with carbide tools which were cooled but not lubricated produced the desired results. Rotary template reproduction was used with careful mounting of the parts to avoid breakage.

The Russians[17] have examined vacuum-extrusion processes for refractory metals. Specimens of molybdenum and niobium heated to 1600°C in hydrogen and argon atmospheres, respectively, were upset in air to determine the effect of ambient atmosphere on their ductility. Other specimens were heated to and upset at the same temperature in vacuum. A special unit which provided either a vacuum or a neutral atmosphere in heating and deformation under 1000-ton pressure was used in the experiments. Heating in argon and deforming in air led to gas impregnation of niobium to a depth of 3 mm, an increase in the CO_2 content from 0.02 to 0.06 wt.%, an increase in the surface microhardness, and significant cracking of semifinished products, whereas none of these changes occurred in niobium that was heated and deformed in vacuum. Similarly, heating in hydrogen and deforming in air produced oxygen saturation of molybdenum to a depth of 0.3 to 0.8 mm, which led to embrittlement and failure with a 43% reduction, whereas vacuum-deformed molybdenum sustained a 60% reduction without cracking.

On the basis of the above experimental results, procedures were developed for extruding Mo–Nb alloy ingots, rods, and tubes in a vacuum. A glass-fiber base plus graphite lubricant was used in vacuum ex-

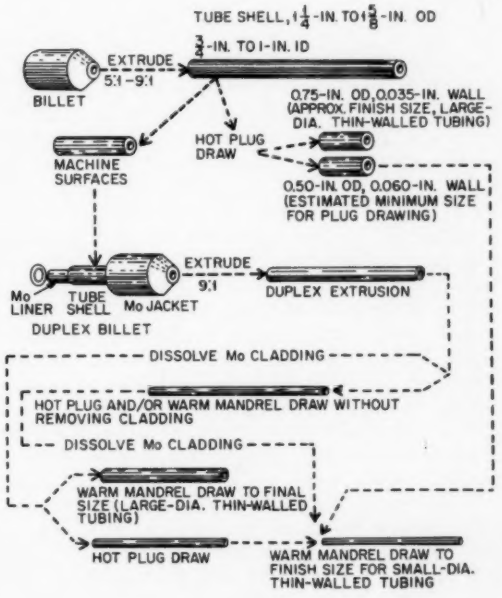
TUBE SHELL, 1¼-IN. TO 1⅝-IN. OD
¾-IN. TO 1-IN. ID
EXTRUDE 5:1–9:1
BILLET
0.75-IN. OD, 0.035-IN. WALL (APPROX. FINISH SIZE, LARGE-DIA. THIN-WALLED TUBING)
HOT PLUG DRAW
MACHINE SURFACES
0.50-IN. OD, 0.060-IN. WALL (ESTIMATED MINIMUM SIZE FOR PLUG DRAWING)
EXTRUDE 9:1
Mo LINER
TUBE SHELL
Mo JACKET
DUPLEX BILLET
DUPLEX EXTRUSION
DISSOLVE Mo CLADDING
HOT PLUG AND/OR WARM MANDREL DRAW WITHOUT REMOVING CLADDING
DISSOLVE Mo CLADDING
WARM MANDREL DRAW TO FINAL SIZE (LARGE-DIA. THIN-WALLED TUBING)
HOT PLUG DRAW
WARM MANDREL DRAW TO FINISH SIZE FOR SMALL-DIA. THIN-WALLED TUBING

Fig. IV-2 General process for extrusion and drawing of tungsten and tungsten-alloy tubing.[14]

trusion at 1400 to 1600°C. For extrusion at lower temperatures (1100 to 1300°C), copper foil was used as lubricant. The technology was successfully applied to the extrusion of rods, tubes, and other semifinished products from two or more dissimilar metals and also for cladding and diffusion bonding of metals. Vacuumtight joints were obtained in rods and tubes fabricated from niobium and steel, molybdenum and steel, and niobium and molybdenum.

The fabricability of yttrium and 12 lanthanide metals was examined by the British.[18] Fabrication by cold working, thereby avoiding excessive oxidation, was found possible for all the lanthanide metals except samarium and lutetium. Work-hardening and recrystallization characteristics were found to be markedly influenced by small amounts of impurities, particularly copper, which form low-melting-point grain boundaries with the lanthanides.

The use of gas plasmas for fabrication of tungsten components has been studied by Brunst.[19] The physical characteristics of gas plasmas are defined as the fourth physical state that is reached when, owing to high thermal agitation, a separation occurs between an atomic nucleus and electrons. Some applications of plasmas are in plasma burners for depositing tungsten films, in fabrication of nozzles by plasma-spraying tungsten powder, and in deposit welding. Tungsten powders melt in the process of plasma spraying and form spherical drops, which permits the fabrication of tungsten parts of controlled porosity. Another application of the plasma technology is in the growing of tungsten single crystals.

A metalworking review by Bryrer and Boulger[20] cited advances in forging lubricants and in developing cemented-carbide tool materials. Lubricants other than heavy-duty cutting fluids—usually composed of sulfur, chlorine, or phosphorus compounds—were developed from considerations of surface chemistry. Experiments showed that the use of iodine-charge-transfer components as additives to hydrocarbon oils produced improvement in lubricating ability for titanium-to-titanium and titanium-to-steel sliding surfaces. Cemented-carbide tools with refractory-metal binders exhibiting exceptional cutting capabilities on 4340 steel contain a Ni–Cr or Nb–Mo refractory matrix in combination with WC–TiC solid solutions plus additions of TaC. The development of extrusion die materials and a pneumatic extrusion system utilizing an inert gas under pressure for extrusion of thin-section steel shapes and problems encountered in the forging of beryllium were also described in the survey.

Two patents were assigned to the U. S. Atomic Energy Commission for unique fabrication processes. One patent covers a method for forming external projections on zirconium tubes by electric heating and pressure.[21] In this method the tube is internally supported on a water-cooled copper-alloy mandrel. A copper-alloy electrode with a concave cylindrical surface portion having a recess is pressed against the outside of the tube, and an alternating current of low voltage and high amperage is applied across the tube wall between the electrode and the mandrel. By this procedure the external projection is formed by thinning adjacent areas of the tube and gathering metal at the projection. The second patent[22] describes a method for extruding molybdenum and tungsten in which a volatile-oxide bearing surface is formed by heating the metal to 2850 to 3700°F (1566 to 2040°C) and exposing the heated metal to an oxidizing atmosphere. This method was used by Oak Ridge in the float-mandrel extrusion of tungsten described earlier.

(S. G. Nelson)

Powder-Metallurgy Materials

Cold Vibratory Compaction

A book[23] on vibratory compaction (published in 1967) includes a discussion of technological and economic advantages of this method over static pressing methods, especially when working with the powders of very hard, strong materials such as carbides, borides, ceramics, and ferrites. There is an annotated bibliography containing 64 references.

McGeary[24] conducted an idealized experimental study on the vibratory-packing characteristics of spherical particles. Spherical metal shot of steel, tungsten, and aluminum in several discrete, small sizes were packed in glass containers by mechanical vibration. Packing arrangements for one, two, three, and four sphere sizes in a given container and the dynamic process of packing were studied visually. One-size spheres were found to pack in an orthorhombic arrangement with a density of 62.5% of theoretical. It was noted that high-density packings could be achieved if several widely different sphere sizes were used together. For instance, a quaternary packing with a density of 95.1% of theoretical was formed from spheres with diameter ratios of 1:7:38:316 and volume ratios of 6.1:10.2:23.0:60.7, respectively. The frequency and acceleration of vibration, density of materials, fineness of components, and state of evacuation of container influenced the rate of packing in tests with both pneumatic and electric vibratory equipment.

Pressing and Sintering

A pressing-sintering technique[25] for fabricating containers for melting high-temperature metals has been developed by Dow Chemical Company. Tungsten, zirconium diboride, various oxides, nitrides, and carbides were formed into containers of high density and low porosity.

A method for producing shaped products of powder materials is described in a British patent.[26] The powders, including metals, alloys of metals, and ceramics either alone or with a binder, are formed into composites of high strength. The powder is loaded into a mold that has an enclosed cavity in which the inner portions of the mold wall are formed of graphite flour and colloidal graphite alternating with layers of graphite stucco. The remainder of the mold is formed of graphite materials or inorganic ceramic materials. Powders processed in this manner included Be, Cr, Nb, Mo, Ta, Ti, W, and Zr, as well as their oxides and metallides. The sintering temperature is 2100°F (1150°C).

A second British patent[27] describes a compaction process in which particles of metallic powders are hot pressed to form a solid body of high density. The particles have an inert solid film that acts as a barrier to the formation of metal–metal bonds. The surface film on the particles remains solid during processing but is penetrated by atoms of the underlying metal, and the lower process temperatures inhibit grain growth.

A British study[28] involved the development of manufacturing procedures for the consolidation of a series of high-density (approximately 17 to greater than 18.5 g/cm^3) sintered W–Ni–Cu and W–Ni–Fe alloys. Physical- and mechanical-property data for these alloys and the effect of sintering variables on their properties were determined.

Sintered bars of two series of W–Os–Re alloys were successfully prepared by the British.[29] The first series, containing nominally 5 wt.% rhenium and up to 2.25 wt.% osmium, was single-phase alloys consisting of an alpha solid solution. The second series, containing nominally 26 wt.% rhenium and up to 11.3 wt.% osmium, consisted of the same solid solution up to 1.67 wt.% osmium, whereas the higher osmium contents yielded two-phase alloys consisting of the alpha solid solution and a hard, brittle sigma phase. The two-phase alloys were of the age-hardenable type, and their properties were thus dependent on thermal history.

The French[30] have prepared Zr–Cu and Zr–Cu–Mo alloys by sintering the hydride powders. This technique was devised so that machining scrap from zirconium alloys could be recovered by powder-metallurgy methods. The mechanical properties of the dense sintered parts were comparable with those of cast parts, except for the hardening influence of the oxygen content.

Kellerer, Saur, and Borchers[31] have processed Al–Al_2O_3 dispersion-strengthened alloys from thin sheets. The technique involved winding aluminum sheets, 3 to 40 μ thick, into spools and oxidizing them in air, water, or water vapor. The spools were then extruded into rods at about 600°C, which caused the superficial oxide layers to break into small particles and become distributed throughout the matrix. Metallography and mechanical-property determinations were used to establish the optimum fabrication conditions for the alloy. The influence of oxide content and foil thickness on mechanical properties was investigated. When foils 3 μ thick and oxide layers 0.2 μ thick were used, maximum tensile strengths of 32 kg/mm^2 at 20°C and 8 kg/mm^2 at 450°C were obtained.

Mechanical properties at elevated temperatures (up to 525°C) of sintered compacts of oxidized Mg–Zr or Mg–MgO of various particle-size ranges (~20 to 800 μ) were determined.[32] The elevated-temperature mechanical properties of the compacts showed a direct dependence on the content and distribution of the oxides and on the particle-size distribution of the oxidized powders. The ductility varied with the size of the original particles.

Porous-Metal Fabrication

The Russians[33] have processed porous parts from tungsten and molybdenum and examined the effects of technological factors on the porosity of these materials. Air penetration and durability of the parts were considered in relation to their porosity.

Porous-metal filters for nuclear applications was the subject of two presentations at an English Symposium on the Role of Powder Metallurgy in Nuclear Technology. The first paper[34] discussed the utilization of sintered porous stainless steel (En58e or 304L) for numerous specialized purposes in chemical engineering, notably filtration. Typical nuclear energy applications, in which corrosion resistance and good elevated-temperature strength of porous stainless steel are of value, were described. In the second paper[35] the utilization of porous bronze and chromized iron filters in nuclear power stations for CO_2 purification was noted. These elements are used for filtering in the submicronic to 25-μ range.

(C. A. MacMillan)

Pressure Bonding

Hot-press bonding of six dissimilar-alloy combinations was investigated by Boeing.[36] The alloy couples studied were as follows:

2219 aluminum: 321 stainless steel
7106 aluminum: 321 stainless steel
2219 aluminum: Ti–5 wt.% Al–2.5 wt.% Sn
321 stainless steel: Ti–8 wt.% Al–1 wt.% Mo–1 wt.% V
321 stainless steel: Inconel 718
Inconel 600: Ti–8 wt.% Al–1 wt.% Mo–1 wt.% V

Good bonds were obtained with all alloy couples except those containing the Ti–8 wt.% Al–1 wt.% Mo–1 wt.% V alloy which formed brittle compounds during the bonding operation. The more promising couples of this group were further evaluated by metallurgical analysis, mechanical- and thermal-shock testing, leak testing, and corrosion tests.

Studies of the primary diffusion parameters[37] showed temperature to be the most influential factor in achieving good bonds. Time at temperature exhibited an intermediate effect. Pressure during bonding was found to be an important factor up to the level at which intimate contact of the mating faces was obtained. No effect was observed at higher pressures.

In evaluating process variables, researchers noted that chemical cleaning provided the best means of surface preparation.[36] Bonding in air led to weak joints because of oxidation, whereas bonding in an argon atmosphere or in a vacuum resulted in consistently high-strength joints. The use of silver electroplates as a diffusion aid was successful in all cases except when bonding the Inconel 718–321 stainless-steel couples, in which case nickel electroplates provided the best results.

A high-pressure, hot-pressing technique for fabricating dense bodies of titanium and zirconium diborides has been described by Clougherty and Kalish.[37] The processing technique does not employ the lower-melting-point metal additives and utilizes pressures on the order of 100,000 psi and temperatures from 1500 to 2000°C.

A patent[38] has been issued describing the production of tungsten-powder ingots with high structural integrity and densities greater than 98% of theoretical. In this process the powders are compacted at temperatures above 900°C and pressures up to 50 kbars. On cooling it is necessary to decompress the compact before reaching 700°C. (S. W. Porembka)

Plating

A method of ion plating which employs a gas discharge independent of the evaporation source and substrate was described by Baum.[39] The gas discharge was set up perpendicular to the path of the depositing vapor. Low substrate potentials could be employed, and the kinetic energy of ionized particles incident upon the substrate could be adjusted from thermal energies up to 400 ev or better. Copper and gold films were deposited by this method on 1.5-in.-diameter stainless-steel substrates mounted in an insulating material with only the front surface exposed. The deposited films were evaluated in terms of adherence, abrasion resistance, and surface appearance. Film thicknesses, calculated from the weight-change data, were 9000 A for gold and 6200 to 12,000 A for copper.

The deposition of thin films of iridium on molybdenum has been studied by field-ion microscopy at Harwell.[40] The choice of the Mo–Ir system was dictated by the ease of imaging molybdenum and iridium in helium gas at 77°K, by their similar lattice constants, and by their alloying behavior. A directly heated coil of high-purity iridium wire 0.020 in. in diameter served as the evaporator. Pressures of the order of 10^{-9} torr used for this work were maintained by a liquid-nitrogen-cooled titanium-evaporation pump. When the substrate was held at low temperature during and after deposition, a localized thin deposit coherently bound to the substrate was formed. At higher substrate temperatures, diffusion of the iridium took place, and thicker films were grown epitaxially on the substrate with the (1 1 1) plane of iridium on the (1 1 0) plane of molybdenum and with the $[\bar{1}\,0\,1]$ direction of iridium parallel to the $[\bar{1}\,1\,\bar{1}]$ direction of molybdenum. Twin crystals caused by multiple positioning and stacking faults were found. There was no evidence of alloy formation by surface interdiffusion of iridium and molybdenum.

The sputtering process was discussed and evaluated by McClanahan, Moss, and Busch,[41] with particular attention to the triode method. The high electron current involved in the triode sputtering produces a plasma of high ion density (10 to 30 ma/cm^2), which promotes adherence of the deposit to the substrate. The sputtering rates obtained were on the order of 100 times that obtained by the diode method, and the inert-gas pressure was in the range 10^{-6} torr. This low operating pressure reduced the concentration of the impurities in the atmosphere. As a specific application of the triode method, hollow stainless-steel cylinders were coated with a specified thickness of uranium. The resulting neutron-detector anodes met specifications for thickness, uniformity, and adherence. The coating apparatus was capable of depositing a second protective coating over the uranium without breaking the vacuum. However, the sputtered uranium was sufficiently resistant to oxidation, and there was no need for the second coating.

Single-crystal thin ferrite films were prepared by Westwood et al.[42] by sputtering in a glow-discharge system from a ceramic cathode of nickel ferrite onto a magnesium oxide substrate cleaved parallel to the (1 0 0) plane. X-ray and electron diffraction analyses gave d values consistent with a nickel ferrite spinel. The iron-to-nickel atom ratio, obtained by chemical analysis, was approximately 2 : 1. Magnetic measurements indicated that the films were single crystal, since the values obtained differed from those for the bulk compound.

Two vacuum techniques, glow-discharge anodization of a metal film and d-c-diode reactive sputtering, were investigated by Vratny[43] for the formation of tantalum oxide films. Dielectrics up to a maximum thickness of 3000 A could be prepared by these methods with equal or larger-than-anticipated capacitance per unit area and with dielectric strengths about one-third that of anodically formed tantalum oxide. The d-c-diode reactive-sputtering process produced thickness variations of 4 to 20% over 50 cm^2, compared with 4% and 1% for glow-discharge anodization and aqueous anodization, respectively. Lower dielectric strengths and lower formation rates were indicated as a limitation of the all-vacuum methods.

Formation of silicon and titanium carbides by chemical vapor deposition at high temperatures from gas mixtures containing tetrachlorides, hydrogen, and methane was studied by Pearce and Marek.[44] For silicon carbide deposits the simultaneous reduction of silicon tetrachloride to silicon and deposition of carbon with subsequent reaction of these two to form the carbide were suggested. For titanium carbide, however, elemental titanium was apparently not involved in the mechanism. It was also suggested that titanium carbide deposition may proceed via lower valency halides that react with methane or hydrocarbon free radicals to form large, complex, pyrolyzable molecules. (J. Zupan)

High-Energy-Rate Processes

A joining technique utilizing magnetic-pulse bonding has been developed by Morin, Peacock, and Zotos.[45] The patented process has been used to produce circumferential socket-type joints in low-carbon-steel pipe, dissimilar stainless-steel tubing, and titanium-alloy tubing. In the process a high-intensity magnetic field is applied to the workpieces in a short time interval, and the tubes are thus driven together at a velocity sufficient to cause bonding. The novelty of this process lies in the fact that the accelerating coil is also used for induction heating of the tubes prior to joining.

Another application of magnetic-pulse bonding has been reported by Douglas United Nuclear.[46] Researchers there have developed a technique for metallurgically bonding end caps to powder-filled aluminum cylinders without change in mechanical properties or "blowout" problems usually associated with fusion-welding techniques. It was found that strong, leaktight bonds could be produced when the annular standoff was between 10 and 65 mils, and the end cap had a taper between 4 and 8°. Advantages of the technique, which is still undergoing development, are speed (6 to 10 sec/per assembly), little or no change in can wall thickness, and no change in metallurgical structure of the bonded materials.

A short review of the explosive-welding field, dealing mainly with British developments, has been published by Gandhi.[47] Briefly and simply discussed are the effects of the many variables on the final properties of the bond. In addition to describing the normally used parallel-plate or angled-plate standoff configuration, the author describes a new arrangement whereby the plates to be bonded are placed in contact with each other, covered with a thick layer of rubber, and subjected to the impulse from a high-explosive charge. The advantages, limitations, and applications of the various techniques are also presented. (D. Laber)

Welding and Brazing

Welding

Development of a readily weldable high-strength aluminum alloy for cryogenic applications has been conducted by Alcoa.[48] Two experimental alloys (X2021 and X7007) showed good promise on the basis of weldability, weld tensile strength, and weld ductility. Alloy X2021 demonstrated excellent weldability with 2319 filler alloy, and its weld tensile strength is slightly higher than that with 2219 filler alloy. Alloy X7007 can be commercially welded with 5356 filler alloy and has a weld tensile strength approaching 60,000 psi. However, it is susceptible to stress-corrosion cracking at 30,000 psi, and further work is being done to overcome this problem.

Techniques for automatic gas tungsten-arc welding of aluminum composite control plates for the High Flux Isotope Reactor have been established at Oak Ridge.[49] These cylindrical control plates regulate the power level of the reactor and have stringent dimensional requirements. Four curved segments were joined by longitudinal weld seams to form the plates, which were 17.842 in. in diameter and $68\frac{3}{8}$ in. long. The diametral tolerance of the welded plate was ±0.005 in., and the straightness tolerance was ±0.030 in. A V-groove joint design and 4043 aluminum filler metal were used in welding the plates.

Results of bend and tensile tests indicated that the welded cylinder would withstand very little deformation before failure occurred in the aluminum–core material interface. This zone tended to yield and fracture long before the weld became significantly stressed. Thus methods and equipment were developed to measure closely the effects of weld shrinkage, weld planishing, and explosive sizing on the diameter and shape of the control plate.

General Electric is examining the inertia welding process for the fabrication of superalloys.[50] The alloys included in the study are Inconel 718, Udimet 700, and Ti–6 wt.% Al–4 wt.% V.

Weldment Studies

Weldment-property studies have been conducted on PH13–8Mo precipitation-hardening stainless steel and on Inconel 718 at General Electric.[51] Tensile and Charpy V-notch impact properties of PH13–8Mo base plate are compared with those for weldments aged after welding (Fig. IV-3). Tensile-strength values for weldments were intermediate between those transverse and parallel to the rolling direction for the base plate. Weldment yield strength varied from 93 to 96% of that for the base plate parallel to the rolling direction over the range from room temperature to 775°F (415°C). The ductility of these specimens was significantly lower and more variable than that for the base plate.

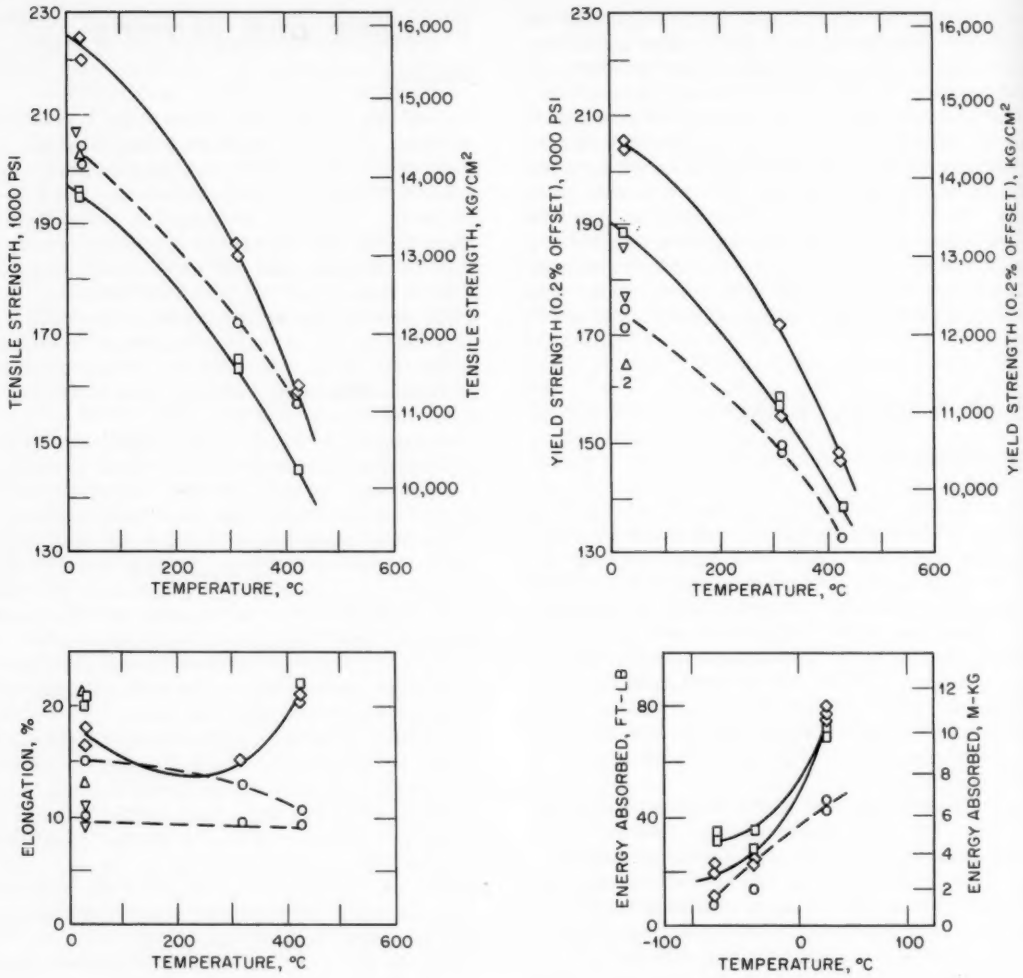

Fig. IV-3 Tensile and Charpy V-notch impact properties of PH13–8Mo precipitation-hardening stainless-steel plate and weldments.[51] □, parallel to rolling direction; ◇, transverse to rolling direction; ○, weld joint (W + A); Δ, all weld (W + A); ▽, all weld (W + An + A). Heat-treatment: W, welded; A, aged 4 hr at 1049°F (565°C), air cooled to room temperature; An, annealed at 1697°F (925°C) for 0.5 hr, air cooled to 50°F (15°C).

Figure IV-4 compares tensile and impact properties for Inconel 718 base plate with those for specimens machined from double U-joint weldments. Strength and ductility of weld specimens were considerably lower than those of similarly treated base-plate specimens. Charpy specimens aged, but not annealed, after welding possessed approximately the same impact strength at 77°F (25°C) as the base plate, but only half as much at −40°F (−40°C), which indicates a possible transition range for the weld metal. Specimens that were both solution-annealed and aged after welding yielded even lower impact-strength values at −40°F.

Tantalum and niobium weldment-property studies have been completed at Lockheed.[52] Single-pass GTA welds were made in 0.015-in.-thick sheets of commercial purity, and tensile and precracked-sheet Charpy tests were performed. Table IV-1 summarizes the tensile test results. The fracture toughness of tantalum was considerably higher than that of niobium.

Brazing

Solar has evaluated several alloys for brazing 10-mil foils of TD nickel, TD nickel–chromium, L-605,

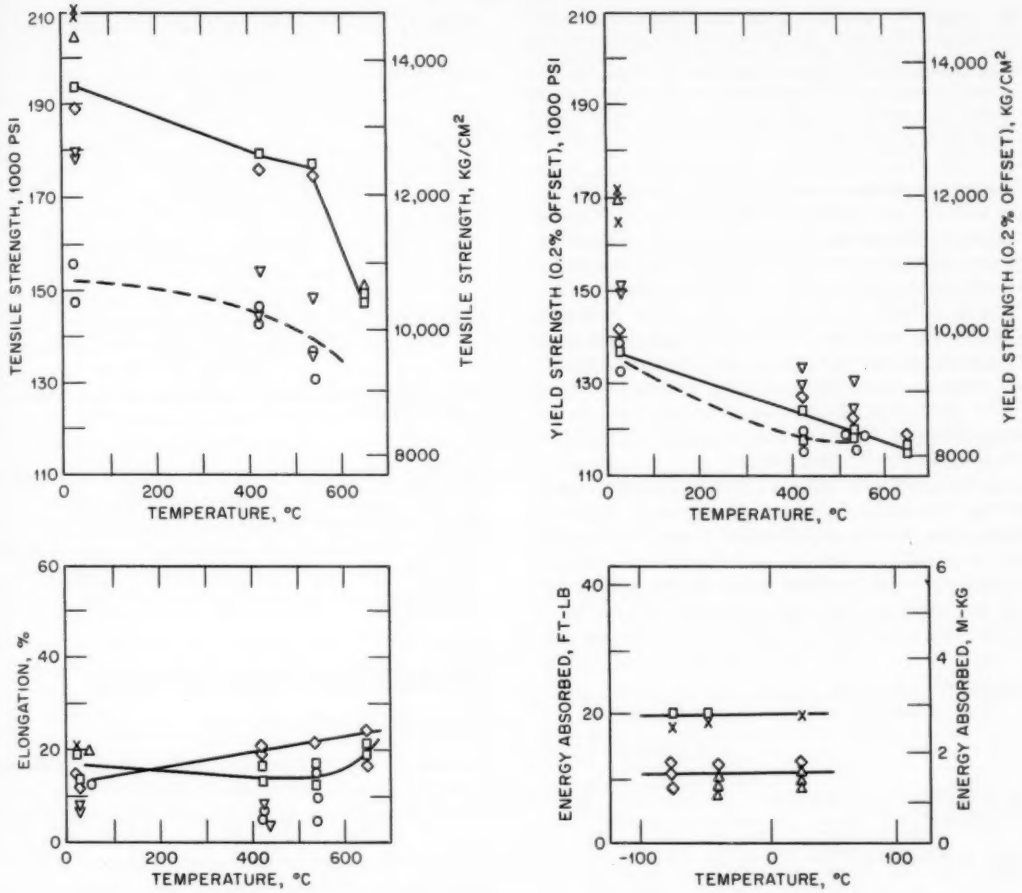

Fig. IV-4 Tensile and Charpy V-notch impact properties of Inconel 718 plate and weldments.[51] □, parallel to rolling direction (I); ◇, transverse to rolling direction (I); ×, parallel to rolling direction (II); △, transverse to rolling direction (II); ○, weld joint (I); ▽, weld joint (II). Heat treatment: (I) 1742°F (950°C) for 1 hr, furnace cool 100 min to 1319°F (715°C), hold 8 hr, furnace cool to 1148°F (620°C), hold 12 hr (including furnace cooling time), then air cool to room temperature; (II) 1742°F (950°C) for 1 hr, air cool to room temperature, heat to 1319°F (715°C), hold 8 hr, furnace cool to 1148°F (620°C), hold 12 hr (including furnace cooling time), then air cool to room temperature.

Table IV-1 TENSILE PROPERTIES* OF TANTALUM AND NIOBIUM WELDED SHEET[52]

Material	Weld orientation	Tensile yield stress, psi	Ultimate tensile stress, psi	Elongation in 1 in., %
Ta	Parallel	35,000	48,400	0.306
Ta	Perpendicular	35,700	50,700	0.277
Nb	Parallel	19,300	31,500	0.167
Nb	Perpendicular	19,100	30,500	0.157

*All values are an average of three specimens.

and Inconel 625 for use at 1800°F (982°C) and above.[53,54] Selections were made on the basis of remelt temperature, high-temperature oxidation, and strength properties. The results of tensile tests on brazed T joints are given in Table IV-2.

Hoppin[55] has emphasized that stress-rupture and creep strength are important in the selection of brazing alloys for superalloys for high-temperature service. Stress-rupture data are plotted in Fig. IV-5 for brazed lap joints in René 41. All these joints had a $2t$ overlap and were aged at 1400°F (760°C) for 16 hr. The following important observation on the usefulness of test data was made by Hoppin:

> Valid comparison of one filler metal to another may be made to aid in selection, but the apparent shear-strength results obtained from lap-joint testing really have no absolute value that can be translated into component design. Brazing-filler-metal selection ultimately must be made on the basis of component requirements and proven on actual or simulated components. There exists today a vast area of ignorance in applying brazed-joint test data intelligently. Far more work in the area of stress analysis

is required to determine what tests are really needed to predict performance. In conjunction with this, available data are inadequate, often not reproducible, and many design engineers have avoided using brazed designs because of their recognition of this situation. The largest single factor holding back the greater use of brazing in superalloy fabrications is the lack of proper data and the knowledge of how to use it.

A program to select a brazing alloy for Zircaloy-2-clad fuel-rod assemblies is being conducted at Illinois Institute of Technology Research Institute.[56] Approximately 150 alloys have been evaluated for brazability and corrosion resistance to static superheated water. Of these, 20 have been selected for further screening in long-term hydrodynamic tests. Eighteen of these are zirconium-based systems (17 binary, 1 ternary) with brazing temperatures ranging from 1769 to 3146°F (965 to 1730°C). The other two alloys are binary platinum systems with brazing temperatures of 1562 and 1652°F (850 and 900°C).

An Al–13 wt.% Si alloy for brazing components of sintered Al–Al_2O_3 has been developed in France.[57] From initial rolling experiments it was found necessary to modify the brazing alloy by adding 0.02 wt.% sodium to prevent depletion of the silicon in the diffusion zone at the high temperatures of 842 to 1040°F (450 to 560°C) likely to be encountered in service.

Table IV-2 TENSILE STRENGTH OF AS-BRAZED T JOINTS AT ROOM TEMPERATURE AND AT $T_{MAX.}$[53,54]

Superalloy	Braze alloy	Test temp., °F	Ultimate tensile strength, 1000 psi	Failure mode*
L-605	J8400	70	109.5	BA
L-605	J8400	1800	21.5	PM
L-605	J8100	70	74.7	BA
L-605	J8100	1800	22.0	PM
L-605	CM52	70	78.9	BA
L-605	CM52	1800	20.1	PM
L-605	J8600	70	132.0	BA
L-605	J8600	1800	0.6	BA
Inconel 625	Palniro X	70	70.5	BA
Inconel 625	Palniro X	2000	3.2	BA
Inconel 625	CM50	70	106.5	BA
Inconel 625	CM50	2000	1.1	BA
Inconel 625	NX77	70	75.9	BA
Inconel 625	NX77	2000	10.5	PM
Inconel 625	J8600	70	109.9	PM
Inconel 625	J8600	2000	6.5	50% PM
TD nickel	TD-20	70	67.8	PM
TD nickel	TD-20	2000	17.4	PM
TD nickel	TD-6	70	60.6	PM
TD nickel	TD-6	2000	15.1	50% PM
TD nickel	J8600	70	59.2	PM
TD nickel	J8600	2000	5.0	BA
TD nickel	60 Pd–40 Ni	70	65.1	PM
TD nickel	60 Pd–40 Ni	2000	9.4	BA
TD nickel–chromium	TD-6	70	111.6	30 to 100% PM
TD nickel–chromium	TD-6	2200	2.3	BA
TD nickel–chromium	CM50	70	103.7	BA
TD nickel–chromium	CM50	2200	1.2	BA
TD nickel–chromium	NX77	70	120.0	PM
TD nickel–chromium	NX77	2200	0.6	BA
TD nickel–chromium	NSB	70	111.0	BA
TD nickel–chromium	NSB	2200	0.7	BA

*BA, braze alloy; PM, parent metal.

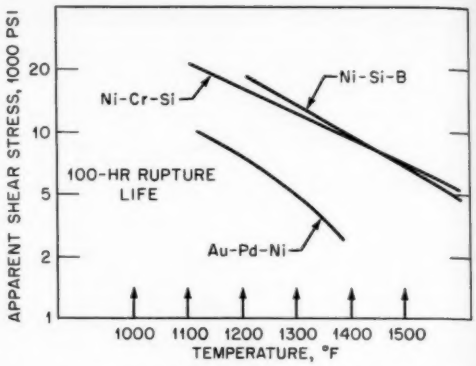

Fig. IV-5 Stress-rupture properties of brazed joints in Renê 41 (Ref. 55).

Brazing tests were carried out with this modified alloy on sheets and on bar-tube units. Good-quality bonds, unimpaired by diffusion, were obtained. Under certain conditions the mechanical properties were superior to those of the base material, and the joints were completely leaktight to helium. (R. M. Evans)

Nondestructive Testing

Ultrasonic Techniques

Ultrasonic nondestructive techniques are preferable to destructive impact methods of determining neutron-irradiation damage in metals, since destructive tests require a large number of exposed specimens. Using the critical-angle method, investigators at Battelle–Northwest[58] developed a preliminary curve that correlates ultrasonic signal amplitude to neutron fluence. They were able to detect radiation-induced property changes in both 304 stainless steel and A-302B steel.

By using an *A*-scan for determining the distance and a *C*-scan for outlining the target, researchers at Atomic Power Development Associates[59] developed an ultrasonic method of locating and identifying an object in high-temperature opaque media such as liquid sodium at 600°F (316°C). The attenuation of ultrasonic energy propagating in molten salt is low, and the lack of transducers that can operate at the required temperature has been a major limitation. Lead zirconate–titanate transducers (Clevite PZT-5) with zirconium lenses were used successfully to locate objects within distances ranging from ¼ in. to 3 ft. How the PZT-5 elements were protected from the 600°F temperature, which is dangerously near the Curie point for PZT-5, was not revealed.

Other research at Battelle–Northwest[60] showed that penetration of the weld in peripheral end caps on SNAP-15A isotope-containment capsules could be measured ultrasonically with an accuracy of ± 5% of full penetration. By careful transducer alignment, it

was also possible to detect intergranular cracking and cavities at the weld root.

Machined longitudinal and transverse notches are being used at Oak Ridge[61] as ultrasonic notch standards for calibration in tubing with 0.050- and 0.180-in. bores. The notches are prepared by electrical-discharge machining. Microcracking has been encountered in the bottom of reference notches in tungsten- and molybdenum-base alloys. This problem was especially severe in unalloyed tungsten. Depths of the notches are determined by means of silicone-rubber replicas of the inner surface of the tube. The replicas were made by spinning the tubes in a small jewelers' lathe while the rubber was curing, then removing the replicas by vacuum.

German investigators[62] have employed pulse methods to detect defects in electrical high-tension insulators. Porcelain and steatite insulators can pass the electrical-breakdown and mechanical-parts test and still contain internal defects, such as shrinkage cavities, cracks, foreign inclusions, closed voids, disk-type fractures, or small pores which weaken the ceramic and lead to fracture of the insulator in service. A standard pulse-echo technique is used to locate large defects, such as shrinkage cavities, cracks, and foreign inclusions. Longitudinal wave velocity serves as a measure of the quality of the ceramic body of the insulator, since the wave velocity is higher in the correctly fired ceramic than in either the underfired or overfired ceramic. Porous insulators can also be detected by this method. (D. Ensminger)

NDT Techniques Other Than Ultrasonic

A diaphragm-type pressure transducer has been designed, constructed, and tested to 165,000 psi by investigators at Lawrence Radiation Laboratory.[63] A differential-phase two-coil eddy-current system operating at 1 Mc detects the deflection of the metal diaphragm, and the phase difference is converted to a d-c output signal. The transducer has a design range of 100,000 psi at full scale, a 1-volt output, a 3000-volt breakdown isolation, and the ability to withstand accelerations up to 5000 g and high gamma and neutron radiation fluxes for short periods. Slowly changing pressures and pressure peaks with periods of a few hundred microseconds are detectable. The performance was observed repeatable to 0.2% or better, and most units had a hysteresis of less than 2% of full scale. Difficulty in working with a range of 200,000 psi would be due only to calibration limitations. Diagrams of the transducers, calibration system, and environmental testing apparatus are presented.

Investigators at Argonne are studying a small isotopic neutron source useful for neutron radiography.[64] Cellulose nitrate layers are also being investigated as neutron-track-etch detectors. With cellulose nitrate layers 8 μin. thick, improved contrast can now be observed in neutron images of 0.5-mm steps in natural-uranium test pieces 1 to 2 mm thick. With older cellulose nitrate layers three times as thick, it was difficult to detect the neutron shadow of 2-mm-thick test pieces of uranium. Useful images are now obtained with neutron exposures about one-fourth of the former value of 2×10^9 neutrons/cm^2. It was not established whether the improved results were due to the smaller layer thickness or to better cellulose nitrate material.

The same investigators have initiated studies of scatter X radiography with a 1.27-cm-diameter aluminum rod with holes of various sizes drilled into the end face to simulate internal voids. When film is wrapped around the circumference of the rod sample, a collimated X-ray beam 0.95 cm in diameter directed along the axis of the sample will resolve several different hole sizes at depths of 0.58 to 1.65 mm.

Acoustic emission as a method for nondestructive testing and failure prediction has been investigated by Hutton.[65] Typical sonic signals were shown, as well as data taken during yield of test specimens. The acoustic-emission approach appears promising for remote and continuous surveillance of operational systems, such as natural-gas pipelines, reactor pressure vessels, and aircraft structures, and for monitoring welds for cracking during cooling, testing of fuel tanks, and fracture research.

(A. F. Leatherman)

References

1. F. H. Hueston and R. S. Barclay, Some Problems in the Melting and Casting of Uranium and Its Alloys, *Can. Mining Met. Bull.*, 60: 795-798 (July 1967).
2. O. J. Wick, Fabrication of Unalloyed Plutonium and Plutonium Base Alloys, *Plutonium Handbook, A Guide to Technology*, Vol. 2, pp. 585-598, Gordon and Breach, Science Publishers, Inc., New York, 1967.
3. J. Herriott, M. Murtha, and G. Burnet, Growing Nickel Single Crystals by Pulling from a Melt, USAEC Report IS-1703, Ames Laboratory, October 1967.
4. J. C. Freche, W. J. Waters, and R. L. Ashbrook, Application of Directional Solidification to a NASA Nickel-Base Alloy (TAZ-8B), Report NASA-TN-D-4390, National Aeronautics and Space Administration, Lewis Research Center, February 1968.
5. E. L. Foster, Jr., S. G. Nelson, W. J. Hildebrand, N. M. Griesenauer, D. P. Moak, and J. M. Allen, Development of a Subscale Manufacturing Process for the Fabrication of Hypereutectic Transition-Metal Carbide Composites, Interim Engineering Progress Report No. 6, Battelle Memorial Institute, Columbus Laboratories, Jan. 15, 1968.
6. H. G. Poole, Metallurgical Progress Report No. 37, Quarter Ending December 1967, USAEC Report USBM-RC-1326, pp. 1-24, Bureau of Mines.
7. C. E. Lundin and A. S. Yamamoto, A Fundamental Investigation of the Alloying Behavior of the Rare Earths and Related Metals, USAEC Report DRI-2437, Denver Research Institute, September 1967.
8. S. Takahashi, Improvement in the Casting of Aluminum–Uranium Alloy, Japanese Patent 12723, July 19, 1966.
9. J. P. Langeron, Application of the Zone Melting Method to the Purification of Zirconium and Study of Certain Properties of the Metal Thus Purified, *Rev. Hautes Temp. Refract.*, No. 2: 137-156 (June 1965).

10. I. V. Milov, D. M. Skorov, and V. V. Nikishanov, Crystallization Front in Electric-Arc Zone Melting, in *High-Purity Metals and Alloys: Fabrication, Properties, and Testing*, pp. 45-49, Consultants Bureau, New York, 1967.
11. V. N. Grinyuk, I. I. Papirov, G. F. Tikhinskii, and I. G. D'yakov, Purification of Beryllium by Zone Refining and by Crystal Pulling from the Melt, *Izv. Akad. Nauk SSSR, Metal.*, No. 4: 77-84 (July–August 1967).
12. R. R. Lowery and G. Asai, An Evaluation of W–25 Re Produced by Both Arc-Melting and Powder Metallurgy, USAEC Report USBM-RC-1274, Bureau of Mines, February 1968.
13. J. F. Kakner, Selected Bibliography of Hydrostatic and Fluid-to-Fluid Extrusion of Metals, USAEC Report UCID-15236, University of California Lawrence Radiation Laboratory, Oct. 23, 1967.
14. R. E. McDonald and G. A. Reimann, Floating-Mandrel Extrusion of Tungsten and Tungsten-Alloy Tubing, USAEC Report ORNL-4210, Oak Ridge National Laboratory, February 1968.
15. C. H. Ross, Try Shear Spinning To Form Tough Alloys, *Tool Mfg. Eng.*, 59: 40-43 (July 1967).
16. G. Clar and W. Reverdy, Production of a Tungsten Jet Pipe Neck at the SEPR Plant, *Tech. Mod.*, No. 6: 24-26 (May 1965).
17. S. B. Pevzner, N. I. Korneev, I. G. Skugarev, A. S. Tugushev, Yu. V. Malashenko, and V. B. Emel'yanov, Extrusion of Refractory Metals in Vacuum, *Tsvetn. Metal.*, No. 8: 86-88 (1967).
18. I. N. Ross, The Recrystallization and Work-Hardening Characteristics of Yttrium and Twelve Lanthanides, *J. Inst. Metals*, 95: 337-342 (November 1967).
19. W. Brunst, Plasma Technology of Tungsten, *Schweissen Schneiden*, 18: 239-240 (May 1966).
20. T. G. Bryrer and F. W. Boulger, Metalworking, Review of Recent Developments, Battelle Memorial Institute, Defense Metals Information Center, May 26, 1967.
21. R. E. Monroe and J. J. Vagi, Forming Projections on Tubes, U. S. Patent 3,354,290, to USAEC, Nov. 21, 1967.
22. R. E. McDonald and C. F. Leitten, Jr., Method for Extruding Molybdenum and Tungsten, U. S. Patent 3,350,907, to USAEC, Nov. 7, 1967.
23. H. H. Hausner, K. H. Roll, and P. K. Johnson (Eds.), *Vibratory Compacting. Principles and Methods. Perspectives in Powder Metallurgy. Fundamentals, Methods, and Applications*, Vol. 2, Plenum Press, New York, 1967.
24. R. K. McGeary, Mechanical Packing of Spherical Particles, *Vibratory Compacting, Perspectives in Powder Metallurgy*, pp. 209-236 of Ref. 23.
25. W. P. Meier, Materials for High-Temperature Metal-Melting Containers, USAEC Report RFP-900, Dow Chemical Company, Rocky Flats Division, Feb. 21, 1968.
26. N. G. Sirones, Method of Producing Shaped Products of Sintered Powders, British Patent 1,088,560, Oct. 25, 1967.
27. J. W. Butcher and R. L. Samuel, Improvements in or Relating to Sintering Processes, British Patent 1,090,263, Nov. 8, 1967.
28. D. J. Jones and P. Munnery, Production of Tungsten Alloy Penetration Radiation Shields, *Powder Met.*, 10: 156-173 (Autumn 1967).
29. A. Leach and D. J. Jones, Preparation and Some Properties of Tungsten–Rhenium–Osmium Alloys, *Powder Met.*, 10: 174-191 (Autumn 1967).
30. H. Demars and R. Meyer, Preparation of Zirconium–Copper and Zirconium–Copper–Molybdenum Alloys by Sintering the Hydride Powders, *Powder Met.*, 10: 145-155 (Autumn 1967).
31. H. Kellerer, G. Saur, and H. Borchers, Production and Properties of Al–Al_2O_3 Dispersion Strengthened Alloys from Thin Sheets, German Report EUR-3497d, Mar. 14, 1967.
32. R. Biais, N. Vitran, F. Dabosi, P. Millet, and J. Pegoud, Structural and Mechanical Properties of Sintered Magnesium Products at Elevated Temperatures, *Powder Met.*, 10: 116-144 (Autumn 1967).
33. E. P. Ponomarenko and A. K. Voropaev, Tungsten and Molybdenum Porous Parts, *Porosh. Met., Akad. Nauk. Ukr. SSR*, No. 9: 92-96 (September 1967).
34. E. Bishop and G. Collins, Stainless Steel Filters for Nuclear Applications, *Powder Met.*, 10: 192-202 (Autumn 1967).
35. R. A. G. Harcourt, A Note on Porous Metal Filters in Nuclear Power Stations for CO_2 Purification, *Powder Met.*, 10: 203-207 (Autumn 1967).
36. C. H. Crane, R. T. Torgerson, D. T. Lovell, and W. A. Baginski, Study of Dissimilar Metal Joining by Solid State Welding, Report NASA-CR-82460, Boeing Co., Oct. 1, 1966.
37. E. V. Clougherty and D. Kalish, Strengthening Mechanisms, in *High Pressure, High Temperature Ceramic Structures*, pp. 431-443, Syracuse University Press, Syracuse, N. Y., 1966.
38. G. E. Zima and J. A. Lakner, Method for Producing High Density Tungsten, U. S. Patent 3,356,495, to USAEC, Dec. 5, 1967.
39. G. A. Baum, Low-Energy Accelerated Ion Deposition, USAEC Report RFP-686, Dow Chemical Company, Rocky Flats Division, Feb. 6, 1967.
40. D. S. Whitmell, A Field-Ion Microscope Study of Thin Films of Iridium on Molybdenum, British Report AERE-R-5608, October 1967 (to be published in *Surface Sci.*, 8: (1968).
41. E. D. McClanahan, R. W. Moss, and R. Busch, Application of Sputtering to the Fabrication of Neutron Detector Anodes, USAEC Report BNWL-553, Battelle–Northwest, November 1967.
42. W. D. Westwood, H. K. Eastman, R. G. Poulsen, and A. G. Sadler, Single-Crystal Ferrite Films Prepared by Cathodic Sputtering, *J. Amer. Ceram. Soc.*, 50(3): 119-123 (March 1967).
43. F. Vratny, Tantalum Oxide Films Prepared by Oxygen Plasma Anodization and Reactive Sputtering, *J. Amer. Ceram. Soc.*, 50(6): 283-287 (June 1967).
44. M. L. Pearce and R. W. Marek, Formation of Silicon and Titanium Carbides by Chemical Vapor Deposition, *J. Amer. Ceram. Soc.*, 51(2): 84-87 (February 1968).
45. T. J. Morin, G. R. Peacock, and J. Zotos, Hydrodynamic Welding—A Major Breakthrough in Tubular Joining, *Weld J. (N. Y.)*, 47(2): 114-117 (February 1968).
46. H. G. Powers, Bonding of Aluminum by the Capacitor Discharge Magnetic Forming Process, USAEC Report DUN-1941, Douglas United Nuclear, Inc., April 1967.
47. S. C. Gandhi, Explosive Welding Today, *Metalwork. Prod.*, 111(17): 58-64 (Apr. 26, 1967).
48. R. W. Westerlund, W. A. Anderson, and H. Y. Hunsicker, Development of a High-Strength Aluminum Alloy, Readily Weldable in Plate Thicknesses, and Suitable for Application at −423°F (−253°C), Report NASA-CR-61423 (N68-14135), Aluminum Company of America, Oct. 13, 1967.
49. W. C. Collins, Welding of the Control Plates for the High Flux Isotope Reactor, *Weld. J. (N. Y.)*, 46: 833-841 (October 1967).
50. K. W. Stalker, Improved Fabrication Methods of Jet Engine Rotors, Interim Engineering Progress Report, October 1–December 31, 1967, General Electric Company, Flight Propulsion Division.
51. General Electric Company, Nuclear Materials and Propulsion Operation, AEC Fuels and Materials Development Program, Progress Report No. 71, USAEC Report GEMP-1002, pp. 111-115, Dec. 29, 1967.
52. K. E. Hays, Crack Propagation Studies of Welds in Tantalum and Columbium Sheet, Report RLMSC-B-70-6718(AD-654150), Lockheed Missiles and Space Co., March 1967.
53. Solar, a Division of International Harvester Co., Join-

ing of Superalloy Foils for Hypersonic Vehicles, Interim Engineering Progress Report, September 1–November 30, 1967.
54. Solar, a Division of International Harvester Co., Joining of Superalloy Foils for Hypersonic Vehicles, Interim Engineering Progress Report, December 1, 1966–May 31, 1967.
55. G. S. Hoppin III, Critical Properties of Superalloy Brazed Joints, Report TM-67-701, General Electric Company, Nov. 8, 1967.
56. Illinois Institute of Technology Research Institute, Research on Zircaloy Braze Alloy Development, USAEC Report IITRI-578-P-29-17, Oct. 17, 1967.
57. J. Herenguel and Cl. Leymonie, Examination of Rolled Alpax/Al–Al_2O_3 Sintered Materials, Application of Brazing to Components of Sintered Al–Al_2O_3 Materials, USAEC Report UCRL-Trans-10144 [translated from *Mem. Sci. Rev. Met.*, 61: 43-54 (1964)].
58. D. O. Hunter, An Ultrasonic Method for Nondestructively Detecting Radiation-Induced Embrittlement in Pressure Vessel Steels, USAEC Report BNWL-SA-1467, Battelle–Northwest, Oct. 16, 1967.
59. C. C. Scott and S. P. Ying, Development of the Under-Sodium Ultrasonic Scanner, USAEC Report APDA-210, Atomic Power Development Associates, Inc., October 1967.
60. R. W. Steffens and F. M. Coffman, Nondestructive Testing of Isotope Containment Capsules, SNAP-15A, USAEC Report BNWL-529, Battelle–Northwest, January 1968.
61. P. Patriarca (Comp.), Oak Ridge National Laboratory, unpublished, April 1968.
62. C. Stueber, The Use of the Ultrasonic Pulse Method for Nondestructive Testing of High Tension Insulators, British Report AERE-Trans-1077 [translated from *Ber. Deut. Keram. Ges.*, 44: 20-22 (1967)].
63. J. E. Field, Design and Testing of a 100,000-psi Eddy-Current Pressure Transducer for Hostile Environments, USAEC Report UCRL-50341, University of California Lawrence Radiation Laboratory, Oct. 10, 1967.
64. Argonne National Laboratory, Reactor Development Program Progress Report, January 1968, USAEC Report ANL-7419, pp. 111-112.
65. P. H. Hutton, Acoustic Emission in Metals as a NDT Tool, USAEC Report BNWL-SA-1262, Battelle–Northwest, September 1967.

AEC SYMPOSIUM SERIES

Available for $3.00 each from: Clearinghouse for Federal Scientific and Technical Information, National Bureau of Standards, U. S. Department of Commerce, Springfield, Virginia 22151.

1 Progress in Medical Radioisotope Scanning (TID-7673), 1962
2 Reactor Kinetics and Control (TID-7662), 1963
3 Dynamic Clinical Studies with Radioisotopes (TID-7678), 1963
4 Noise Analysis in Nuclear Systems (TID-7679), 1963
5 Radioactive Fallout from Nuclear Weapons Tests (CONF-765), 1964
6 Radioactive Pharmaceuticals (CONF-651111), 1965
7 Neutron Dynamics and Control (CONF-650413), 1965
8 Luminescence Dosimetry (CONF-650637), 1965
9 Neutron Noise, Waves, and Pulse Propagation (CONF-660206), 1966
10 Use of Computers in the Analysis of Experimental Data and the Control of Nuclear Facilities (CONF-660527), 1966
11 Compartments, Pools, and Spaces in Medical Physiology (CONF-661010), 1967
12 Thorium Fuel Cycle (CONF-660524), 1968

LEGAL NOTICE

This journal was prepared under the sponsorship of the U. S. Atomic Energy Commission. Neither the United States, nor the Commission, nor any person acting on behalf of the Commission:

A. Makes any warranty or representation, expressed or implied, with respect to the accuracy, completeness, or usefulness of the information contained in this journal, or that the use of any information, apparatus, method, or process disclosed in this journal may not infringe privately owned rights; or

B. Assumes any liabilities with respect to the use of, or for damages resulting from the use of any information, apparatus, method, or process disclosed in this journal.

As used in the above, "person acting on behalf of the Commission" includes any employee or contractor of the Commission, or employee of such contractor, to the extent that such employee or contractor of the Commission, or employee of such contractor prepares, disseminates, or provides access to, any information pursuant to his employment or contract with the Commission, or his employment with such contractor.

☆U.S. GOVERNMENT PRINTING OFFICE: 1968-345-339/1

NUCLEAR SCIENCE ABSTRACTS

The U. S. Atomic Energy Commission, Division of Technical Information, publishes *Nuclear Science Abstracts* (*NSA*), a semimonthly journal containing abstracts of the literature of nuclear science and engineering.

NSA covers (1) research reports of the U. S. Atomic Energy Commission and its contractors; (2) research reports of government agencies, universities, and industrial research organizations on a worldwide basis; and (3) translations, patents, books, and articles appearing in technical and scientific journals.

Complete indexes covering subject, author, source, and report number are included in each issue. These are cumulated quarterly, semiannually, and annually providing a detailed and convenient key to the literature.

Availability of *NSA*

SALE *NSA* is available on subscription from the Superintendent of Documents, U. S. Government Printing Office, Washington, D. C., 20402, at $30.00 per year for the semimonthly abstract issues and $22.00 per year for the four cumulated-index issues. Subscriptions are postpaid within the United States, Canada, Mexico, and all Central and South American countries, except Argentina, Brazil, Guyana, French Guiana, Surinam, and British Honduras. Subscribers in these Central and South American countries, and in all other countries throughout the world, should remit $37.00 per year for subscriptions to semimonthly abstract issues and $25.00 per year for the four cumulated-index issues.

EXCHANGE *NSA* is also available on an exchange basis to universities, research institutions, industrial firms, and publishers of scientific information. Inquiries should be directed to the Division of Technical Information Extension, U. S. Atomic Energy Commission, P. O. Box 62, Oak Ridge, Tennessee, 37830.

UNITED STATES
ATOMIC ENERGY COMMISSION
P.O. BOX 62
OAK RIDGE, TENNESSEE 37830

OFFICIAL BUSINESS

POSTAGE AND FEES PAID
U.S. ATOMIC ENERGY COMMISSION

MR. R.E. CHAPIN
DIRECTOR OF LIBRARIES
MICHIGAN STATE UNIVERSITY
EAST LANSING, MICHIGAN 48823

1

DOCUMENTS
OCT 14 1968
MICHIGAN STATE UNIVERSITY
LIBRARIES

TECHNICAL PROGRESS REVIEWS may be purchased from Superintendent of Documents, U. S. Government Printing Office, Washington, D. C. 20402. *Nuclear Safety* at $3.50 per year (six issues) for each subscription or $0.60 per issue; each of the other journals at $2.50 per year (four issues) or $0.70 per issue. The use of the order form below will facilitate the handling of your order.

POSTAGE AND REMITTANCE: Postpaid within the United States, Canada, Mexico, and all Central and South American countries except Argentina, Brazil, Guyana, French Guiana, Surinam, and British Honduras. For these Central and South American countries and all other countries: add, for each annual subscription, $1.00 for *Nuclear Safety* and $0.75 for each of the other journals; for single issues, add one-fourth of the single-issue price. Payment should be by check, money order, or document coupons, and MUST accompany order. Remittances from foreign countries should be made by international money order or draft on an American bank payable to the Superintendent of Documents or by UNESCO book coupons.

order form

SUPERINTENDENT OF DOCUMENTS
U. S. GOVERNMENT PRINTING OFFICE
WASHINGTON, D. C. 20402

Please send — 1, 2, or 3 years

- ☐ Isotopes and Radiation Technology ____
- ☐ Nuclear Safety ____
- ☐ Reactor and Fuel-Processing Technology ____
- ☐ Reactor Materials ____

Enclosed: document coupons ☐ check ☐ money order ☐

Charge: Superintendent of Documents No._____

SUPERINTENDENT OF DOCUMENTS
U. S. GOVERNMENT PRINTING OFFICE
WASHINGTON, D. C. 20402

(Print clearly)

Name

Street

City, State, ZIP Code